IVW - Schriftenreihe Band 75
Institut für Verbundwerkstoffe GmbH - Kaiserslautern

Rudi Velthuis

Induction Welding of Fiber Reinforced Thermoplastic Polymer Composites to Metals

Bibliografische Information Der Deutschen Bibliothek

Die Deutsche Bibliothek verzeichnet diese Publikation in der Deutschen Nationalbibliografie; detaillierte bibliografische Daten sind im Internet über <http://dnb.ddb.de> abrufbar.

Bibliographic information published by Die Deutsche Bibliothek

Die Deutsche Bibliothek lists this publication in the Deutsche Nationalbibliografie; detailed bibliographic data is available in the Internet at <http://dnb.ddb.de>.

Herausgeber: Institut für Verbundwerkstoffe GmbH
Prof. Dr.-Ing. Alois K. Schlarb
Erwin-Schrödinger-Straße
TU Kaiserslautern, Gebäude 58
67663 Kaiserslautern
http://www.ivw.uni-kl.de

Verlag: Institut für Verbundwerkstoffe GmbH

Druck: Unionprint Satz und Druck GmbH
Saarbrücken

D 386

Als Manuskript gedruckt. Printed in Germany.
ISSN 1615-021X
ISBN 978-3-934930-71-1
ISBN 3-934930-71-9

Induction welding of fiber reinforced thermoplastic polymer composites to metals

Vom Fachbereich für Maschinenbau und Verfahrenstechnik

der Technischen Universität Kaiserslautern

zur Verleihung des akademischen Grades

Doktor-Ingenieur (Dr.-Ing.)

genehmigte Dissertation

von

Rudi Velthuis

aus Zwolle, Niederlande

Vorsitzender der Prüfungskommission:	Prof. Dr.-Ing. Alois K. Schlarb
1. Berichterstatter:	Prof. Dr.-Ing. Peter Mitschang
2. Berichterstatter:	Prof. Dr.-Ing. Paul L. Geiß
Tag der mündlichen Prüfung:	31.08.2007

D 386

Preface

The following doctoral thesis was made during my work as research assistant at the Institut für Verbundwerkstoffe GmbH (Kaiserslautern, Germany) at the University of Kaiserslautern during the period from 2002 to 2007.

My special thanks are for my supervisor, Prof. Dr.-Ing. Peter Mitschang, for giving me the opportunity to do my doctoral thesis on the metal/composite joining topic and for the interesting and motivating discussions we had. Furthermore, I would like to thank Prof. Dr.-Ing. Paul L. Geiß for examining my thesis and for the valuable input from him and his employees. I am grateful to Prof. Dr.-Ing. Alois K. Schlarb for his support in welding of polymers and for the chairmanship in the examination board.

I also want to thank my colleagues at the IVW and the student assistants (especially Mr. Sven Hennes) for the pleasant working atmosphere and for their support during the material manufacturing, preparation of the samples, and further analyses. In the thermoplastic fiber reinforced polymer composite processing group I would like to affirm my gratitude to Mr. Lars Moser, Mr. Uwe Schmitt, and Mr. Peter Mang. Special thanks go to Mr. Markus Steeg for proofreading and Mr. Christoph Collet for his assistance in various welding topics. Furthermore, I would like to thank my former colleagues Dr. Amol Ogale, Dr. Jens Schlimbach, and Mr. Florian Weyrauch.

The Deutsche Forschungsgemeinschaft is acknowledged for funding the project “Diskontinuierliches Induktionsschweißen von Metall/Faser-Kunststoff-Verbunden” (MI 647/10-1 and MI 647/10-3) in the frame of the DFG-Research-Group 524 „Herstellung, Eigenschaftsanalyse und Simulation geschweißter Leichtbaustrukturen aus Metall/Faser-Kunststoff-Verbunden“. The members of this research group are also thanked for their contribution - especially Dr. Stefan Emrich for providing assistance with pre-treatment methods.

My parents are thanked for giving me the possibility to study. I express my deepest gratitude to my wife Birgit Steiner and my daughter Mareike for exercising patience and for their confidence during the time I was working on my thesis. Only with their help, along with the support of Erika Steiner, I was able to finish and defend my Ph.D.-thesis successfully.

Kaiserslautern, November 2007

Für Birgit und Mareike

Table of content

Abbreviations

Short form	Description
AF	Adhesion failure
Al	Aluminum
$Al(OH)_3$	Aluminumtrihydroxide
Al_2O_3	Aluminumoxide
APC-2/AS4	Commercial uni-directional CF/PEEK-laminate
ASTM	American Society for Testing and Materials
AT	Acetone treatment
BC	Bond line corrosion
CF	Carbon fiber fabric
CF/PA66	Carbon fiber reinforced polyamide 66
CF/PEEK	Carbon fiber reinforced poly(etherehterketone)
CFRPC	Carbon fiber reinforced polymer composite
Co	Cobalt
CoF	Cohesion failure
–COOH-group	Carbonyl-group
CSL	Coupe Sport Leicht
DC01	Steel type
DIN	Deutsches Institut für Normung
DSC	Dynamic scanning calorimetry
EDX	Energy Dispersive X-Ray
Fe	Iron
FE	Finite element
FRPC	Fiber reinforced polymer composites

GF	Glass fiber
GMT	Glass mat reinforced thermoplastic
GPa	Giga Pascal
H_3PO_4	Phosphoric acid
HNO_3	Sulfuric acid
IVW	Institut für Verbundwerkstoffe GmbH
J	Joule
J-Nose	J-shaped leading edge wing section
JB	Joining partner breakage
JP1	Joining partner 1
JP2	Joining partner 2
kW	Kilowatt
LFT	Long fiber reinforced thermoplastic
m	Meter
Mg	Magnesium
MHz	Mega Hertz
mm	Millimeter
Mn	Mangan
MPa	Mega Pascal
NaOH	Sodium hydroxide
NCF	Non-crimped fabric
–OH-group	Hydroxide-group
PA12	Polyamide 12 or Nylon 12
PA66	Polyamide 66 or Nylon 66
PEEK	Poly(etherehterketone)
PE-HD	Polyethylene (high density)

PEI	Poly(etherimide)
PEKEKK	Poly(etherketoneetherketoneketone)
PES	Poly(ethersulfone)
PET	Poly(ethyleneterephthalate)
PE-X	Cross-linked polyethylene
P_h	Power due to hysteresis
P_i	Power induced by induced currents
PP	Polypropylene
PP-GM 25	Glass mat reinforced polypropylene, wt.-% 25
PP-GM 30	Glass mat reinforced polypropylene, wt.-% 30
PP-GM 40	Glass mat reinforced polypropylene, wt.-% 40
PPQ	Poly(phenylquinoxaline)
PPS	Poly(phenylenesulfide)
PTFE	Poly(tetrafluorethylene)
RH	Relative humidity
RT	Room temperature (23 °C)
SEM	Scanning electron microscopy
TGA	Thermogravimetric analysis
Ti	Titan
TP-FRPC	Thermoplastic fiber reinforced polymer composites
TSA	Thermal elastic load analysis (German: Thermische Spannungsanalyse)
WBL	Weak boundary layer
XPS	X-ray photoelectron spectroscopy

Symbols used

Symbol	Unit	Description
α	[-]	Contact angle
α_{heat}	[W/(m²·K)]	Heat transfer coefficient
δ	[mm]	Penetration depth
π	[-]	Value of approx. 3.14
γ^{D}_{lv}	[mN/m]	Disperse contribution of liquid-vapor energy
γ^{D}_{s}	[mN/m]	Disperse contribution of the free surface energy
ρ	[kg/m^3]	Density
ρ_{el}	[Ω·m]	Electrical resistivity
γ_{lv}	[mN/m]	Liquid-vapor energy
σ_{n-1}	[-]	Standard deviation
γ^{P}_{lv}	[mN/m]	Polar contribution of liquid-vapor energy
γ^{P}_{s}	[mN/m]	Polar contribution of the free surface energy
γ_{sl}	[mN/m]	Solid-liquid energy
γ_{sv}	[mN/m]	Solid-vapor energy
μ	[-]	Relative permeability
σ	[MPa]	Tension load
A	[m^2]	Surface area
b	[m]	Sample thickness
c	[J/g·K]	Specific heat capacity
c_p	[J/g·K]	Specific heat capacity at constant pressure
c_v	[J/g·K]	Specific heat capacity at constant volume
E_0	[eV]	Electric potential
f	[Hz]	Frequency

h	[J/g]	Specific enthalpy
H	[J]	Enthalpy
H_e	[T]	Magnetic field
I	[A]	Current
M	[mol/dm³]	Molarity
n	[-]	Amount of measured points
Q	[J]	Heat generation
Q_{in}	[J]	Inserted heat
p	[MPa]	Pressure
R	[Ω]	Ohmic resistance
R_a	[µm]	Roughness parameter
t	[s]	Time
T_0	[K]	Starting temperature
T_{Al}	[K]	Aluminum temperature
T_g	[°C]	Glass transition point
T_m	[°C]	Melting point
T_R	[K]	Room temperature
u	[J/g]	Specific inner energy
U	[J]	Inner energy
v	[m³/g]	Specific volume
V	[m³]	Volume
$x_{average}$	[-]	Mean average value
$x_{measured}$	[-]	Measured value
z	[-]	Factor for calculating the 95 % confidence intervals

Kurzfassung

Induktionsschweißen kann sowohl für das Schweißen von thermoplastischen Faser-Kunststoff-Verbunden als auch für das Verbinden von Metall/Faser-Kunststoff-Verbunden eingesetzt werden. Nach Betrachtung der Möglichkeiten einer solchen Verbindung wurde festgestellt, dass die Verbindungsqualität durch die Oberflächenvorbehandlung des metallischen und des polymeren Fügepartners und durch die Prozessbedingungen bestimmt wird.

Verschiedene neue Werkzeuge (z.B. spezielle Probenhalterungen, temperierbarer Anpressstempel, Erwärmungs- und Konsolidierungsrolle) wurden entwickelt und in die Induktionsschweißanlage zur Herstellung von Metall/Faser-Kunststoff-Verbunden integriert. Topografische Analysen mittels Rasterelektronenmikroskopie und Laserprofilometrie zeigen einen großen Einfluss der Vorbehandlungsmethoden auf die Oberflächenrauhigkeit. Zusätzlich ändert die Vorbehandlung die physikalischen (Oberflächenenergie) und die chemischen Eigenschaften (Atomkonzentration). Die Eigenschaften der Verbindungen wurden zuerst anhand von Zugscherprüfungen und parallel durch Oberflächenanalysen untersucht. Die Ergebnisse dieser Untersuchungen zeigen:

- Die Vorbehandlungsmethoden Korundstrahlen und Sauerbeizen führen bei dem metallischen Fügepartner zu den höchsten Verbundfestigkeiten. Die Atmosphären-Plasmareinigung des polymeren Fügepartners ergibt eine Zunahme der Zugscherfestigkeit von ca. 10 % sowie auch eine Verkleinerung des Vertrauensbereiches.
- Die Zugscherfestigkeit hängt vom Prozessdruck und damit vom Fließverhalten des Polymers in der Fügezone ab.
- Die Orientierung der Prüfkraft relativ zur Faserorientierung hat keinen Einfluss auf die Zugscherfestigkeit der eingesetzten faserverstärkten Materialien.
- Die Leinwand-Bindung, mit mehr polymerreichen Zonen, führt zu einem geringen Anstieg der Zugscherfestigkeit im Vergleich zu einer Atlas 1/4-Bindung. Die Gelege-Struktur ergibt durch Faserverschiebungen ähnliche Festigkeiten wie die Leinwand-Bindung. Es zeigt sich, dass die Verbundfestigkeit durch das Polymer bestimmt wird.

- Die Zugscherfestigkeit gewinnt einen großen Anstieg durch eine zusätzliche Polymerfolie in der Fügezone. Die Schliffbilder zeigen eine polymere Zwischenschichtdicke von 5 bis 20 µm für AlMg3-CF/PA66.
- Durch den gezielten Einsatz verschiedener Vorbehandlungsmethoden (Korundstrahlen mit zusätzlichem Polymer) kann die Zugscherfestigkeit auf bis zu 14 MPa für AlMg3-CF/PA66-Verbunde und 18 MPa für DC01-CF/PEEK-Verbunde gegenüber dem unbehandelten Zustand verdoppelt werden.

Weitere Untersuchungen an den Prozessparametern ergaben für DC01-CF/PEEK-Verbunde, dass folgende Einstellungen zu einer weiteren Steigerung der Zugscherfestigkeit auf 19 MPa führen:

- Eine Starttemperatur des Anpresstempels von 370 °C.
- Eine Haltezeit von 7 Minuten.
- Eine Abkühlrate von 6 °C/min.

Für AlMg3-CF/PA66 zeigte sich, dass eine Anpresstemperatur von 10 °C zu einer Zugscherfestigkeit von 14,5 MPa führt. Diese beiden Zugscherfestigkeiten sind lediglich 10 – 15 % geringer als die unter optimalen Bedingungen hergestellten Klebeverbindungen.

Erste Untersuchungen zeigen, dass bei galvanischer Korrosion von Metall/FKV-Verbunden eine schnelle Abnahme der Zugscherfestigkeit erfolgt. Hierfür wurden die Proben drei Wochen in Wasser gelagert. Beim direkten Kontakt zwischen Kohlenstofffaser und Aluminium erklärt sich dies durch Korrosion in der Fügezone. Dabei sinken die Zugscherfestigkeiten der Proben bis auf 5 MPa. Bei Proben mit einer Glasfaserlage als Isolationsschicht zeigen sich keine Korrosionsprodukte und die Zugscherfestigkeit nimmt um 30 % bis auf 8 – 9 MPa ab.

Bei in Salzwasser gelagerten Proben ist die galvanische Korrosion deutlich stärker ausgeprägt. Bereits nach einer Woche besitzen die acetongereinigten Proben mit zusätzlichem Polymer lediglich eine Restzugscherfestigkeit von 3 bis 4 MPa. Die korundgestrahlten Proben zeigen Korrosionsprodukte am Rande der Fügezone und in der Fügezone, weisen aber dennoch eine Zugscherfestigkeit von ca. 10 MPa auf. Die glasfaserverstärkten Proben zeigen weder Korrosionsprodukte noch eine Abnahme der Zugscherfestigkeit.

Dynamisch thermografische Analysen wurden in verschiedenen Umgebungsgasen durchgeführt, um die Zersetzungstemperatur des faserverstärkten Polymers zu bestimmen. Im Falle von CF/PA66 führte dies nicht zu einer Vergrößerung des Prozessfensters, da die Zersetzung hauptsächlich thermisch und nicht thermo-oxidativ ist. Die festgestellte Zersetzungstemperatur von CF/PEEK in Luft betrug 550 °C. Die Vergrößerung des Prozessfensters ist für CF/PA66 gering und zeigte auch keinen Anstieg in der Zugscherfestigkeit nach dem Schweißen in Stickstoff. Trotzdem hat das Induktionsschweißen unter Schutzgas ein großes Potential für gesättigte Kohlenwasserstoffe wie z.B. glasfaserverstärktes Polypropylen. Hier wurde die Zersetzungstemperatur von 230 °C in Luft auf 390 °C in Stickstoff erhöht.

Es wurde ein Demonstrator bestehend aus einem Aluminium-Profil und einer CF/PA66-Platte hergestellt, womit gezeigt werden konnte, dass die erworbenen Kenntnisse auch für die industrielle Anwendung umsetzbar sind. Mittels analytischer Modelle und FE-Berechnungen wurde die induktive Erwärmung erfolgreich nachgebildet.

1 Introduction and objectives

1.1 Fiber reinforced polymer composites

Fiber reinforced polymer composites (FRPC) are used in a broad range of industrial applications, e.g., in civil engineering, medical engineering, mechanical engineering, the aerospace and aeronautic industries, and automotive engineering. Rotor blades for wind mill applications could only be designed with composites as they have nowadays a blade length up to 55 meter and a weight of 23 tons. Aerospace also uses large amounts of composites. An Airbus A380 contains a composite amount of about 25 % by weight [1]; the planned Boeing 787 will have a composite amount of about 50 % by weight [2]. Most of the composites are so far made out of conventional thermoset resins, but the manufacturing of thermoplastic composites offers many advantages.

Especially in automotive engineering thermoplastic molding compounds, like GMT (glass mat reinforced thermoplastic) and LFT (long fiber reinforced thermoplastic), are used for the manufacturing of components [3-6]. Typical applications for fibrous molding compounds are underbodies, instrument panels, structural door carpeting, front end carrier, and cover sheets. These components show complex and large surface geometries and a high functional integration [7-10].

The use of continuous fiber woven fabrics increased in the last years. Typical applications of these fabrics are bumper beams [11]. More and more lightweight structures, especially those made of metal/thermoplastic fiber reinforced polymer composites (metal/TP-FRPC), are available. This allows innovative product designs and developments in many different industrial areas. Hybrid lightweight structures formed with metal/TP-FRPC enable a new generation of products with applications in the automotive and aircraft industry. The development of joining techniques which are able to combine TP-FRPC with lightweight metals to form hybrid structures reduce the specific disadvantages of the individual material groups and combine their advantages. For a better understanding the process chain of TP-FRPC is discussed in the following sections.

1.2 Process chain TP-FRPC

Manufacturing of TP-FRPC begins with textiles (e.g. woven or non-crimp fabrics) and polymers (film, powder, or fibers), which have to be impregnated and consolidated in a static, intermittent, or continuous process (Figure 1.1) [8].

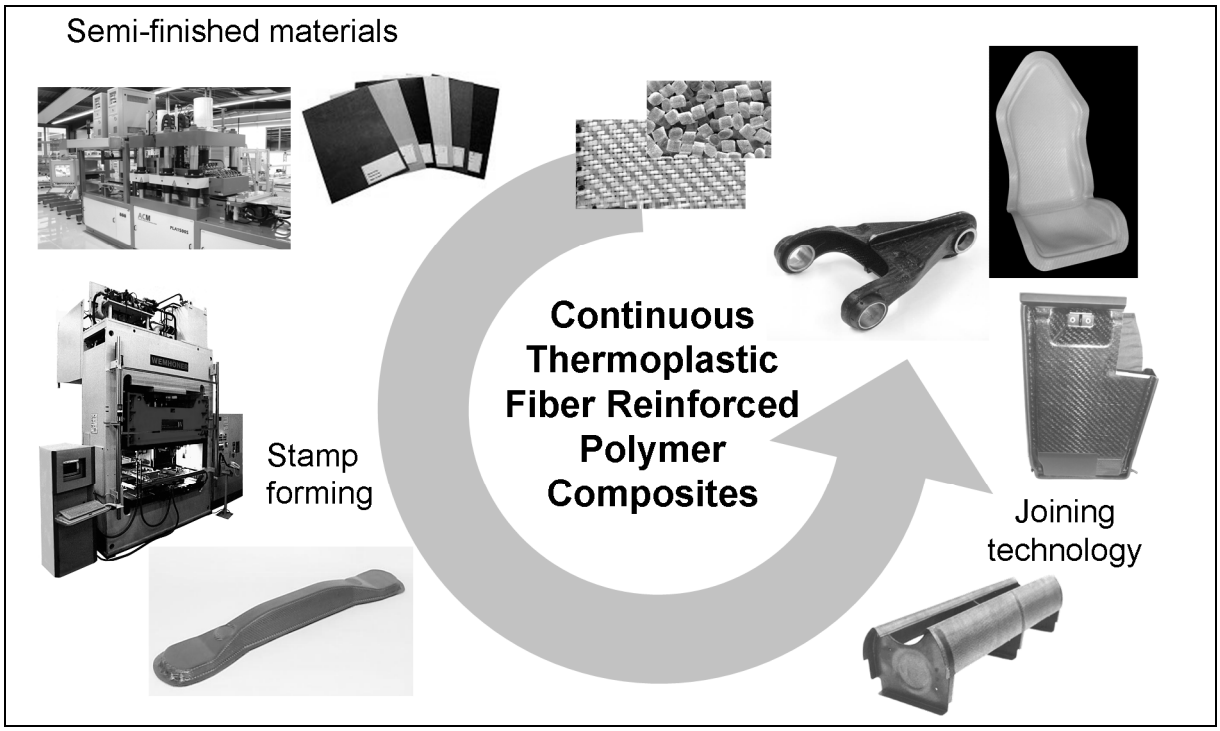

Figure 1.1: Process chain of TP-FRPC

In a second step the semi-finished sheets are reheated and thermoformed to a shaped part. Finally, these thin-walled shaped parts are joined with other TP-FRPC parts or even with metallic structures.

1.2.1 Manufacturing of semi-finished sheets

The manufacturing of semi-finished sheets can be divided into three phases: impregnation and wetting, consolidation, and solidification phases [12]. During the impregnation phase the matrix is changed into a liquid state by increasing the temperature. In the second phase the consolidation takes place under pressure. Due to the applied pressure the air is pressed out of the spaces between the rovings and thus a void-free structure with good fiber-matrix bonding is obtained. Subsequently, in the last phase the material is cooled down by heat extraction resulting in a solidified sheet or component.

Three types of press processes are available and one can distinguish as follows:

- Static pressing (e.g., hot pressing)
- Semi-continuous pressing (e.g., continuous compression molding)
- Continuous pressing (e.g., double belt pressing)

For example, Figure 1.2 shows the continuous compression molding press available at the Demonstration and Application Center of the Institut für Verbundwerkstoffe GmbH (IVW).

Figure 1.2: Continuous compression molding press at the IVW

It is feasible to use the continuous compression molding press for small and medium-sized production series. This new technology has separately adjustable heating and cooling zones through which the material is transported and consolidated during the periodical opening and closing of the press. An advantage of this is that some of the manufacturing parameters (e.g., pressing time, pressing force, and feed rate) are more variable compared to a double belt press. These parameters have a significant influence on the impregnation quality [13]. Additionally, it is possible to choose any laminate structure and the possibility of manufacturing fiber reinforced profiles is also given. Moreover the investment volume needed is significantly lower than that for a double belt press.

The continuous compression molding press at the IVW contains various heating sections (heating temperatures up to 410 °C), two pressing sections (up to 25 bar), and different hydraulic circulations. These circulations enable sheet manufacturing as well as the manufacturing of profiles in several shapes. So far double V-profiles are manufactured at the IVW (Figure 1.3), but closed profiles can also be developed. These continuous fiber reinforced profiles are used in aerospace applications such as stringers or stiffening structures [14].

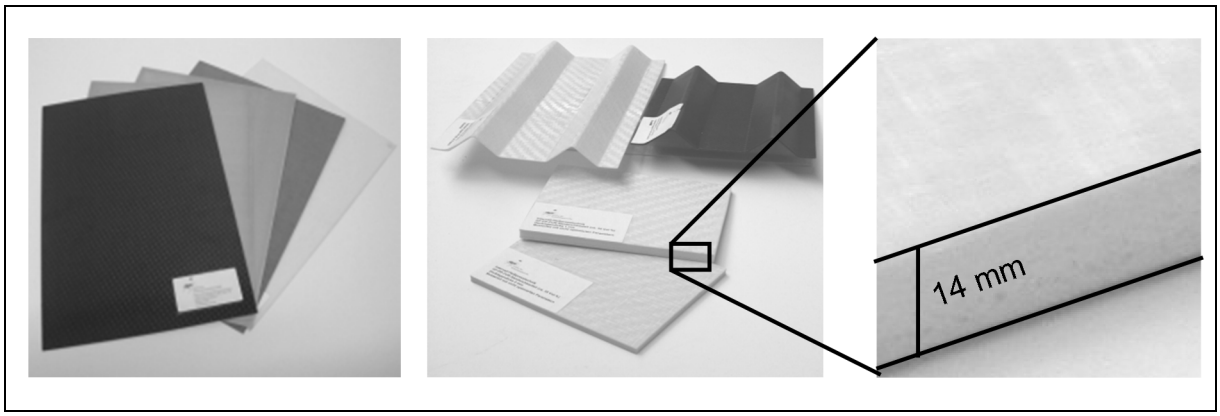

Figure 1.3: Organic sheets and profiles made by continuous compression molding pressing [15]

The continuous compression molding technique also enables the manufacturing of continuous sandwich structures up to a thickness of 40 mm (Figure 1.3). In one step non-consolidated starting materials are impregnated to become cover layers and are directly bonded to the core material.

1.2.2 Thermoforming

By means of thermoforming continuous fiber reinforced thermoplastic composite sheets can be shaped into complex structures. In order to do this the material is heated in an infrared heating field (Figure 1.4). After reaching the desired thermoforming temperature the sheet is transported into the press. The press is then closed applying a pressing force during a fixed time. A three-dimensional component is formed in the press, which usually needs to be trimmed [16].

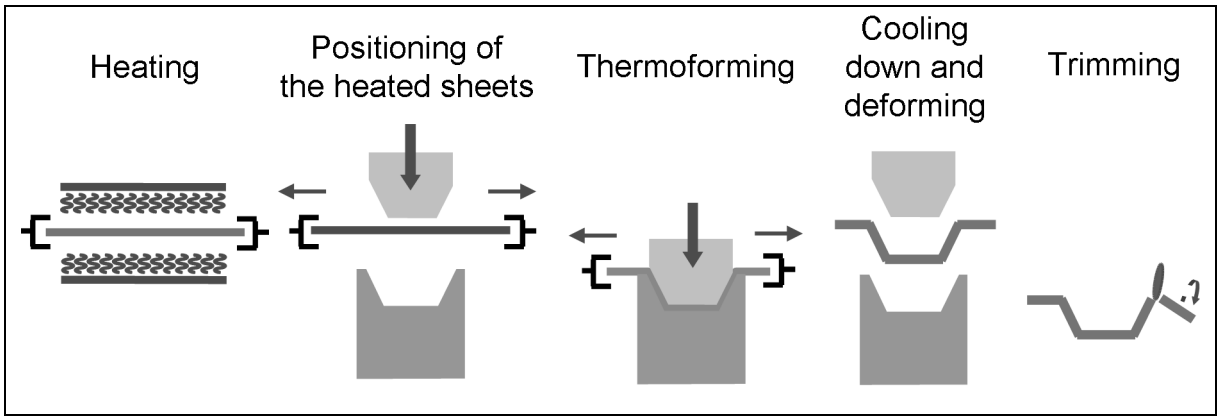

Figure 1.4: The thermoforming process

Thermoforming is suitable for large-scale production of shell-shaped components, which are mainly joined to other components in a second step.

It is not necessary to heat up the entire sheet. This means that partial and local heating e.g. by induction heating can be applied to thermoform organic sheets. This technique reduces the heating time and therefore increases the production rate [17].

1.2.3 Joining technologies for TP-FRPC

The manufacturing of complex structures out of sheets of thermoformed parts requires the application of joining technologies. In general the joining technologies can be divided into three groups (Figure 1.5). First of all undetachable joints are discussed. The joints can only be opened after applying external force to destroy the joint as the joining partners (JP) are interlocked by form fittings (mechanical fastening), chemically bonded by an adhesive, or physically bonded by polymers (welding). Secondly, partially detachable joints can be opened for recycle or repair applications. In case of induction or resistance welding the joining partner can again be used as a heating element to disassemble the welded joints. Another example of a partially detachable joint is a riveted joint. Thirdly, bolted joints can be opened with an external force without destroying the joint and are therefore assigned into force fitting detachable joints [18].

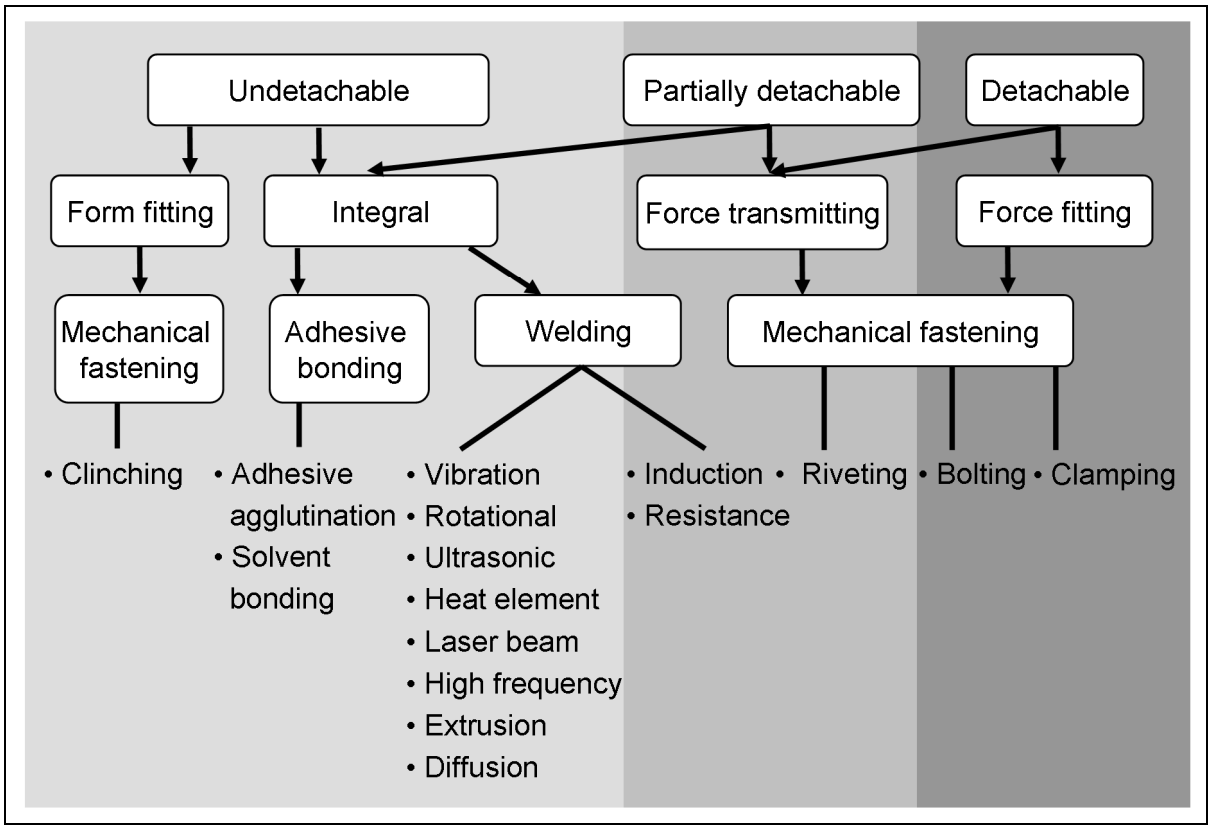

Figure 1.5: Overview of joining techniques [18]

Compared to riveting and adhesive bonding the welding process has the following advantages:

- Reducing the amount of parts needed for bonding compared to fasteners
- Reduction of surface treatment time
- Short process cycle time, usually in the range of minutes
- Possibility of field repair
- Elimination of stress concentrations

However, the frequently uneven laminate heating, which can lead also to delaminations and distortions of the fibers in the joining zone, is a disadvantage.

First of all a closer look is taken at the mechanisms during welding. Subsequently, the possibilities of FRPC-welding are illustrated by two examples in the aerospace and automotive industries.

1.3 Welding

A joining technique for TP-FRPC is the welding process. For this welding process five steps are distinguished [19]:

1) Surface treatment: The surface has to be free of contamination and can be activated.
2) Heating: There are several methods to heat up the polymer matrix, some will be examined later more closely.
3) Pressure: The welding pressure is needed to generate a good contact for the polymer diffusion and also to prevent material delamination.
4) Diffusion: If two homogenous polymers are located in direct contact and are joined at temperatures above the glass transition temperature (T_g), the contact area will progressively disappear and an adhesion between both joining areas is formed.
5) Cooling down: After cooling down, the polymer is solidified, being the last step of the joining process.

Every welding technique needs to go through these steps, but there are of course large differences in the way the surfaces are treated before joining, and how the joining partners are heated. Resistance and induction welding for aerospace and automotive applications will now be examined in more detail.

1.3.1 Leading edge section (J-Nose) in aerospace applications

In the aerospace industries more and more thermoplastic composites are used to replace metal or even thermoset composite components. Stork Fokker AESP b.v. developed many fiber reinforced components for the Fokker and Airbus aircraft. One of these components is a J-Nose, which is a wing leading edge section. The reasons to substitute the regular aluminum component were the reduction of weight and manufacturing costs [20]. At first, the development was made for the Airbus A340-500/600, but after the successful replacement of the aluminum, the Airbus A380 was also equipped with the fiber reinforced J-Nose. The manufacturing process starts with one-layer glass fiber fabrics (GF) being only partially impregnated with polyphenylenesulfide (PPS). These single layers are positioned in a mold and

consolidated in an autoclave to a shaped structure. The autoclave is needed due to the large dimension and various thicknesses of the lay-ups. Finally, stiffening ribs profiles, or stringers are inserted and joined by resistance welding. PPS impregnated steel meshes are connected to a current source. Heat is generated in the mesh along the bond line due to electrical resistance. An Airbus A340 has a TP-FRPC J-Nose of about 7 meter length; an Airbus A380 now has a J-Nose of 64 meter, divided into 16 sections of 4 meters each.

Figure 1.6: J-Nose mounted on a wing for an Airbus A380 (© Airbus United Kingdom)

Smaller components, like for example the tail leading edge, are also made out of TP-FRPCs. These thermoformed components are bonded by adhesive bonding or by mechanical bonding, like riveting. Carbon fiber reinforced PPS (CF/PPS) components are also joined by induction welding as demonstrated for a leading edge section of an Airbus A330-200 [21]. Thermoformed profiles are also welded to stringers for stiffening purposes [22].

1.3.2 Rear seat-back support in automotive applications

The IVW developed in co-operation with AC.S GmbH and Jacob Composite GmbH an induction welding technique to enable assembling of a profile to a rear seat back support [23]. The lightweight rear seat back support consists of two face covers and a PES foam core, as shown in Figure 1.7.

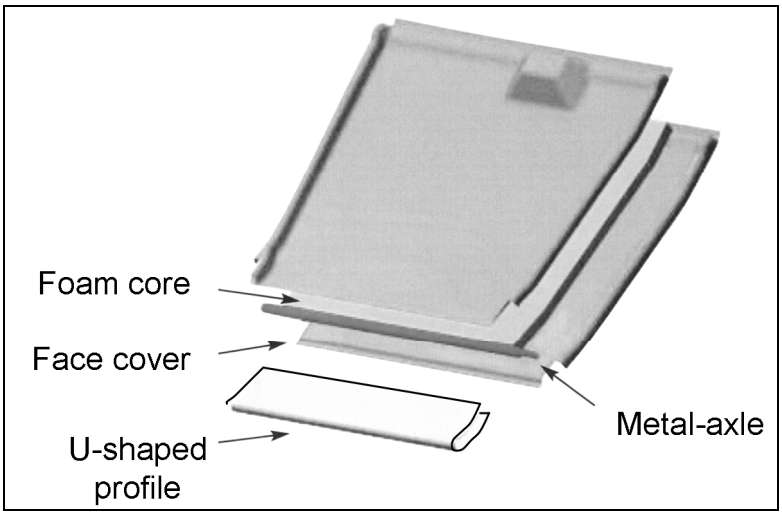

Figure 1.7: Set-up of the lightweight rear seat back support (© AC.S GmbH)

Figure 1.7 illustrates the U-shaped profile, which will be joined. In Figure 1.8 a finished lightweight rear seat back support is shown. In the detailed illustration, the welding zone can be recognized.

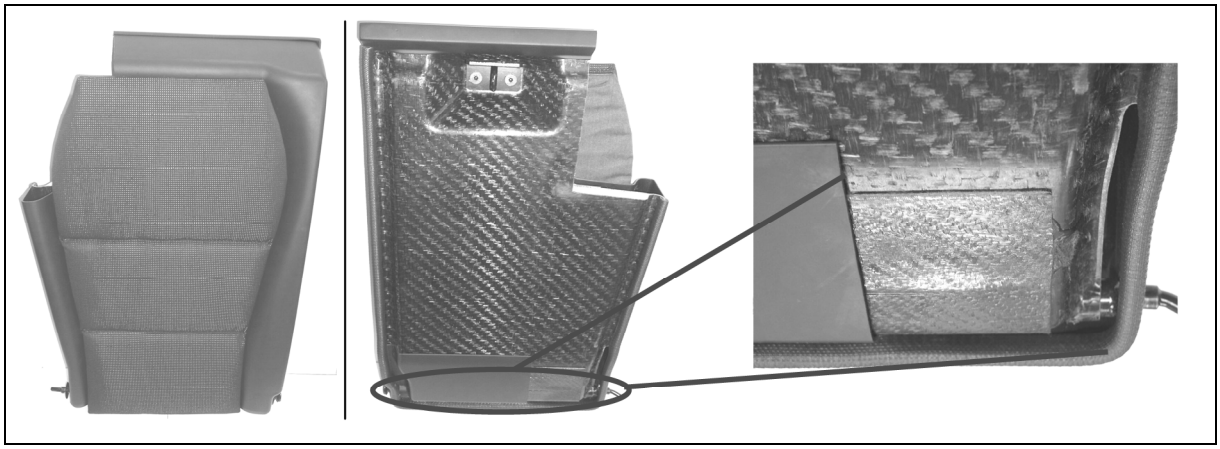

Figure 1.8: A finished lightweight rear seat back support

The newly developed lightweight rear seat back support is about 50 % lighter than a regular one, resulting in a weight reduction from 11 kg to 5.5 kg. In crash tests the lightweight rear seat-back support proved to be as safe as the two times heavier standard steel version [24]. Moreover, the sound insulation is better than in the standard steel version.

The welding process was optimized for large-scale production and represents the first application of induction welding of fiber reinforced thermoplastic composites in the automotive sector [23].

1.4 Metal-polymer joints

Recent developments show an increase in the use of bonding dissimilar materials to optimize the specific applications. In transportation applications joints between metal and fiber reinforced composites are being investigated. In the BMW M3 CSL a thermoset composite roof was adhesively bonded to the steel frame structure. The roof was only 6 kg lighter than the standard roof, but improved the driving quality as the center of gravity was lowered [25, 26]. Due to the success in the M3 CSL, BMW also used this concept for the BMW M6 in 2005 (Figure 1.9).

Figure 1.9: CFRPC-roof of a BMW M6 (© Autobild)

Thermoset carbon fiber reinforced composites structures are also used for roof structures in an Audi A2 test vehicle [27]. Here, the composite was clinched to aluminum carrier structures. The implementation of composites in the metallic roof and in floor structures led to a weight reduction of 26 % and an increase of stiffness by 6 %.

1.5 Objectives

The above given examples show that there is an increasing interest in joining metallic structures to composites. This material combination has a high mechanical potential and offers design engineers new design possibilities. The goal of this thesis is to investigate the metal to composite bonding by means of induction welding. The induction welding is chosen as it has many advantages including a very high-energy input, cost-effective equipment and tooling, a high degree of automation, and high flexibility.

The goals of the performed investigations are:

- Evaluation of the achievement potential of a hybrid joint out of metal and composite.
- Designing, constructing, and building equipment for the discontinuous induction welding.
- Determination of the influence of surface treatments on the welding quality.
- Sensitivity analysis of significant process parameters by employing discontinuous induction welding with several process conditions and experimental set-ups with various environmental conditions.
- Enlarge the process window for welding of thermoplastic composites.
- Verification of the experimental results by thermal models to predict heating times.

This thesis is divided into various sections. After the state of the art, the experimental part is given. This is followed by the topographical and elemental analysis of the joining partner. Finally, the results of the performed experiments and developed thermal model are given and discussed.

2 State of the art

This chapter starts with a description of the state of the art of the welding of polymers and FRPC and is followed by a discussion of the joining of metal and polymer. For a better understanding of the bonding mechanisms a close look at the surface properties of both metal and polymer is taken. An intensive literature search gives valuable information about applied surface treatments and their influence on the bonding quality. Several parameters that influence the bonding strength are discussed and used as basic principles for the investigations in this thesis. The last part of the chapter is dedicated to a description of the material and equipment parameters used for induction welding, and discussion of existing models to predict the heating time for an optimal process window during fusion bonding of FRPCs.

2.1 Welding of polymers / FRPC

Welding of TP-FRPC belongs to the fusion bonding technology [28, 29, 30]. The fusion of the joining partners occurs basically by contacting the surfaces, subsequently elimination of the boundary layer by macromolecule diffusion and finally consolidation. During fusion and pressing polymer flows are usually induced, through which the macromolecules penetrate into the joining partners and become solid during cooling. In extensive investigations it has been shown that these melt flows have a large influence on the bonding strength. Potente showed in 1977 that for non-reinforced thermoplastics a certain intermediate melt flow velocity has to be exceeded in order to obtain high bonding strengths [31]. Schlarb showed that for vibration welding a critical elongation velocity in the joining zone should not be exceeded in order to prevent the super molecular structures from orientating in a lower quality bonding [32, 33]. In [34, 35] the characteristic composition of the joining area is investigated and described (Figure 2.1). Depending on the process conditions various zones of different polymer structures are observed.

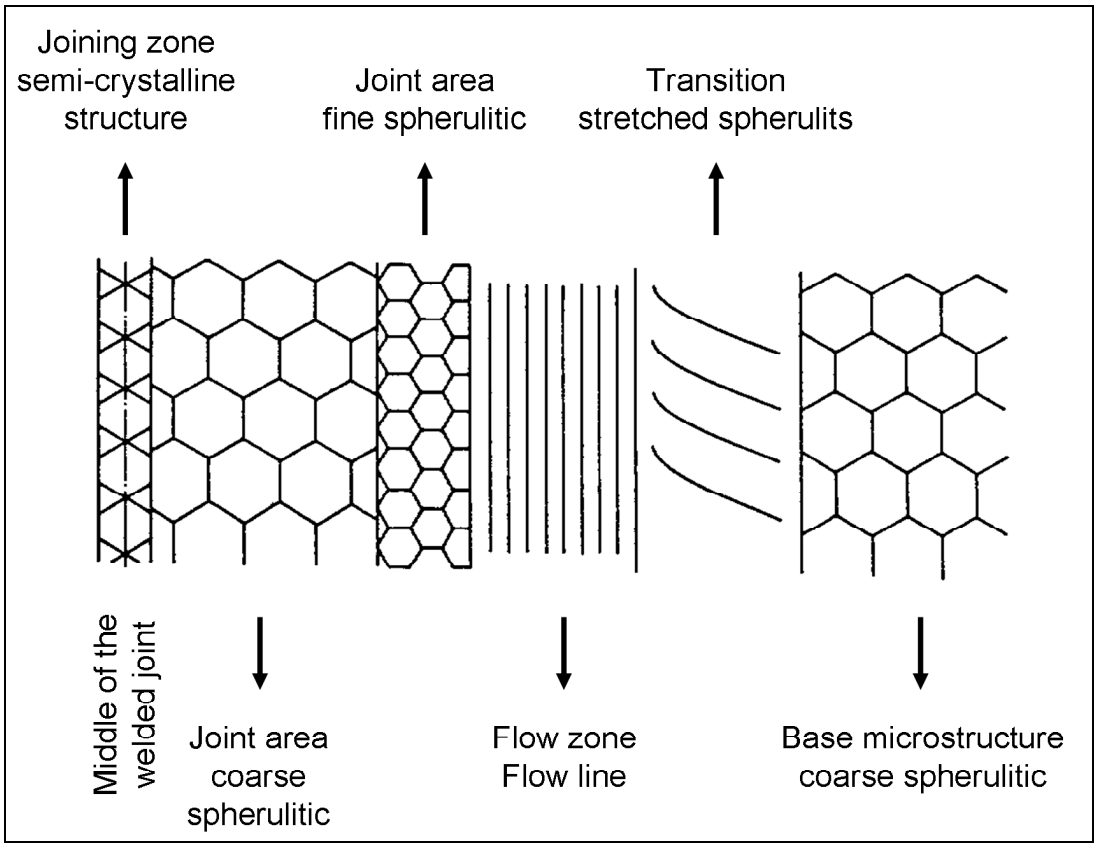

Figure 2.1: Characteristic composition of the joining area for semi-crystalline polymers after vibration welding [32]

Important for the joining behavior is the morphology in the transition solid / melted zone as well as the structure in the joining zone itself. Therefore, several authors decided to consider the melting zone thickness as a criterion for controlling the bonding quality [36, 37, 38]. Ehrenstein's investigations [39] on vibration welding establish that the various zones in the joining area are dominantly influenced by the swinging behavior of the tool and the fixed joining partner after the set welding time or depth is reached.

Bonten et. al. described diffusion bonding for welding of the semi-crystalline polymers and a new hypothesis for bonding of cross-linked thermoplastics [40]. The movement of PE-X (cross-linked polyethylene) entanglements and the resulting force fitting after cooling is described. A relation between the presence of lamellar links (such as tie-molecules, mutual entanglements, and micro-fibrils) in the joint after recrystallization and with its force transmission is established as well. The weld is estimated to be a few nanometers wide.

Comparative investigations for welding of glass fiber reinforced PES were performed by Potente et al. [41]. Hot plate, vibration, and laser welding were used as joining technologies, and the results showed a change in the fiber direction in the joining area of the samples that were manufactured by using the hot plate and vibration welding. After welding a large amount of fibers lay parallel to the joining area, so the highest welding factor possible was around 0.6. Laser welded samples show in the joining area a high fiber volume fraction in their original orientation resulting in measured short-time welding factors of around 0.8. In this paper the welding factor is defined as the quotient of the strength of welded material and the base material strength. As in the case of fiber reinforced composites the base composite material strength is highly influenced by the fiber reinforcement and the bonding strength is mainly influenced by the original polymer strength, low welding factors are obtained for the polymer composites.

Short fiber reinforced polypropylene and short fiber reinforced nylon in respect to their influence of the process conditions on the welding are investigated by Potente et al. [42]. Here, it is shown that the fiber volume fraction itself has a large influence on the bonding strength. An increase in the fiber amount results in a decrease in the welding factor. This behavior is also verified by the investigations on long fiber-reinforced polypropylene (PP-GM 25, PP-GM 30, and PP-GM 40) in [43] und [44]. Here welding factors of 0.23 up to 0.4 were achieved. Also Messler [45] obtains in the case of uni-directional fiber reinforced composites a similar outcome.

Rudolf showed that with vibration welding a very good shear tensile strength could be achieved [46]. In the case of GF/PA6, shear tensile strength of 31 MPa is achieved. This value equals or is even slightly higher than the interlaminar shear strength of the non-reinforced PA6. This high value is explained by interlocking of the fibers. A comparison of vibration and induction with adhesive bonding and riveting to bond CF/PPS shows that welding techniques result in a higher shear tensile strength (25 - 30 MPa) than the adhesive bonding or riveting (up to 10 MPa). Ehrenstein shows the same tendency [30]. As can be seen, polymer welding results in higher shear tensile strength than mechanical fastening. Not reactive materials (like GF/PP) which are difficult to bond adhesively can be joined with good shear tensile strength up to 15 MPa as polymer chains are entangled due to polymer diffusion [46].

2.2 Welding of FRPC/metal

2.2.1 Theory of adhesion

An important condition for adhesion of metal and polymer is the full wetting of the metal surface by the polymer. The surface free energy of solids represents a quantity that cannot be directly quantified. The contact angle measurement is a method used to determine the wetting behavior and therefore, the surface free energy of solids [47]. The contact angle of a liquid droplet on a solid surface is defined by the mechanical equilibrium of the droplet under the action of three interfacial tensions:

- Solid-vapor energy(γ_{sv})
- Solid-liquid energy (γ_{sl})
- Liquid-vapor energy (γ_{lv})

This equilibrium equation is known as Young's equation:

$$\gamma_{lv} \cdot \cos(\alpha) = \gamma_{sv} - \gamma_{sl} \tag{2.1}$$

where α is the contact angle.

This contact angle is the angle between the tangent of the fluid surface and the solid surface. Figure 2.2 illustrates the contact angle α in relation with the surface and interfacial tension during wetting. The specific wetting behavior of the surface is influenced by these three parameters.

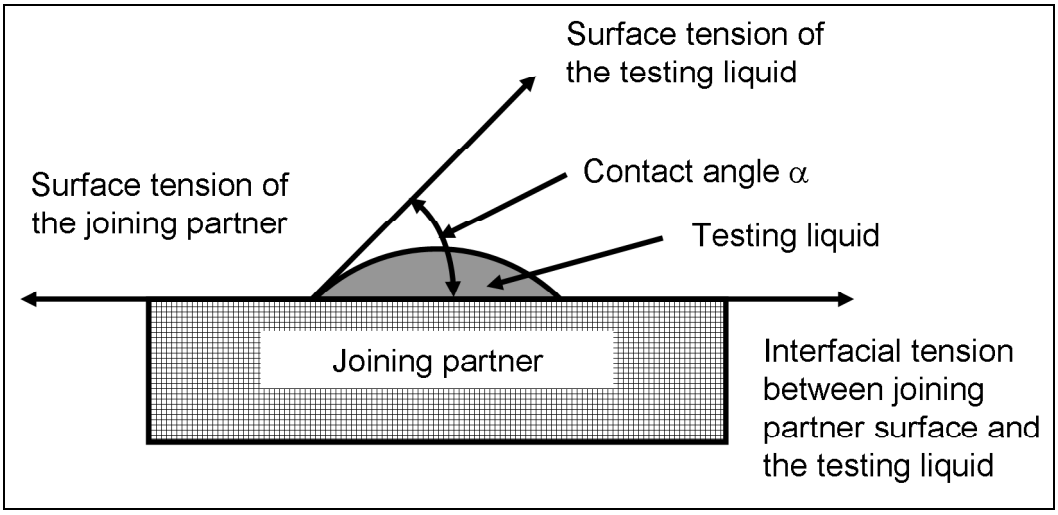

Figure 2.2: Contact angle, surface, and interfacial area tension during wetting

To determine the dynamic contact angle a droplet of the testing liquid is deposed on the joining partner surface. Demineralized water, glycerol, and di-iodomethane are used as liquids because their surface tension properties are known (Table 2.1).

Table 2.1: Surface free energies of liquids used for contact angle measurements (disperse, polar, and total) [48]

Liquid	**Surface free energy (mN/m)**		
	γ^D_{lv}	γ^P_{lv}	γ_{lv}
Water	22.0	50.2	72.2
Glycerol	34.0	30.0	64.0
Di-iodomethane	48.5	2.3	50.8

This method enables the separation of the disperse and polar contributions of the measured surface energy on different pre-treated surfaces. The disperse contribution is based on dispersion forces (London forces) which stands for a temporary attractive force that results when the electrons in two adjacent atoms occupy positions and make the atoms form temporary dipoles. The polar contribution is based on permanent dipole-dipole interactions and appears in contrary to the disperse forces not in every material [48].

In Table 2.2 the disperse (γ^D_s) and polar (γ^P_s) surface free energy values of selected solid polymers at room temperature are presented.

Table 2.2: Surface free energies of various solid polymers (disperse, polar, and total)

Polymer	**Surface free energy (mN/m)**		
	γ^D_s	γ^P_s	γ_s
Nylon 66 [48]	33.6	7.8	41.4
Polypropylene [49]	30.5	0.7	31.2
Polytetrafluorethylene [48]	18.6	0.5	19.1
CF/PEEK [50]	40	4.0	44

Table 2.2 shows that the surface free energy value does not indicate a good possibility for bonding. Polytetrafluorethylene (PTFE) is used as heat resistant release agent on cookware to prevent sticking of the food on the pans. This already indicates that the polar part of the surface free energy of the polymer plays an

important role in polymer bonding. In [50] the surface energy of PEEK treated by various corona conditions was measured. It was illustrated that only the polar surface free energy was increased by the treatment, the disperse surface energy (γ^D_s) remained unchanged. This increased polar surface free energy (γ^P_s) corresponded to higher bonding strengths of the CF/PEEK composites.

The reason for the relatively high polar surface energy can easily be seen in the structural formulas of PA66 and PEEK (Figure 2.3).

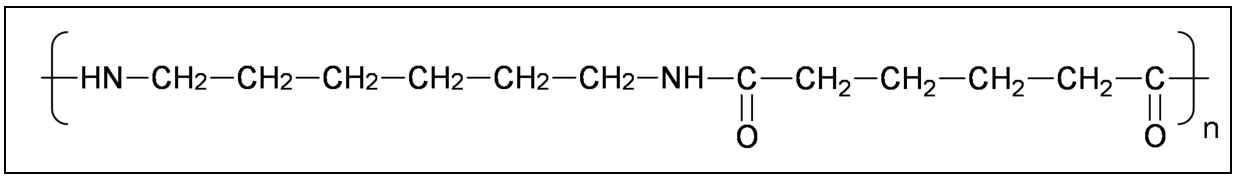

a

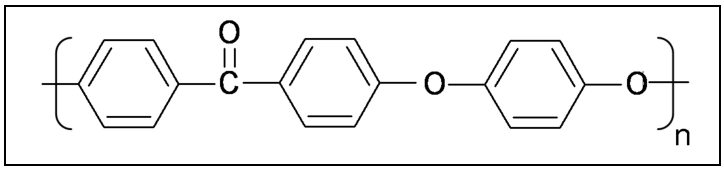

b

Figure 2.3: Structural formulas of a) PA66 and b) PEEK

Due to the different electrical affinities of the atoms, charge difference on the atoms appears as some atoms attract electrons more than other atoms. This results in local charge differences and also in polarity of the polymer chains [51]. The oxygen atom bonded to the carbon atom attracts electrons and is therefore a little bit negatively charged. The same also counts for the nitrogen atoms. In the benzyl-groups also secondary electrons are available for intermolecular bondings.

For mechanically treated samples the barrier effect of the roughness profile can lead to an increase of the contact angle. Capillary effects can lead to a reduction of the contact angle. For the corundum blasted samples these two effects influence the determined values and therefore the surface free energy value should be critically validated.

2.2.2 Influence of the surface treatment

When manufacturing metal/polymer structures, the surfaces of the partners to be joined are brought together, in order to create a permanent joint. Complex physical and chemical mechanisms take place on the interfacing surfaces. In addition to mechanical adhesion, due to penetration of polymer into pores on the surface of the metal joining partner, the adhesion models describe also specific adhesion. This kind of adhesion is divided into physical, chemical, and thermodynamical mechanisms.

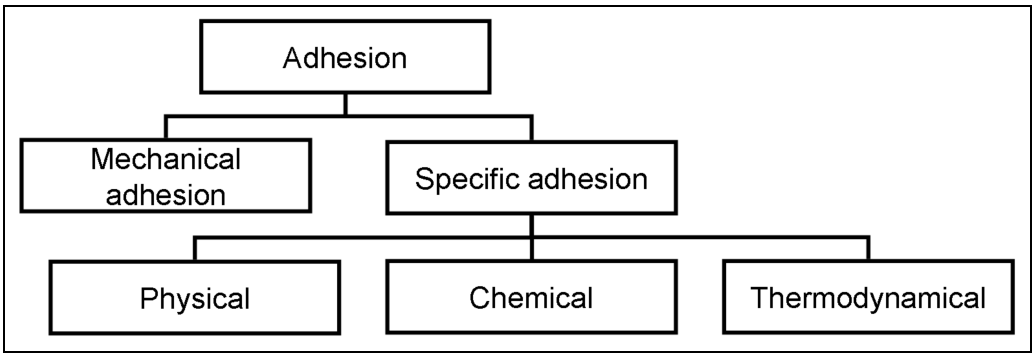

Figure 2.4: Different adhesion models [52]

With the physical mechanisms the entire range of physical bonding forces, like dipole-forces, dispersion forces, and hydrogen bridges take place. Chemical bonds are due to functional polymer groups, which are able to build strong bonds with the metal partner. Specific surface and interface energies play an important role in the wetting and compatibility of the joints. This is also called thermodynamical adhesion.

The joining partners are usually treated before joining to improve the surface area properties. Some treatments and their effects are shown in Table 2.3.

Table 2.3: Surface treatment methods and their properties [52]

Method	Treatment	Effect
Cleaning, degreasing	• Washing with a solvent, like acetone	• Cleaning of the joining partners
Mechanical treatment	• Grinding • Sandblasting • Polishing	• Geometrical changes of the surface → roughness • Removal of contamination layers
Chemical treatment	• Etching in NaOH • Pickling in acid	• Change in the chemical structure of the surface (e.g. oxidation)
Physical treatment	• Plasma cleaning	• Removal of organic compounds • Surface activation

For aluminum many investigations on adhesive bonding can be found. In [53] it is shown that pickling influences the essential bonding mechanisms. This is ascribed to the hydrophobic layer between the aluminum surface and the polymer.

Brockmann reports in [54, 55] fundamental investigations on adhesive joints with aluminum as bonding partner. Here, it is proved that besides the mechanical adhesion specific adhesion also occurs (Figure 2.4). These results are also confirmed in [56, 57]. The development of a metal-oxide-polymer boundary layer with a composite character is described. Comparative short and long-time experiments were performed and illustrate that conclusions about the bonding mechanism from short-time investigations have limited validity.

Extensive investigations in [58] showed that the blasting material for the mechanical abrasive treatments has an influence on the shear tensile strength of adhesively bonded metal joints. Joints made out of AlMg1 show, compared to AlMg3, slightly higher shear tensile strength in accordance with DIN EN 1465. The mechanical surface treatments show only for AlMg3 a positive influence. Blasting of AlMg3 with corundum led to high shear tensile strength up to 20 MPa and also showed least reduction of the bonding strength after long-time conditioning of the samples.

The abrasion of material on the surface leads to:

- A clean and activated surface
- An increase of the surface roughness

To enable a better understanding, the plasma treatment is discussed in more detail. The influence of the other treatments on the surface properties is discussed in chapter 4. The plasma treatment consists in the excitation of atoms due to a high voltage electrical charge, and the subsequent escape of the electrons from their orbits on the surface. Therefore, free electrons and ions are generated which can be beamed. When beaming onto a polymer surface polymer fragments are induced.

The plasma treatment can have the following effects on the polymer surface [59, 60]:

- Cleaning of the surface
- Activation or generation of functional groups
- Deposition of a polymer layer

For the deposition of a polymer layer the atmospheric plasma technique is combined with feeding in a precursor to the beam to deposit a polymer layer on the joining partner after treatment.

Comyn shows, that the plasma treatment leads to higher concentration of oxygen atoms on the surface. After the plasma treatment –COOH and –OH-groups are identified [61]. These active-end groups influence the bonding quality, so the mechanical investigations of the joint strength were performed. Sand paper treated steel joining partners (steel type is not given, sample width: 25 mm, overlap length: 12 mm) were bonded by an adhesive layer out of a PEEK-film (Stabar K200, ICI, film thickness: 0.25 mm) with epoxy resin on both sides (AF-163-2K, 3M). The shear tensile strength values of samples obtained without a plasma treatment were about 17 MPa, whereas the values for plasma treated PEEK-film samples were as high as 30 MPa.

Lommatzsch reported that the plasma activation clearly improves the adhesive bonding quality of polymers (Figure 2.5) [62]. The polymers were bonded with a 2-k polyurethane adhesive and the aluminum with a 2k-epoxide adhesive. Testing was performed in accordance with DIN EN 1465.

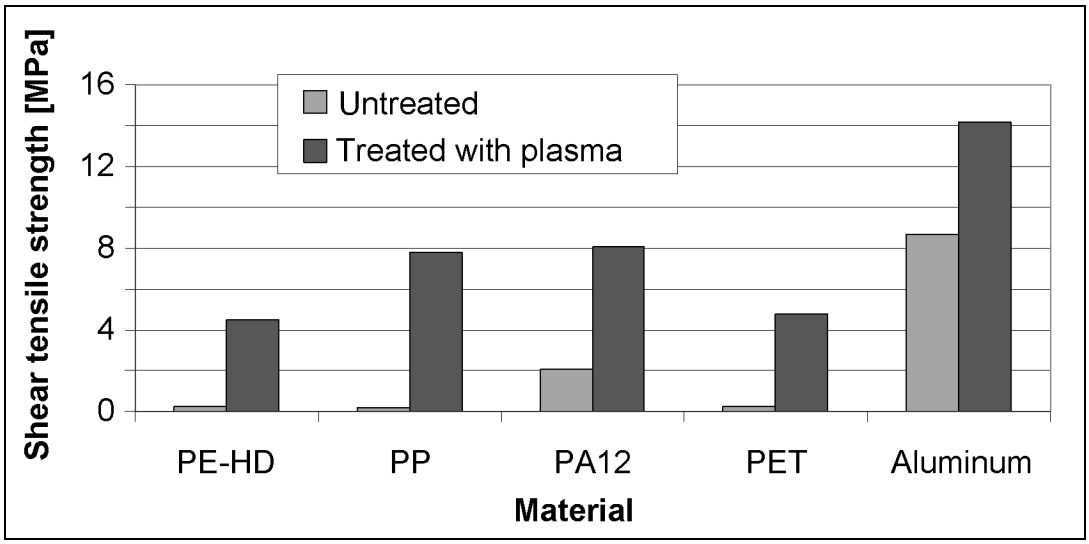

Figure 2.5: Shear tensile strength of various polymers and aluminum with and without plasma treatment [62]

The plasma treatment clearly increases the shear tensile strength of the adhesively bonded samples.

2.2.3 Overview of metal-polymer composites and the influence of thermal properties on the bonding quality

As a basis for the validation of the achieved results an extensive literature review was performed. However, few contributions are available in the field of material joints (hybrid joints) made of metal and polymers and even less in the field of fiber reinforced composites. The relevant literature is given in Table 2.4.

Table 2.4: State of the art of metal-polymer joints

Manufacturing process	Joining partner 1	Joining partner 2	Pre-treatment	Testing method	Joining strength [MPa]	Refer-ence
Hot pressing	Al (6061-T6)	PP	Metal: Anodising in phosphoric acid PP: Plasma	ASTM 3163	19	[63]
Resistance welding	Al (7075-T6)	CF/ PEEK	Metal: Cleaning with trichloroethane, anodising in H_3PO_4, Coating with PEI	ASTM 3163	Up to 20	[64]
Heat bonding with PEKEKK	Ti-6Al-4V	PEKEKK	Grit blasting with 60 grit Al_2O_3 and anodising in NaOH	Bar with ∅ 19 mm	95 - 130	[65]
Heat bonding	Ti-6Al-4V	Ti-6Al-4V	PPQ, GF/PEI, PEI and PES	ASTM D-1002	17 - 34	[66]
Heat bonding with polyimide 422	Ti-6Al-4V	Ti-6Al-4V	Polyimide 422	ASTM D-1002	30 - 41	[67]
Heat bonding	Ti-6Al-4V	Ti-6Al-4V	Ti: Nitric-hydrofluoric acid and chromic acid anodised Al: FPL as well as grit blasting, chromic acid, with and without primer	ASTM D-1002	44 - 55	[68]
Induction welding	Al (2024-T3)	CF/ PEEK	Metal: pickling in chromic acid	ASTM D-1002	31 - 33	[69]
Heat bonding with PEEK	DC01	DC01	Metal: Acetone treatment, grit blasting, polishing	DIN EN 1465	20 - 45	[70]
Adhesive bonding with 1K, 2K epoxide; 2K polyurethane	AlMg4,5 Mn0,4	AlMg4,5 Mn0,4	Metal: acetone – corundum blasting – acetone	DIN EN 1465	15 - 18	[71]
Adhesive bonding with epoxy resin	AlMg3	AlMg3	Sulphuric acid pickling, phosphoric acid pickling, NaOH-pickling, grit blasting, polishing	DIN EN 1465	4 - 19	[72]

For hot plate joining of a PEEK-based material with 3 mm thick steel plates process cycle times of about 34 minutes are obtained in [70]. The samples were taken out of the mold at 300 °C and cooled down under room conditions. Figure 2.6 shows the temperature profile during joining.

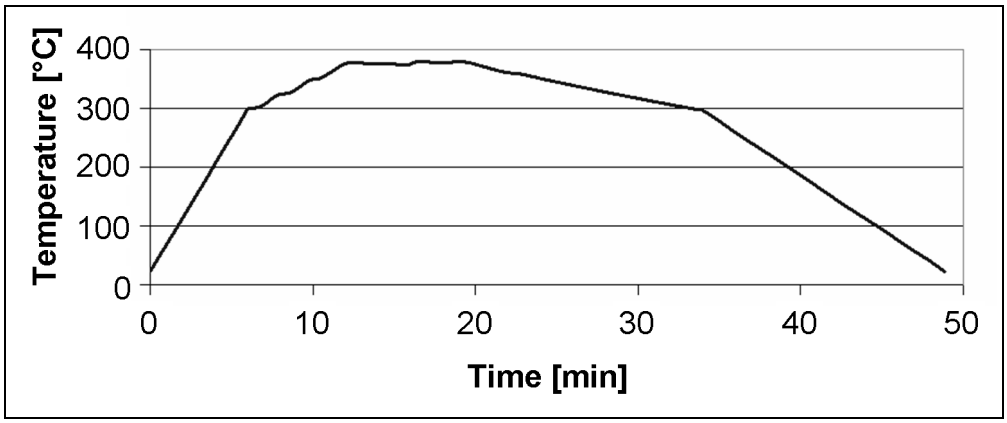

Figure 2.6: Temperature profile during joining of PEEK-based material to steel

A high fraction of the total process time goes by during the cooling phase under pressure (consolidation). This time compared to the consolidation time of standard thermoplastics is a long pressing time. The importance of the cooling rate for the bonding quality is presented in several publications. Ramani performed investigations on bars made out of titanium and polyetherketoneetherketoneketone (PEKEKK) as hot melt [73]. The investigated parameters were:

- Holding time above the melting temperature (5, 10, 15, and 20 minutes) and
- Various cooling rates (20 °C/min and 100 °C/min).

The achieved tensile strengths clearly show that longer holding times (up to 15 min.) increase the bonding quality (Figure 2.7). The samples manufactured with a low cooling rate show the highest shear tensile strength. Apparently, an optimum is shown, when using both long holding times and low cooling rates. In [73] this result is explained by changes in the morphology of PEKEKK (crystallinity).

For PEEK the holding time above melting point is also influencing the polymer structure. Investigations of Day [74] show that the degradation of PEEK in air starts after 10 minutes at a temperature of 380 °C.

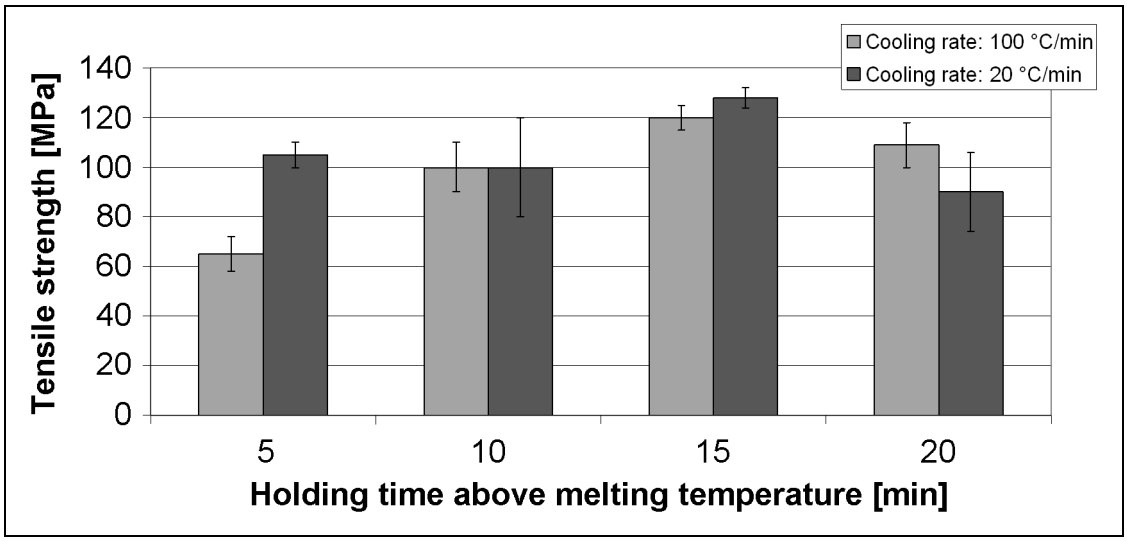

Figure 2.7: Tensile strength in dependence of the holding time above the melting temperature at various cooling rates [73]

Kadi investigated the influence of molding conditions on the CF/PEEK-sample morphology [75]. As was to be expected the level of crystallinity of the PEEK matrix in the laminate depends on the molding temperature and the cooling rate. A decrease of the molding temperature from 400 °C to 365 °C resulted in a variation of the crystalline structure without a change in the level of crystallinity. The polymer in samples manufactured at a molding temperature of 365 °C is non-spherulitic, the samples with the molding temperature of 400 °C show spherulits in the size of around 10 µm. Also for short beam shear strength (three point bending in accordance with ASTM D2344) the variation of the cooling rate influenced the mechanical properties. A high short beam strength (approx. 90 MPa) was observed for the slow-cooled specimens (0.8 °C/min), the specimens cooled at 19 °C/min showed 80 MPa, the fast cooled specimens (70 °C/min) had around 72 MPa.

For welding GF/PPS by means of PSU-film containing nickel particles it is observed that the isothermal fusion bonding time (time of constant temperature above the fusion bonding temperature) strongly influences the bonding strength [76]. The shear tensile strength is increased 40 % to 50 % if the isothermal bonding time is increased from 0 second to 100 or 200 seconds. This is explained by a combination of mainly intimate contact and by a lower extent to healing mechanisms.

A similar behavior was illustrated by [19, 77] for steel/PEEK and Al/CF-PEI-composite. These studies clearly show that a high cooling rate will reduce the bonding strength of metal-CF/PEEK joints.

The information obtained from the various publications show that the highest shear tensile strength value is achieved, when:

- The PEEK-samples are heated up to approx. 370 °C for about 7 minutes
- For PEEK a cooling rate of about 6 °C/min

is chosen. For PA66 no information about the influence of holding time and temperature is found. The crystallinity of PA66-composites is to a large extent influenced by the crystallization temperature [78]. Here it is reported that, below 234 °C the phase transition is too fast to measure differences in the crystallinity by DSC or transmitted light microscopy, above 250 °C the crystallization takes place very slow. For the performed experiments the samples were made in accordance with DIN EN 1465 and shear tensile strength values of 4 up to 25 MPa are reported for this norm and sample thickness of 2 mm (Table 2.4).

2.2.4 Comparison of the testing methods

Table 2.5 shows a comparison of the sample geometry of the several standards and the resulting reference surface area for the shear tensile strength determination:

Table 2.5: Sample geometries of several standards

ASTM 3163	ASTM 1002	DIN EN 1465
Sample width: 25.4 mm Overlap length: 25.4 mm Reference surface area for the bonding strength determination: 645.2 mm^2	Sample width: 25.4 mm Overlap length: 12.5 mm Reference surface area for the bonding strength determination: 322.6 mm^2	Sample width: 25.0 mm Overlap length: 12.5 mm Reference surface area for the bonding strength determination: 312.5 mm^2

If the sample geometry or the testing conditions used are slightly changed, the determined shear tensile strength values cannot be quantitatively compared to those of other investigations anymore. Elsner described several sample geometries used for evaluation of adhesively bonded metal-polymer joints [79]. The single-lap joint is considered to be appropriate because the joint can easily be made and, therefore, has a high comparison value. These single-lap joints are described in DIN EN 1465 [80] and in the similar ASTM 1002. The overlap length is 12.5 +/- 0.25 mm and the sample width is 25.0 +/- 0.25 mm.

This geometry is also criticized because the overlap lengths and lap areas in engineering applications are much larger than those used in the DIN EN 1465. Another point is that the shear state in the sample is not uniform. The overlap sample as force is applied is shown in Figure 2.8 [49].

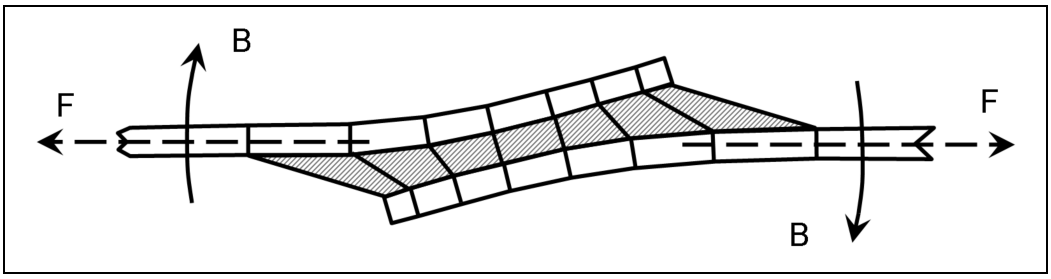

Figure 2.8: Bending (B) and strain of thin single-lap joints under load (F)

The centre of the lap does not move, however the ends of the lap region must move in order to linearize the stress. This is achieved by bending the lap ends of the specimen. Now a combination of shear load and bending (normal) loads takes place. The two different joining partners used give another contribution to the non-uniform shear state in the specimen. The metallic joining partner is only 1 mm thick, whereas the carbon fiber reinforced joining partner has a thickness of 2 mm. The inhomogeneous stress distribution is determined by Schmeer [81] and is shown in Figure 2.9.

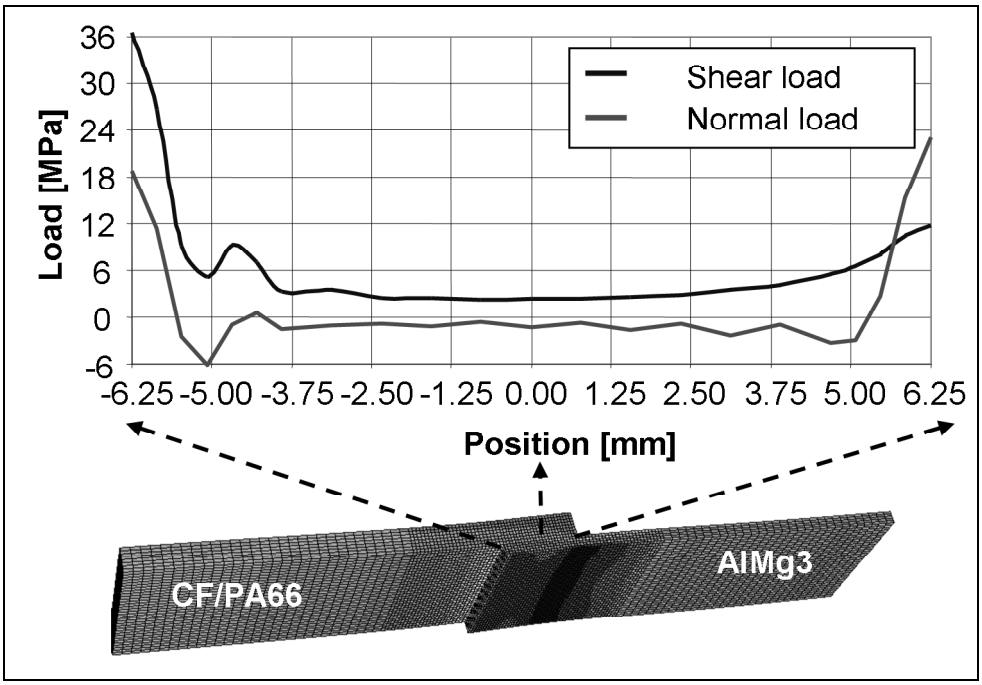

Figure 2.9: Simulated normal and shear loads in the joining zone of an induction welded sample

Here it can be seen that at the composite side (position: -6.25 mm) much higher loads are determined than in the middle (position: 0 mm) of the sample. The used mechanical values of the CFRPC and metal are given in the appendix (page 119, Table 8.1 and 8.2).

A way to prevent the bending is by the use of thick lap shear specimen as in DIN EN 14869-2 [82] or by double-lap shear joints in accordance with ASTM 3586. As is known from several publications [49, 83] an increase of the overlap area leads to a reduction of the lap shear strength. The geometries and the testing conditions used are discussed in more detail in chapter 3.5. Now, a closer look at the state of the art of material degradation mechanisms is presented.

2.2.5 Degradation mechanism of dissimilar materials due to galvanic corrosion

Generally metals react with oxygen and form an oxide layer. This process, called galvanic corrosion, takes place when the metal is electronically connected to carbon fiber reinforced polymer composites and both joining partners have a direct contact to an electrolyte solution (like salt water). The galvanic corrosion of aluminum in contact with carbon fibers is driven by the reduction of oxygen from the electrolyte solution and results in an electrical current [84]. The requirements for galvanic corrosion between dissimilar materials are:

- An actively corroding material
- An electrically conductive composite, e.g., carbon fiber reinforced composite
- An electrical connection between the composite and the corroding metal
- An electrolyte (e.g., salt water)
- Oxygen

Not much can be found about this type of degradation mechanism, although it is largely influencing material properties. The schematic view of the corrosion process in [84] is presented in Figure 2.10.

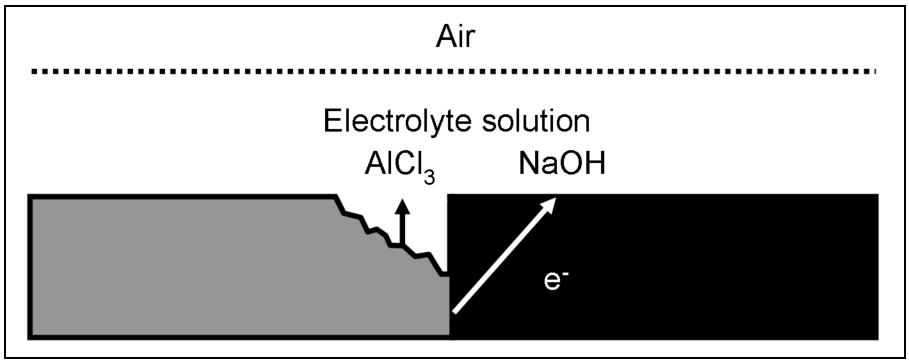

Figure 2.10: Galvanic corrosion of aluminum and carbon fiber reinforced composite

The corresponding chemical reactions given by Boyd et al. [84] are:

At the aluminum surface:

$$Al + 3Cl^- \longrightarrow AlCl_3 + 3e^- \tag{2.2}$$

At the carbon fiber reinforced composite surface:

$$4e^- + O_2 + 4Na^+ + 2H_2O \longrightarrow 4NaOH \tag{2.3}$$

These reactions are only partially correct, as the meant half-reactions with the potential difference are [85]:

$$O_2 + 2H_2O + 4e^- \longrightarrow 4OH^- \qquad E_0 = 0.40 \text{ eV} \tag{2.4}$$

$$Al \longrightarrow Al^{3+} + 3e^- \qquad E_0 = -1.67 \text{ eV} \tag{2.5}$$

For these reactions the electric potential is 2.07 eV, which means that a galvanic cell is formed and a spontaneous process takes place. The insoluble salt aluminumtrihydroxide ($Al(OH)_3$) is assumed to be formed, so the generated OH^- and Al^{3+}-ions are directly used for this reaction. The reactions given in equations (2.4) and (2.5) can be stopped if no O_2, H_2O, or Al is available. This can happen due to the deposit of the $Al(OH)_3$ on the aluminum surface. It is not clear why in [84] NaOH is given to be formed in reaction equation (2.3) as NaOH is very soluble in water.

In order to prevent the corrosion, one of the previous given requirements must not be fulfilled. Therefore, it is usual in aerospace industry applications to place a single layered glass fiber fabric between the carbon fiber composite and the metal to prevent an electrical connection. Another possibility is using a polymer coating on the metal surface [53, 86, 87]. This method is also used in [27] as a polymer tube with 1 mm thickness covers the clinches.

In [84] it is reported that the galvanic corrosion does not influence the bonding strength of bolted aluminum and composite structures. It should be noted that in this case the bonding of the bolted samples is mainly due to mechanical bonding. Also Deinzer performed corrosion tests on mechanical bonded CFRPC to aluminum [27]. Here, no influence on the shear tensile strength can be observed. It was noted that due to the larger volume of the rivet as a result from the corrosion, the clamping force of the rivet was increased.

To prevent the galvanic corrosion the direct contact of carbon fibers to metals should be avoided.

2.2.6 Thermal degradation of polymers and consolidation

Temperature plays an important role on the polymer properties for fusion bonding of polymer composites. Therefore, a temperature control is needed to guarantee a good bonding quality. The minimum temperature of the polymer needed to enable welding is the melting point. Higher temperatures lead to a reduction of the polymer viscosity according to an Arrhenius-type equation [88] and results in a higher diffusion rate [89]. The maximum temperature to which polymers can be exposed is determined by various factors. The main factors are:

- Type of polymer (the melting point is determined by the chemical structure)
- Heating rate of the polymer (during processing or testing)
- Environment (surrounding or purging gas)

The process window for fusion bonding is defined between the minimum and maximum temperature.

Degradation of a polymer has been defined broadly as an irreversible change in its chemical structure when exposed to e.g. heat, light oxidation, or chemical attacks [90]. Several methods are used to determine the thermal degradation of polymers [91]. One of these methods is the thermogravimetric analysis (TGA). This is a thermal method in which the mass change of a sample is recorded during heating within a defined heating rate. The thermogravimetric analysis is frequently used to study the overall thermal degradation kinetics of polymers. An example of a dynamic thermogravimetric measurement with PA66 is illustrated in Figure 2.11.

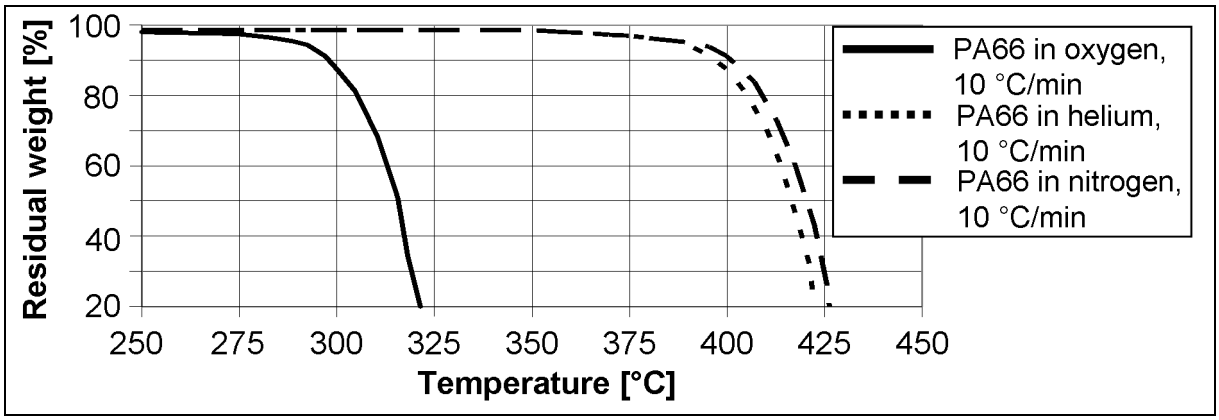

Figure 2.11: Dynamic thermogravimetric analysis of PA66 at 10 °C/min in oxygen, helium, and nitrogen. Specimen mass: approx. 8 mg [92]

Figure 2.11 illustrates that the weight loss of PA66 starts at a temperature of around 300 °C. This temperature is the highest temperature that can be reached without weight loss being detected and is therefore called decomposition temperature. For fusion bonding it forms the upper limit of the manufacturing process window. Overheating of the polymer should therefore be prevented. As polymeric materials have a low heat transfer coefficient, high heating rates usually lead to a slightly higher decomposition temperature. A large increase of degradation temperature is observed, when using an appropriate surrounding gas. For PA66 the degradation temperature shifts from approx. 300 °C in pure oxygen up to 410 °C for helium and argon.

The thermal degradation of PA66 leads to formation of decomposition products, like cyclopentanone, hydrocarbons, nitrils, and vinyl fragments. This cyclopentanone is formed by a degradation mechanism in the adipic acid unit [90, 93]. The thermal stability of PEEK can also be increased by using a non-oxidative environment [91].

In [94] two mechanisms of degradation during electromagnetic induction heating of AS4-CF/PEI at a frequency of 1 MHz are studied. First of all, no significant change in polymer properties from exposure to the high electromagnetic field was observed. Secondly, by means of TGA-measurements it was shown at temperatures above 500 °C that the weight loss of neat PEI could be significantly reduced in a nitrogen atmosphere rather than in air atmosphere. From various samples with different heat treatment and atmospheric conditions, the molecular weight was determined. Here, it was concluded that the cross-linking tends to be the dominant degradation mechanism instead of the chain scission.

Another factor to be considered influencing degradation during the welding of composites is the consolidation pressure. In [95] it is shown that in order to reduce the void content a certain pressure during heating and consolidation is necessary. By applying a pressure of 1.0 MPa, the void content is reduced from 10 % at 0.1 MPa to its initial value of 1 % at 1.0 MPa. This influence of the consolidation pressure is only observed for fiber reinforced thermoplastics. Experiments with neat thermoplastic blocks without a fiber reinforcement do not show this dependence. This example clearly shows the importance of using a multitask tool which enables induction heating and simultaneous application of pressure.

2.2.7 Long-time behavior of CFRPC and joints

In [96] it is shown that the long-time behavior contributed important information about the bonding mechanism of adhesively bonded aluminum samples. Covalent bonding shows less reduction of the shear strength compared to physically bonded samples. Due to higher water absorption these effects are amplified. This also directly results in a reduction of the bonding strength [56, 57].

For pressure sensitive adhesives it was observed that the creep behaviour does not solely depend on the environmental conditions (e.g. testing temperature and humidity), but also on the substrate material and its surface composition. Moreover, it was shown that the shear tensile strength depends on the testing velocity. A high testing speed (100 mm/min) leads to lap shear strength that are 2 to 5 times higher than that of samples tested at 1 mm/h [97].

The creep of the composite gives an additional parameter for the long-time behavior of the composite. In [98, 99] the creep behavior of CF/PA66 (woven carbon fabric, twill weave, fiber volume fraction 0.47) was investigated. The samples were tested in the +/-45°-direction under a load of 50 MPa. The testing direction of +/-45° to the warp direction of the fabric was chosen to determine the maximum polymer influence on the creep behavior.

The increase of the strain of the +/-45°-CF/PA66-sample is under the static load of 50 MPa in 168 hours approximately 30 % of the starting value. For induction welded metal-composite joints the achievable bonding strength is about 50 % of the in Figure 2.12 used tension and additionally the fiber orientation of the welded samples is in

the load direction, so only minor effects on the bonding strength are to be expected due to creep of the polymer.

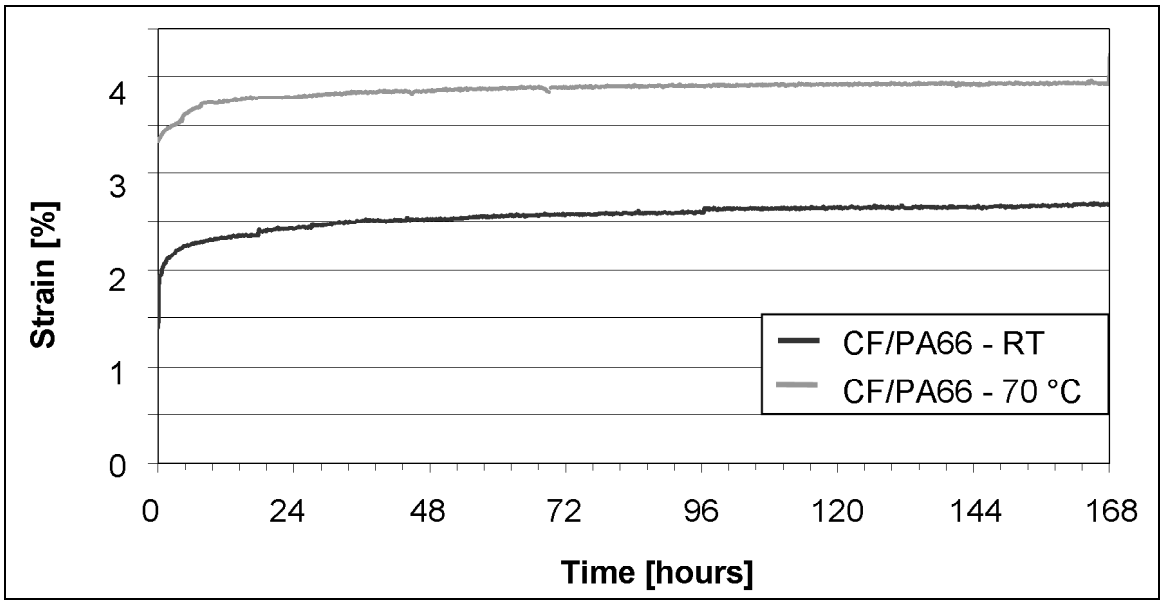

Figure 2.12: Strain as a function of time and temperature of CF/PA66, +/- 45° fiber direction, constant load of 50 MPa

2.3 Induction heating

An alternative method to the conventional processes used to melt polymers is to use induction heating in a high frequency alternating magnetic field. This heating method can only be used with electric conductive materials, like metal and CFRC. The heating is based on two mechanisms [100], which are the energy dissipation due to Joule heating and energy dissipation due to magnetic hysteresis. For ferromagnetic metals, like carbon steels, the heating occurs by these two mechanisms. For non-magnetic materials (like aluminum, copper, and austenitic stainless steels) only heating by joule effect takes place. The heat generation is described by

$$Q = I^2 \cdot R \cdot t \tag{2.6}$$

This means that heating is dependent on the time (t), the ohmic resistance (R), and the square of the current (I) [101]. The current is induced by an alternating magnetic field, so it therefore depends on the inductor geometry (amount of windings and coil size), the coil current, and the distance to the material, if the material is not inside the coil. This situation is schematically illustrated in Figure 2.13.

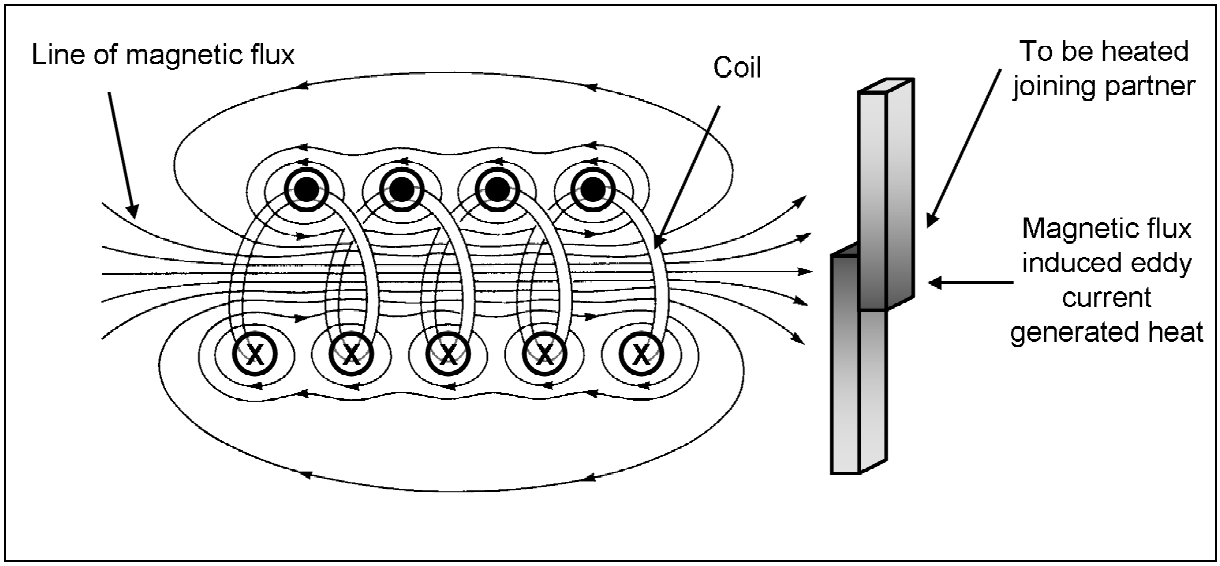

Figure 2.13: Schematic illustration of a magnetic field generated by a coil and the generated heat [100]

In the overview given in [102] the heating process for composites is divided into three categories based on the above given two mechanisms:

- Joule loss – Fiber heating

  Heating is the result of Joule losses due to the inherent resistance heating of fibers [103].

- Junction heating – Dielectric hysteresis heating

  A very thin layer of matrix material at the bonding line separates fibers from the consolidated laminates. A capacitor is created and the dielectric heating occurs due to the movement of charge and rotation of the molecules between the fibers [104].

- Junction heating – Contact resistance heating

  Heating occurs on locations where the fiber-fiber contact is high, this is, in the junction in the case of woven fabric [105]. This theory explains why several fabric types have a different heating generation [46].

So far no evidence has been found in publications for the theory suggested in [104, 106], concluding that the primary heating mechanism for carbon fiber reinforced composites is dielectric losses in the polymeric region between fibers in adjacent planes. A combination of both fiber heating and contact resistance heating occurs during induction of carbon fiber reinforced composites.

As will be discussed in chapter 2.4.2 it is not a necessary condition for the welding implant to be ferromagnetic as is reported in various publications [107, 108]. Usually thermoplastic tapes or films are impregnated with conductive materials, e.g., iron particles, stainless steel, ferrite, and graphite [109].

Yarlagadda et al. [110] studied the effects of a metal mesh implant design on the heating distribution during induction bonding of thermoplastic composites. By selective removal of segments from the uncut mesh, the resultant heating pattern and temperature distribution was made more uniform, resulting in a better weld quality.

Another publication written by Mathur [111] shows the two key requirements for an implant (susceptor), namely:

- Uniform temperature distribution in the susceptor layer and
- temperature control to avoid thermal degradation of the susceptor.

A solution to optimize the properties of a susceptor is given in algorithms to optimize the susceptor (metal mesh) design.

A special type of induction welding is the so-called Emaweld-bonding. Here thermoplastic pastes with metal particles are extruded in various shapes. They form the bonding between the joining partners. The shapes of the extruded pastes depend on the welding zone geometry [28]. The Emaweld-process is fast compared to conventional induction welding. Due to the metal particles in the welding filler, even small cracks lead to notches in the welding zone and reduce the quality of the mechanical properties of the joint [107].

Rudolf investigated the welding of various materials like GF/PP and CF/PPS [46]. Here, good mechanical properties are achieved. Shear tensile strengths of both induction as well as vibration welded CF/PPS-joints of up to 30 MPa are reported.

Ahmed performed comparative investigations of resistance and induction welding [112]. Here, GF/PPS-plates were welded using a metal mesh as heating element in the joining area. The results show that at equal heating conditions, the induction welded samples have a higher shear tensile strength for the single-lap joints up to 30 MPa.

Also in [113] resistance and induction welding of fiber reinforced PPS are compared. When using a metallic mesh the shear tensile strength for resistance welding is above 20 MPa in accordance with the ASTM D1002. Unfortunately, this result cannot be compared to induction welding as no tests with this material's set-up were presented. For the expanded foil the induction welding resulted in higher shear tensile strength (10.1 MPa) than the resistance welding (8.7 MPa).

The examples above show that induction heating can be used for welding of thermoplastic fiber reinforced composites and good bonding properties are obtained.

2.4 Material properties and equipment parameters for induction welding

As is shown in [114] the induced current at the location x (I_x) is described by:

$$I_x = I_0 \cdot e^{-2\pi x \sqrt{\frac{f \cdot \mu}{\rho_{el} \cdot 10^{-7}}}} \tag{2.7}$$

Usually the term in the exponent is replaced by:

$$\delta = \frac{1}{2\pi} \sqrt{\frac{\rho_{el} \cdot 10^{-7}}{f \cdot \mu}} \tag{2.8}$$

δ is the so called penetration depth and is given in millimeters. In this equation it can be seen that the electrical resistivity (ρ_{el}), as well as the frequency (f), and the relative magnetic permeability (μ), influence the penetration depth δ and therefore the current density I_x.

After inserting equation 2.8 in 2.7 this induced current at position x is described by:

$$I_x = I_0 \cdot e^{-\frac{x}{\delta}} \tag{2.9}$$

The penetration depth at x = δ, therefore, represents the depth in which 36.8 % of the current at position x = 0 flows. Therefore, 63.2 % of the current flows between position x = 0 (surface) and the penetration depth δ. As can be seen in equation 2.6 the generated heat is a quadratic function of the current density, therefore, about 86 % of the heat is generated between the surface of the work piece and the depth of the penetration (Figure 2.14). The used material properties and equipment conditions will be discussed in more detail in this sub-chapter.

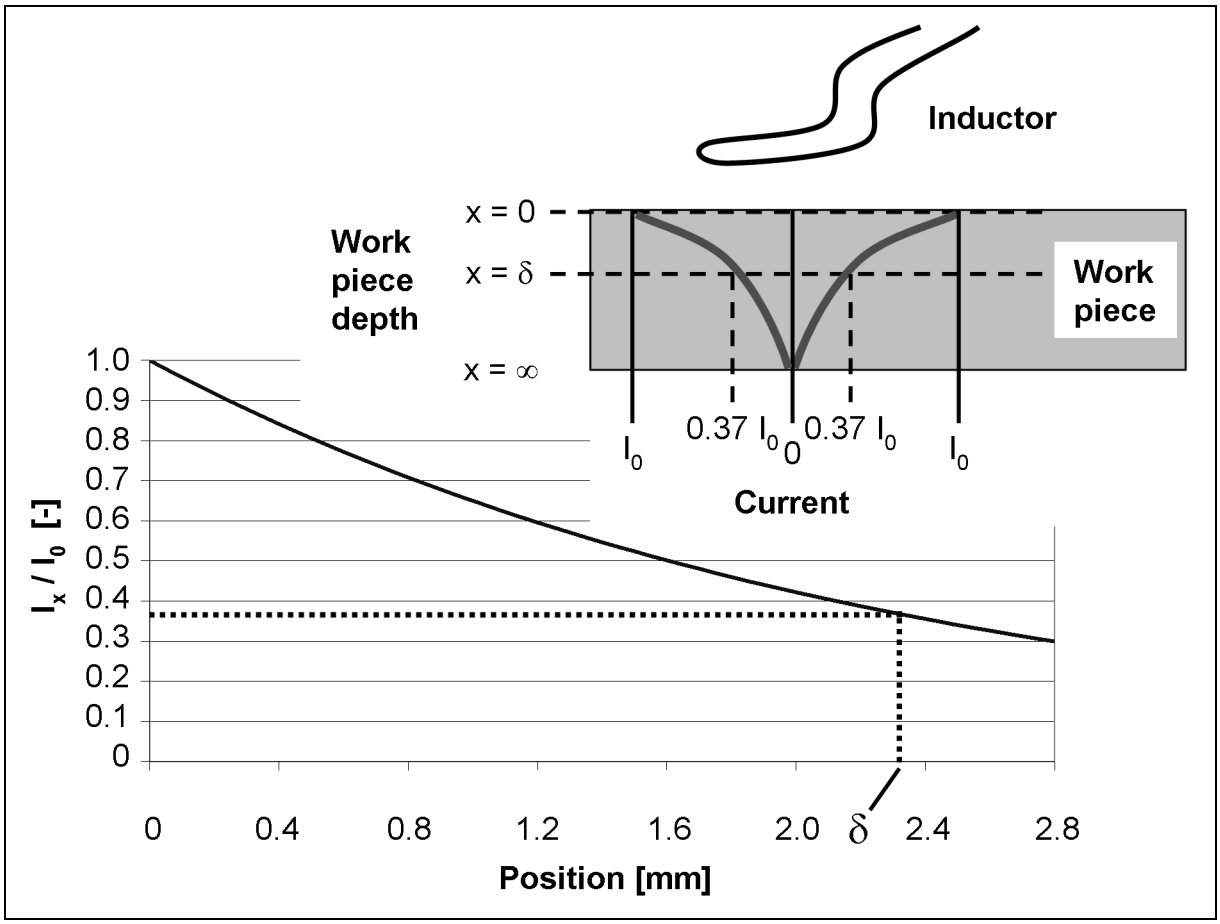

Figure 2.14: Current density in dependence of the position for carbon fiber type T300 (f = 800 kHz, μ = 1, $\rho_{el} = 1.7 \cdot 10^{-5}$ Ωm)

If the work piece thickness is smaller than the penetration depth, the highest current densities would still be on the side facing the inductor. Homogenous heating through the thickness as posted in [46] cannot be observed [17] for fiber reinforced composites.

2.4.1 Frequency

Equations 2.8 and 2.9 show that at high frequencies (range of 500 kHz up to 10 MHz) the penetration depth is much smaller than at low frequencies (range of up to 500 kHz) (Figure 2.15). High frequencies are used for induction heating of carbon fiber reinforced composites and for heating of small metal particles or powder [107, 115]. In some mechanical engineering applications, like hardening of gears, low frequencies are used, because a gear should be hardened a few millimeters underneath the surface [101].

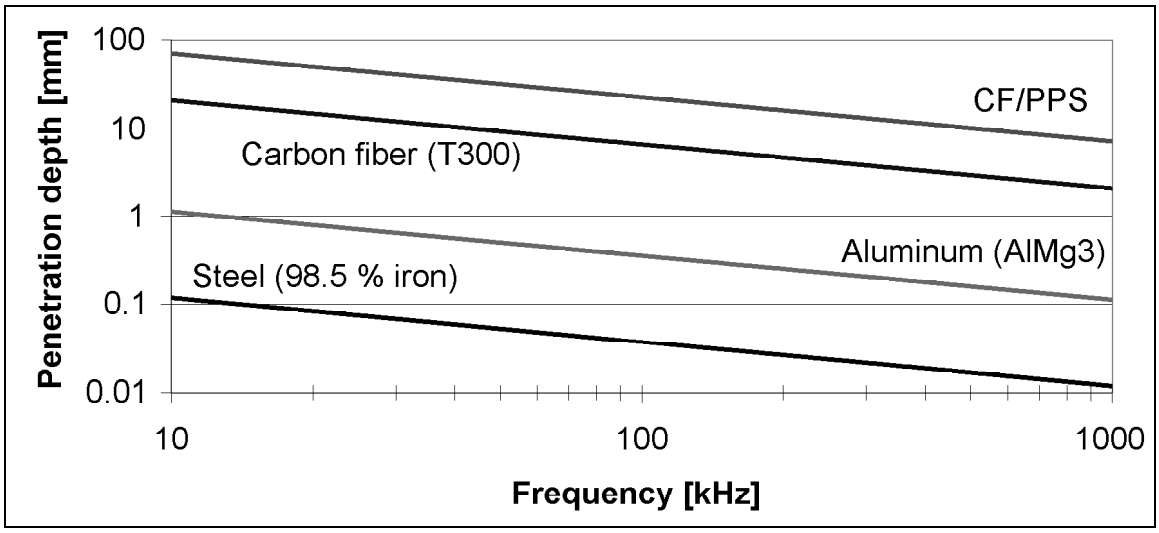

Figure 2.15: Penetration depth in dependence of the frequency [46, 85, 123]

The heat generation induced by the current depends on the frequency. The heating by hysteresis depends linearly on the applied frequency. The resistance losses due to Eddy currents therefore increase quadratically with the frequency [101, 116]. With increasing frequency the ratio of the resistance losses with respect to the hysteretic losses quickly tends to infinite values. In Figure 2.16 these two contributions are schematically illustrated. Below frequencies of 60 kHz mainly hysteretic losses appear, above 60 kHz mainly resistance losses.

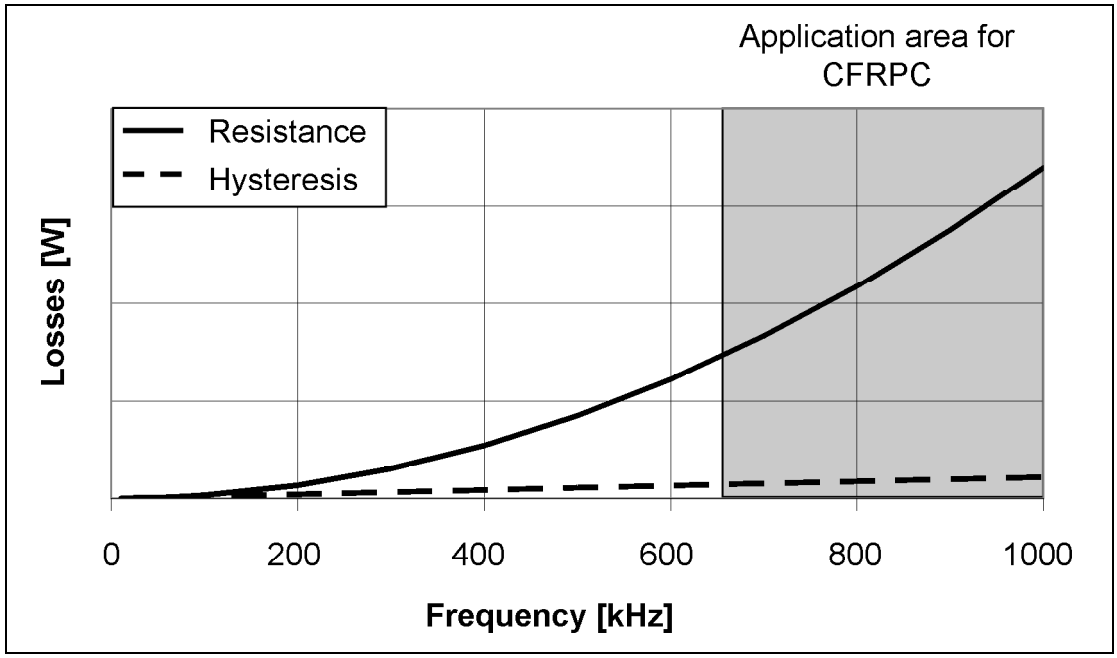

Figure 2.16: Heat losses depending on the frequency

A similar observation is also given by Orfeuil in [117]. Here is the relationship between energy developed by induced eddy currents and magnetic hysteresis expressed by:

$$\frac{P_i}{P_h} \propto f \cdot H_e^{0.4} \tag{2.10}$$

where,

P_i = Power induced by induced currents [W]

P_h = Power due to hysteresis [W]

f = Frequency [Hz]

H_e = Magnetic field [T]

The frequency is an equipment parameter and can be changed by using different frequency generators. It can also be seen that resistance and hysteretic heating have a different amount of heat conversion. To explain the behavior at lower frequencies a closer look into the various magnetic conditions (relative magnetic permeability) needs to be taken.

2.4.2 Relative magnetic permeability

The relative magnetic permeability (μ) also influences the heating behavior of the work piece. This relative magnetic permeability is a material property so the value depends on the type of material and can be divided into three groups due to various responses to magnetic fields. These three groups are:

- Paramagnetic materials ($\mu \approx 1$):

  Paramagnetic materials are attracted to magnetic fields and therefore have a relative magnetic permeability greater than unity. Paramagnets do not retain any magnetization in the absence of an externally applied magnetic field. In general, the relative magnetic permeability is in the order of 1.001 to 1.00001 for most paramagnets. Examples are aluminum and molybdenum.

- Diamagnetic materials ($\mu < 1$):

  Diamagnetism results from changes in the orbital motion of electrons due to the application of an externally applied magnetic field. This field creates a magnetic force on a moving electron, which changes its speed in its orbital motion. This modified electron speed changes the magnetic moment of the orbital in a direction opposite to the external field. Diamagnetic materials have a relative magnetic permeability just lower than 1. Examples are copper, silver, and gold.

- Ferromagnetic materials ($\mu >> 1$):

  Ferromagnetic materials (e.g. steel) have a magnetic moment, also in absence of an external field. They have a relative magnetic permeability that is much higher than 1. Examples are iron, nickel, and cobalt.

The hysteretic losses lose their meaning at higher frequencies. When at lower frequencies (< 60 kHz), if the work piece is heated above a certain temperature, called the Curie point, then the contribution of the heating by hysteretic losses is largely decreased, because ferromagnetic materials lose the ferromagnetic properties above the Curie point [118, 119]. The Curie points of some metals are given in Table 2.6.

Table 2.6: Curie points of various materials [120, 121]

Metal	**Co**	**Fe**	**Ni**	**MnSb**	**Invar 36**
Curie point [°C]	1115	770	354	314	220

It can be seen that the Curie point of nickel is in the range of the manufacturing temperatures of polymers. By blending selected materials this property can be used for temperature control. In [122] experiments are performed with various frequencies (275 kHz, 4 MHz, and 6.5 MHz). First of all it is shown that the low frequency of 275 kHz results in a lower heating rate compared to the higher ones. Furthermore, the Curie points are in some cases reached while in other cases the maximum temperature was below the Curie point. As the Curie point is a material property it does not depend on the applied frequency. The fact that in some cases the temperatures are reached and in some not, indicates that not only hysteretic heating occurs.

In [76] are PSU-polymer films foreseen with Ni-particles in four different diameters, namely, 79 nm; 0.7 µm; 3 µm; and 22 µm. These particles were mixed in the polymer in volume fractions of 0.1 and 0.2. The induction welding equipment was operated at a frequency of 2.25 MHz and 20 kW power. Here, it is reported that further heating of the susceptor is stopped as the contribution of the hysteretic losses is reduced when the Curie temperature of nickel (Ni) is achieved. Unfortunately, no further evidence is given for this high contribution of the hysteretic heating at this high frequency as this observation is in contraire to general accepted theories in [100, 101].

When using the high frequency equipment (650 kHz to 1 MHz), available at the Institut für Verbundwerkstoffe GmbH, the heat generated by the resistance losses in the fibers and at junctions dominates. This is also proved by the fact that stainless steel metal meshes are able to melt thermoplastic polymers in a few seconds [23].

2.4.3 Electrical resistivity

The electrical resistivity (ρ_{el}) depends on e.g. the type of material and on the temperature. Increasing the temperature for metals usually leads to an increase of the electrical resistivity (Figure 2.17).

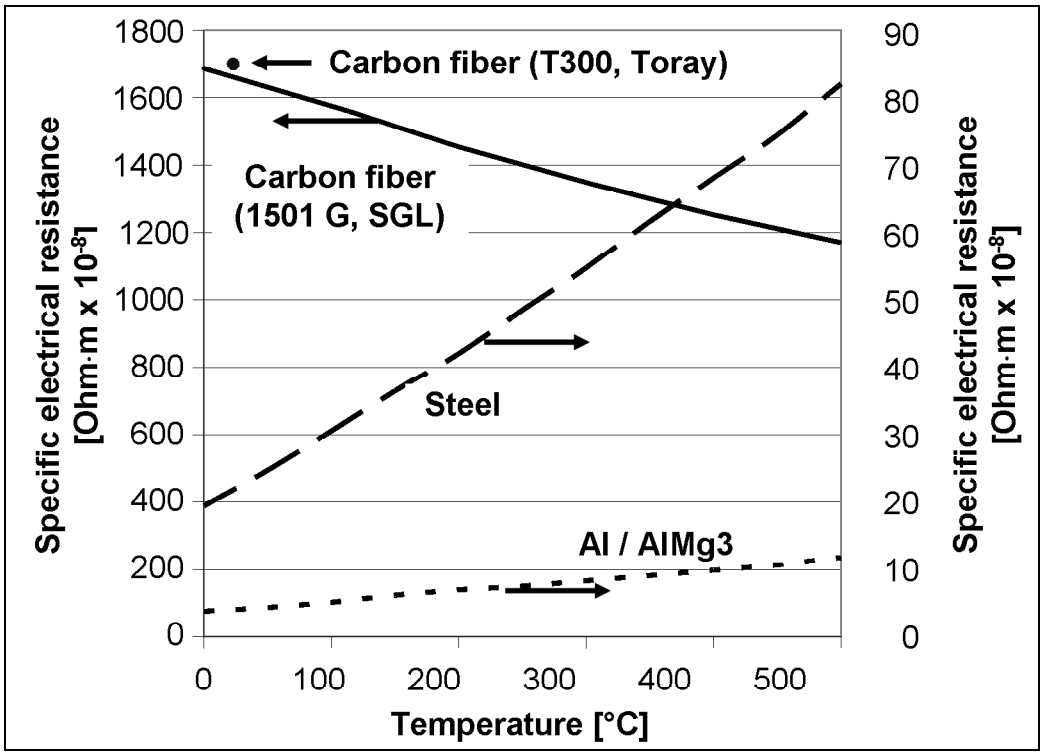

Figure 2.17: Electrical resistivity as function of the temperature according to [101, 123, 124]

For carbon fibers it can be observed that the resistivity decreases with rising temperature. This indicated that less heat is generated at higher temperatures. Although the resistivity value of the carbon fibers is between 300 and 400 °C about 20 times higher than that of steel, less current flows as the penetration depth is much higher for the carbon fibers and so less heat is generated.

2.4.4 Specific heat capacity

When heating materials, the specific heat capacity parameters (c_v and c_p), plays an important role. The specific heat capacity is the amount of heat that is needed to increase the temperature of 1 g of a material by 1 K. As can be seen in Figure 2.18, the specific heat capacity also depends on the temperature. More detailed information about the thermal properties of the materials used is given in chapter 8.2. These thermal properties are needed for performing modelling of the welding.

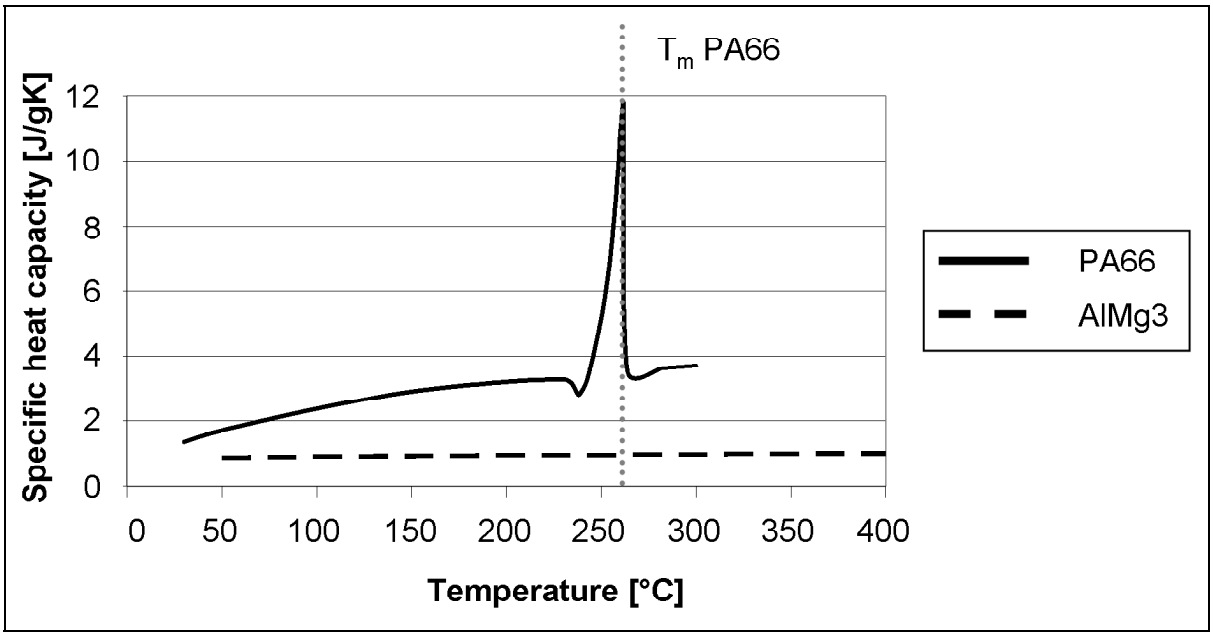

Figure 2.18: Specific heat capacity in dependence of the temperature [125, 126]

2.5 Existing models for welding time estimation

High temperature and long welding time can reduce welding performance because the polymer is degraded and squeezed out of the joint [127]. Low temperature and short-time produce insufficient flow across the bond, resulting in low weld performance. Therefore, optimizing welding time and temperature is essential to obtain a high-quality weld [128].

In [46] a model is given to determine the heating time of carbon fiber fabrics. A disadvantage of this model is that the temperature dependence on the material properties is not considered. Additionally, first investigations with Ansys® FE-toolings are made to illustrate the heat generation on the surface of carbon fiber fabrics. In [129] the Ansys® simulation software is used to simulate the heat transfer dependence on the pressing tool material and the power level. The pressing tool material has a large impact on both the welding time and the temperature gradient through the weld thickness. Power levels between 1.0 and 2.5 GW/m³ are applied to simulate the effect of the power level on welding of APC-2/AS4 (CF/PEEK) laminates. As expected the lower power level resulted in a larger processing window. Moreover, it was shown that for the applied resistance welding configuration it is impossible to obtain a uniform temperature distribution at the weld interface. This can partially be explained by the temperature dependence on the used stainless steel meshes. As was shown in chapter 2.4.3 a higher temperature results in a higher specific resistance and therefore a higher heat generation.

The Joule heating within the heating element was simulated as a volumetric heat generation corresponds to the applied input power level [130]. Due to recent developments also these effects can be implemented in FE-modelling programs, like Ansys® Workbench 10. This will be discussed in more detail in chapter 6.

3 Experimental part

The experimental part starts with an equipment and tool list used to perform the experiments. Many of the tools were specifically designed and constructed to enable researching the specific objectives (chapter 1.5) and are therefore discussed in more detail. This section continues with a description of the polymers used, the reinforcement structures, and the manufacturing conditions. Finally, the design of experiments and testing conditions are presented.

3.1 Equipment

In this section all equipment used is presented e.g. the induction welding machine, the sample holder, the pressing tool, and various other equipments.

3.1.1 Induction welding equipment

Modifications for the planned experiments had to be carried out to convert the existing continuous working equipment (Figure 3.1) to a discontinuous one.

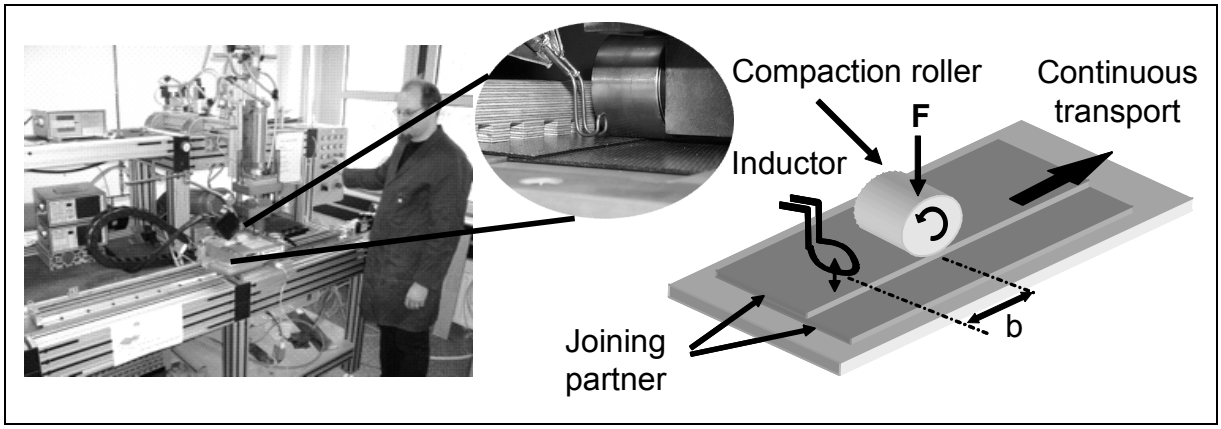

Figure 3.1: Continuous working induction welding equipment (IVW)

A significant advantage of the discontinuous operation mode is the improved reproducibility of the parameter variations. The applied process pressure clarifies this advantage. The continuous operation mode needs a compaction roller that is inherent to the system, whereas with the discontinuous operation mode a punching tool can be used. In the first case the pressing force is an equipment parameter, as the pressing area is unknown. In the second case the force and contact area are

directly available and adjustable for pressing as well as for consolidation. The pressure is now a process parameter.

Initial process and concept plans were made to perform this conversion (Figure 3.2).

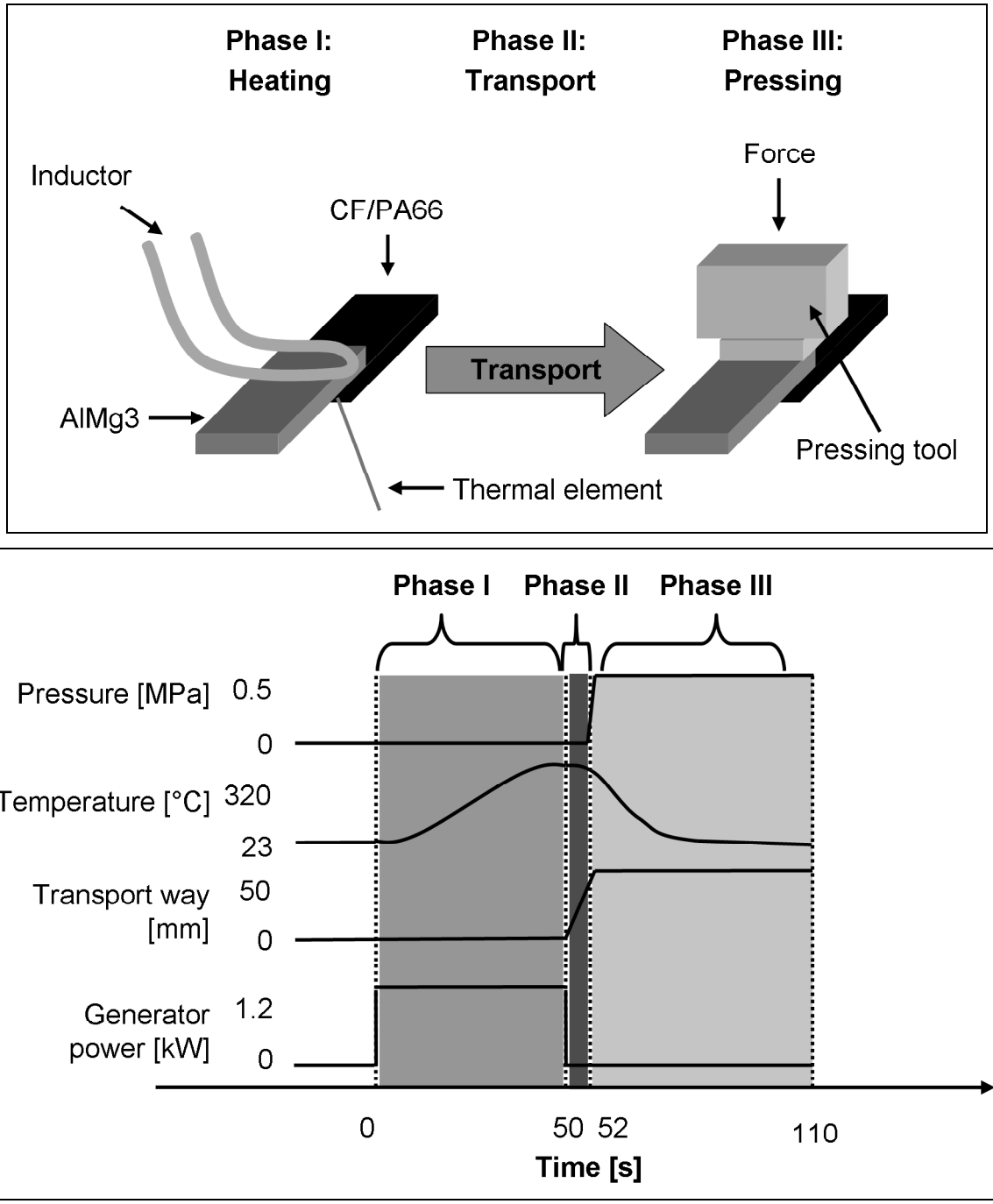

Figure 3.2: Concept and scheme of the process control [131]

Figure 3.2 shows the chronologically matched characteristic process parameters for discontinuous induction welding.

These are:

- Pressure force (consolidation)
- Process temperature (induction heating, transport/convection, and heat extraction/conduction)
- Feeding rate of the transport unit (speed)
- Power of the high frequency generators (energy entry)

In this configuration the joining partner nearest to the inductor (e.g. the metal part) is heated up so the polymer matrix of the semi-finished sheet (e.g. CF/PA66) in the joining zone is melted due to heat conduction (phase I).

After the inductor is switched off, the joining partners are transported underneath the pressing or punching tool (phase II) and the joining pressure is applied.

In the process phase III the joining partners are cooled down under pressure. Here, the semi-finished sheets are reconsolidated and the joint is consolidated. The significant process parameters are the temperature in the joining area and the consolidation pressure. These process parameters are recorded by means of thermal couples and an integrated load cell. For realization of the targeted process sequence, appropriate changes in the equipment were made. The control of the welding equipment was adapted to the requirements, so that the discontinuous welding experiments could also be performed automatically by computer control.

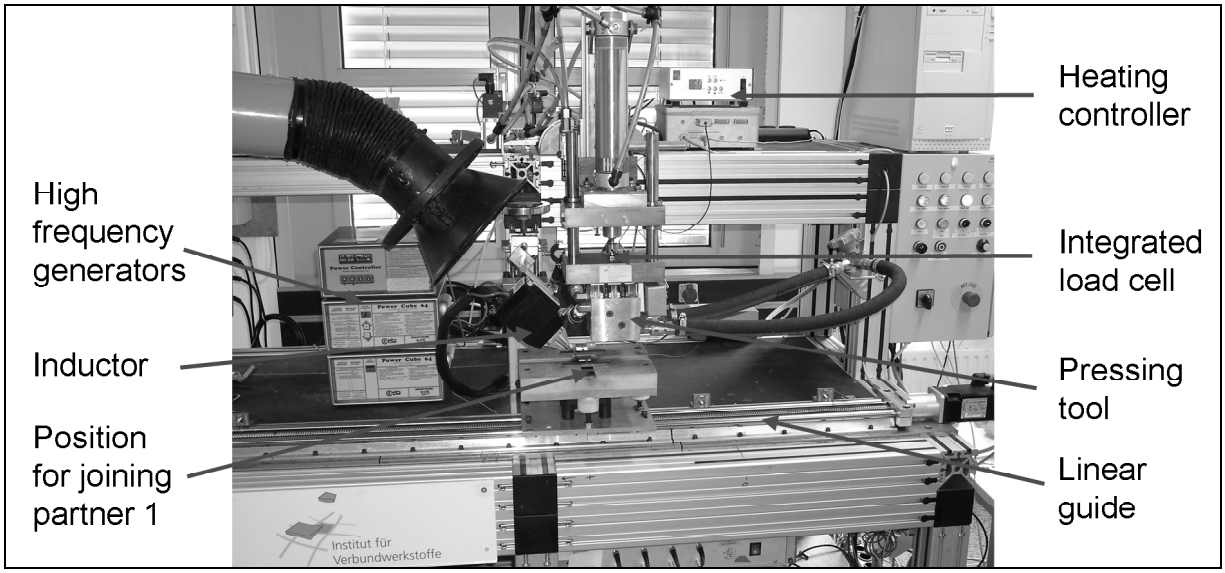

Figure 3.3: Overview of the equipment for discontinuous induction welding (IVW)

The controlling and measurement recording software DIADEM® operates the equipment. The logging of experimental data is greatly improved due to the automated experimental operation. All set points for the experimental operation are already available for the equipment control, so that these can directly be transferred to the experimental journal. Figure 3.4 shows a screenshot taken while performing an experiment.

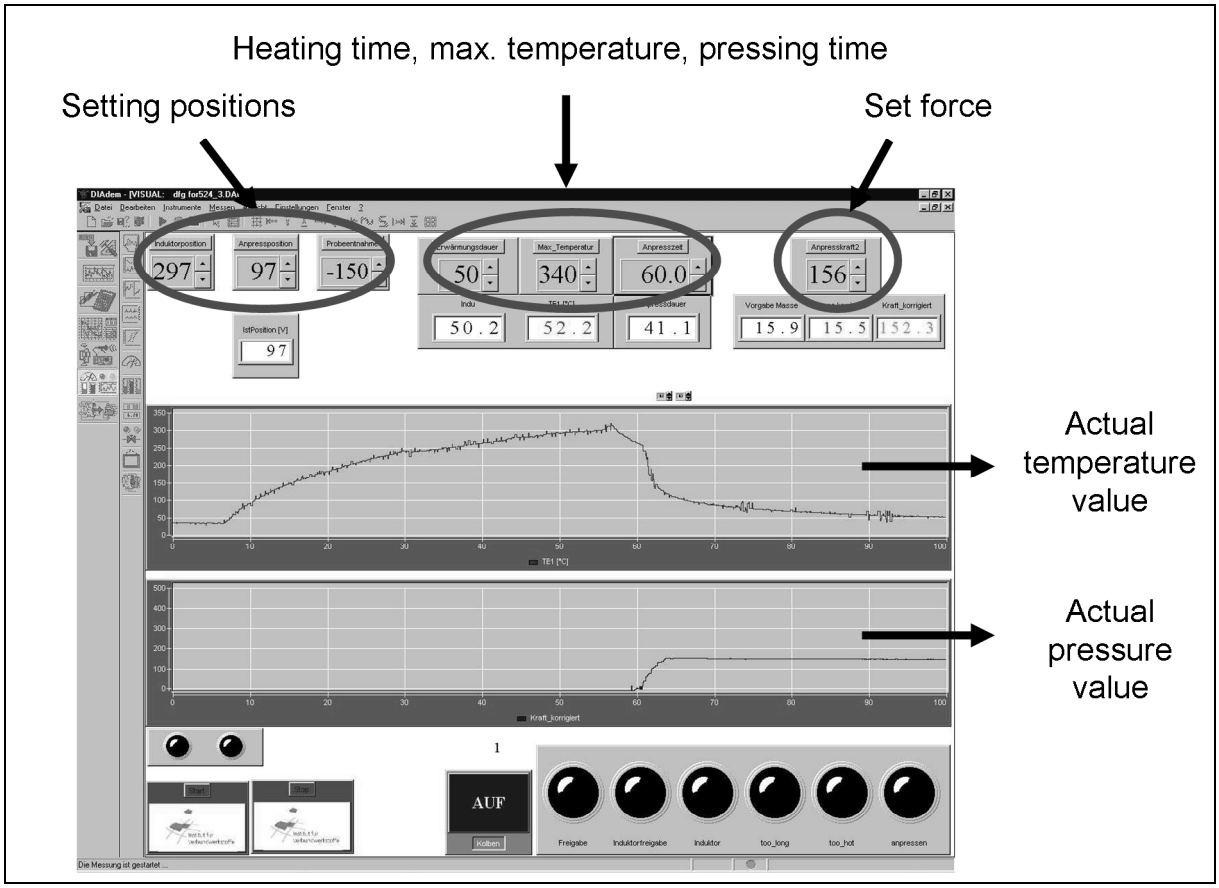

Figure 3.4: Screenshot during performance of an experiment

Here, various positions, like the inductor position for heating of the joining partners, the pressing position, and the sample release position are evident. Furthermore, the heating time, the maximum temperature, and the pressing time are also given. The last adjustable parameter is the set or pressing force.

3.1.2 Inductor

The resulting heated area is influenced by the geometrical configuration of the inductor. The inductor is designed to create a homogeneous heating area. Figure 3.5 shows the constructed inductor.

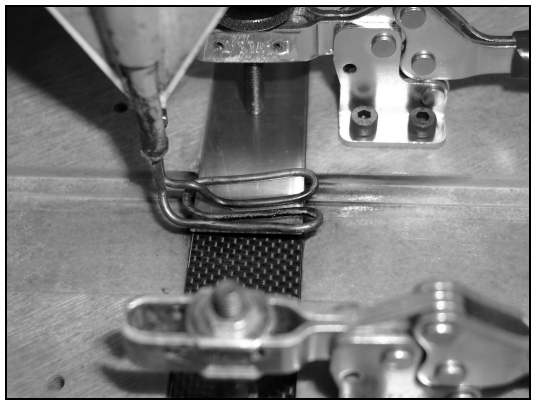

Figure 3.5: Inductor for the surface heating [132]

3.1.3 Sample holder

After the first experiments it was noted, that the sample holder has a significant influence on the reproducibility of the equipment. Therefore, the sample holder had to be designed in a way that the applied process force is completely transferred into the welding area and also no misalignments in the welded sample are induced. To guarantee this, a holder was designed that enables an easy and reproducible sample positioning which is shown in Figure 3.6.

a

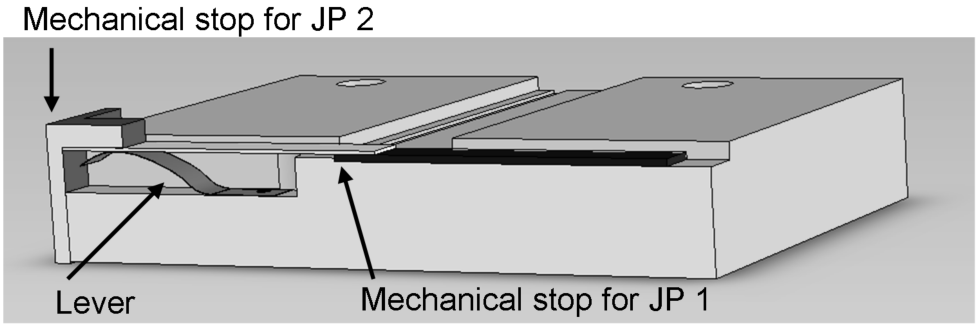

b

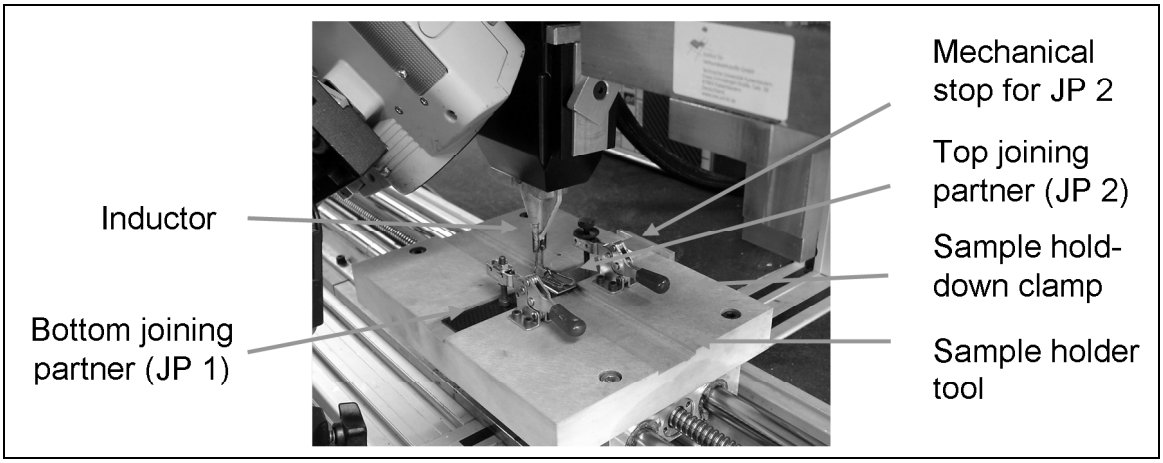

Figure 3.6: a) Sectional representation and b) used tool as sample holder

During induction welding electrical currents are induced in the joining partners. For this reason the sample holder cannot be manufactured out of an electrical conductive material, therefore, glass fiber reinforced insulation material (Doglas ® 250M of the company Dotherm) is used. The glass fiber reinforced insulation material offers:

- High mechanical strengths
- Good electrical insulation properties
- Good thermal insulation properties

This material has good machining properties so accurate sample holders can be constructed to ensure a defined single-lap length. Due to the use of additional horizontal handle hold-down clamps the samples are reproducibly inserted and fixed in the tool.

The procedure used to perform the experiment is as follows:

The carbon fiber reinforced sample is inserted in the bottom joining partner position. The metal sample is then pushed into the top joining partner position and is fixed at a height of 2 mm to the sample holder by an integrated lever. This guarantees that both joining partners overlap parallel and that joints are made with a constant overlap of 12.5 mm according to DIN EN 1465. Also the TP-FRPC partner is used as top joining partner.

The sample holder and the pressing tool are very difficult to be mounted in an absolute plan parallel position. Even small deviations in the parallelism, especially for metal-polymer joints, can lead to a reduction of the shear tensile strength as no homogeneous pressure distribution is available. Therefore, the sample holder is mounted on a flanged bearing (KFSM-GT50A, Igus) to prevent any misalignment (Figure 3.7).

This design enables the sample holder to obtain a parallel position to the pressing tool as it can be moved freely in every direction.

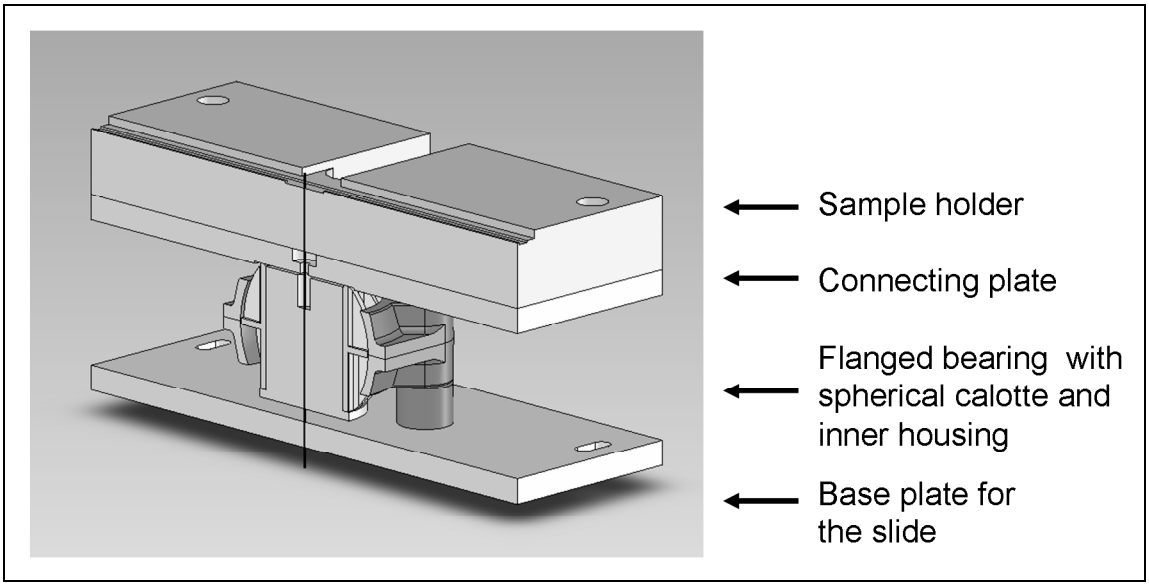

Figure 3.7: Sectional representation of the tool with a flanged bearing

3.1.4 Pressing tool

As shown in the state of the art section the pressing conditions and tools influence the consolidation of the composites. In this section various pressing tools used for the experiments will be shown. The force during pressing is measured by an integrated load cell (Figure 3.3) and with the contact area of 25 x 12.5 mm the pressure on the sample can be determined.

3.1.4.1 Standard pressing tool

Figure 3.8 shows the pressing tool with defined pressing area, which applies the joining pressure. The tool has a width of 12.5 mm and thus covers the joining area in length and width.

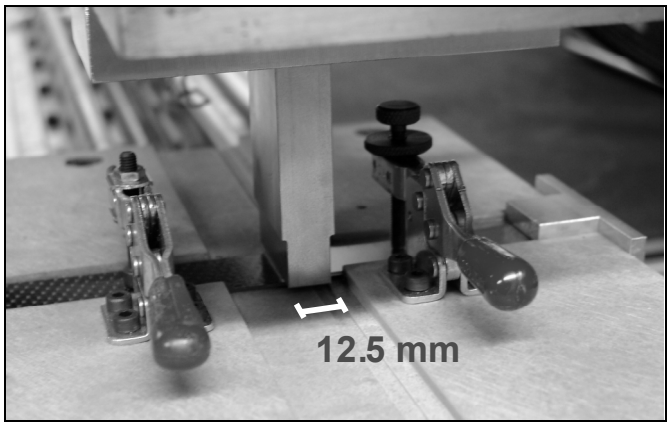

Figure 3.8: Standard pressing tool

Slotted holes in the tool enable a precise positioning of the tool on the joints. A disadvantage of this tool is that the pressing tool temperature for pressing is the room temperature. During pressing the temperature in the joining area of AlMg3-CF/PA66 is rapidly decreased from 310 °C to 70 °C in only six seconds. To prevent these very high cooling rates a tempered pressing tool was designed.

3.1.4.2 Tempered pressing tool

Figure 3.9 shows the designed and constructed tempered pressing tool.

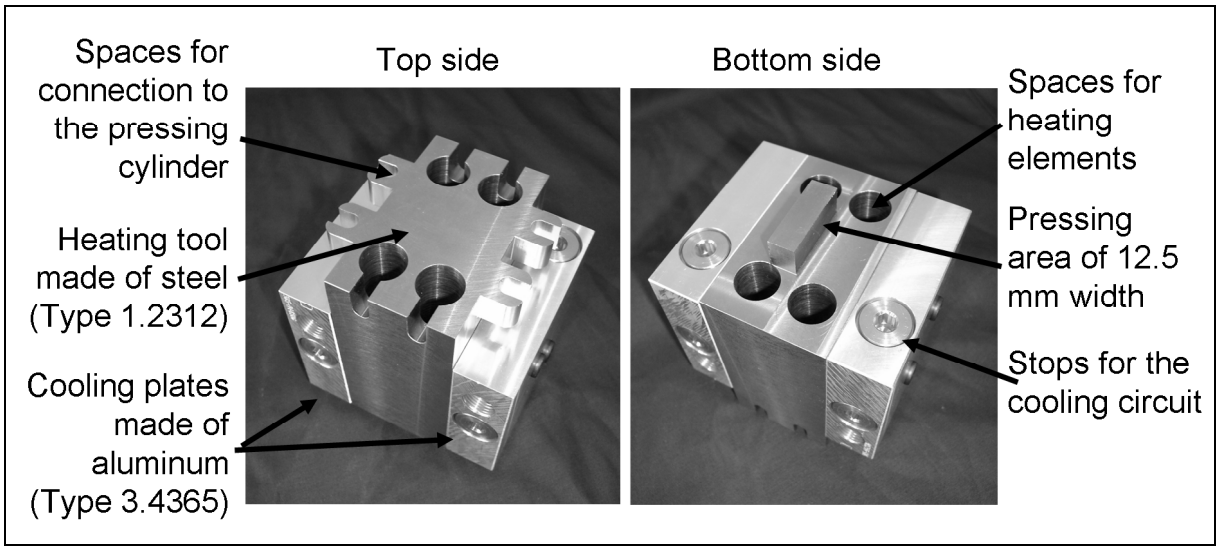

Figure 3.9: Tempered pressing tool

In the pressing tool, four through-going holes for the 800 W heating elements (HS-2050/800/230, HS Stegmeier GmbH) were made and two aluminum plates for cooling with water were arranged on the side. The pressing area on the bottom side of the tool has a width of 12.5 mm, which is the overlap length of the single-lap joints. The heating controller (HS W35 / M, HS Stegmeier GmbH) was used to heat up the heating elements. Two thermal couples are inserted in the pressing area. The first one is used to operate the heating controller; the other is used to determine the temperature as near as possible to the joint and is recorded in the manufacturing journal. This tool enables pressing at a given temperature for a certain time and with a certain pressure. This means that the important process parameters (temperature, time, and pressure) can be investigated.

3.1.5 Equipment used for contact corrosion experiments

For the contact corrosion experiments a two-liter vessel was used in which the welded samples could be stored in a liquid during a defined time. The samples were stuck through a wood plate and were fixed by clamps. Two different condition settings were considered. In one case the samples were submerged in demineralized water, whereas in the other case an artificial sea water solution in accordance with DIN 50905-4 [133] was used. The single components used to make this solution are:

- 985 ml demineralized water
- 28 g NaCl
- 5 g $MgCl_2 \cdot 6H_2O$
- 2.4 g $CaCl_2 \cdot 2H_2O$
- 7 g $MgSO_4 \cdot 7H_2O$ and
- 0.20 g $NaHCO_3$.

The samples were submerged into this sea water solution as is presented in Figure 3.10.

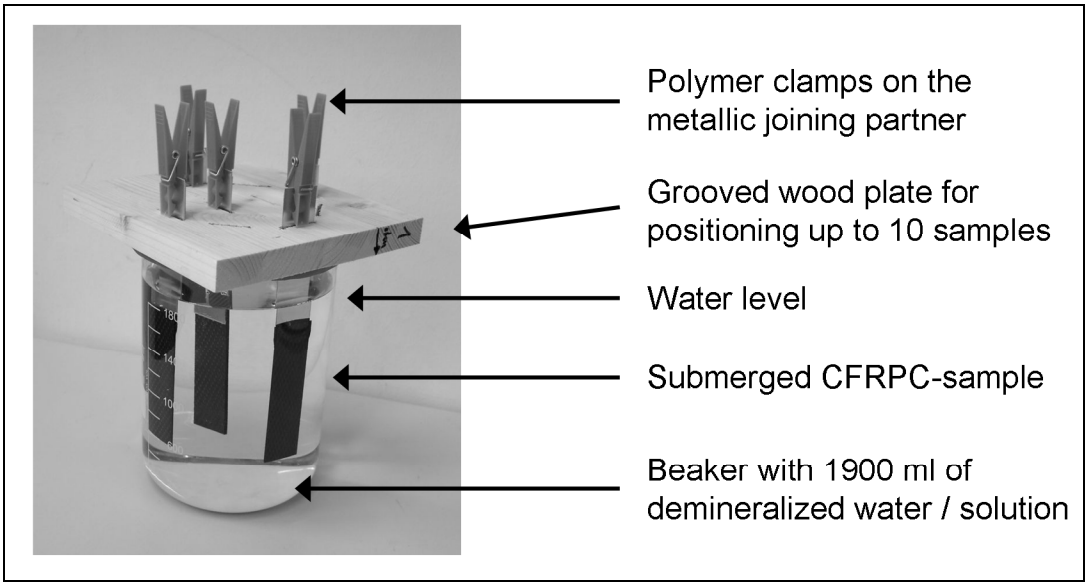

Figure 3.10: Set-up of the beaker with the submerged samples

Resistance measurements were performed to determine whether there is a direct contact between the AlMg3 and the carbon fiber. Figure 3.11 shows the sectional representation of the copper clamp and the set-up for the resistance measurements.

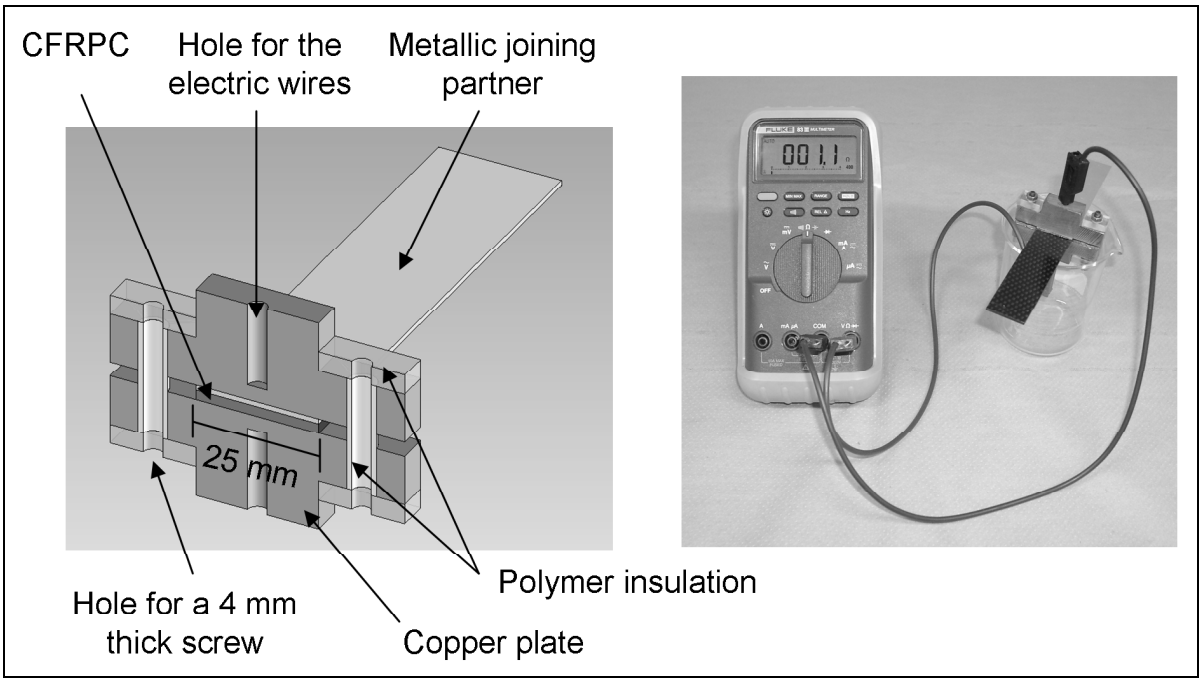

Figure 3.11: Sectional representation of the copper clamp for measuring the resistance through the thickness of the metal/composite joint, and measuring set-up

The resistance is measured by means of a multimeter (Typ 83 III, Fluke) and two copper clamps (dimension: 60 x 12.5 x 20 mm³, hole diameter: 4 mm, hole depth: 17 mm). To guarantee a good and reproducible contact between the measuring clamps and the single-lap joint, the clamps were closed by means of insulated steel screws and a torque of 10 Nm.

3.1.6 Chamber for oxygen exclusion

To perform welding experiments in absence of oxygen, a new experimental set-up had to be designed. A sealed polymer vessel surrounded the entire welding assembly. The vessel was connected to a gas supply to ensure an oxygen free environment. This set-up is presented in Figure 3.12.

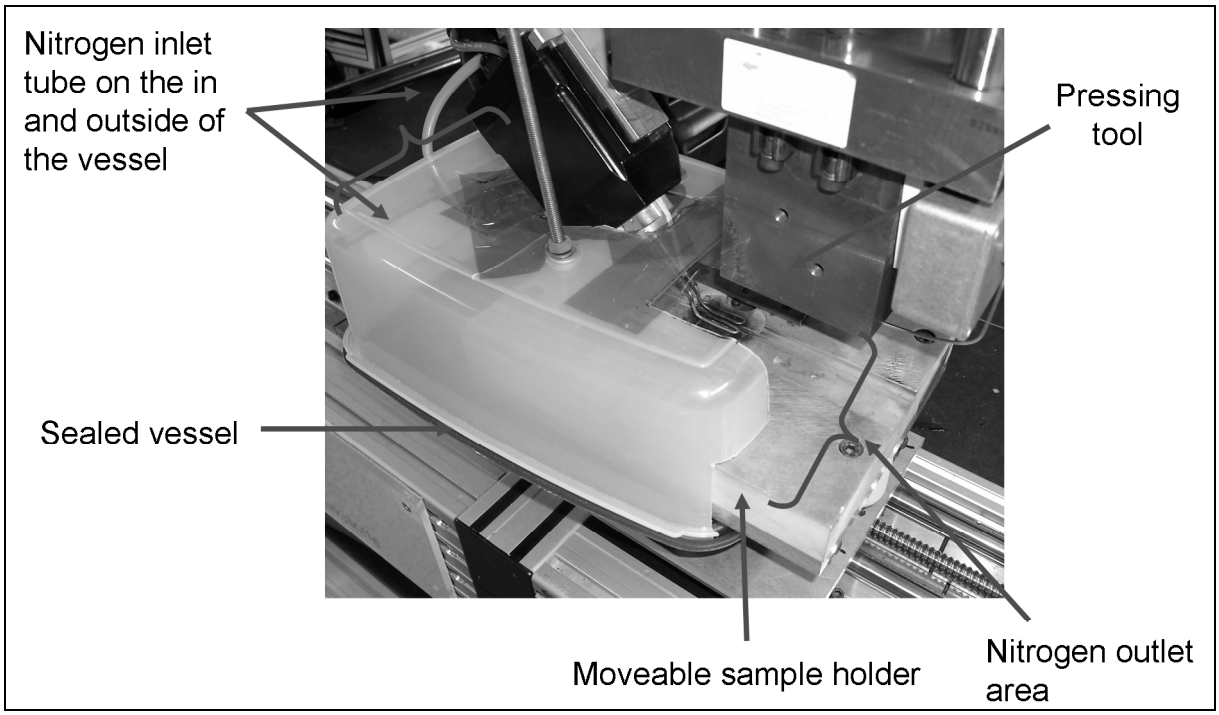

Figure 3.12: Set-up for performing experiments in absence of oxygen

The nitrogen gas (4.0) had a purity of 99.9 %, the gas flow was determined to be 4.5 l/min. After heating in the oxygen-free environment the heated samples were quickly transported to the pressing tool, pressed, and finally reconsolidated.

3.2 Material used and manufacturing parameters

The polymer materials used are selected as they are frequently used in automotive applications (in combination with GF/PA66) and in aerospace applications (CF/PEEK). Carbon fibers were chosen as they can be heated by induction and they offer much potential for future lightweight applications. For semi-finished sheets manufacturing standard woven fabrics (Satin 5H, plain weave) based on 3k carbon fibers (Torayca, T300) were used. For the non-crimped fabric a similar fiber (Fortafil 80k carbon fiber) was used. The glass fiber fabric had a twill weave and was made out of an E-glass fiber.

For the polymer nylon 66 (polyamide 66 or PA66) and polyetheretherketone (PEEK) were used. Table 3.1 shows a summary of these materials.

Table 3.1: Fabrics used for semi-finished sheet manufacturing

Material	**CF-fabric**	**CF-fabric**	**CF-NCF**	**GF-fabric**
Designation	CD 0282.040.000.0000	Style 475	MCX0481270	W140210
Fabric type	Satin 5H, 3k, 285 g/m²	Plain weave, 3k, 285 g/m²	+/- 45°, 80k, 300 g/m²	Twill weave, 3k, 400 g/m²
Supplier	Ten Cate Advanced Composites b.v.	ECC GmbH & Co KG	Sigmatex Ltd.	Verseidag-Indutex GmbH

Figure 3.13 shows the schematic set-up of the fabrics used as well as the supply condition of the Satin 5H-fabric.

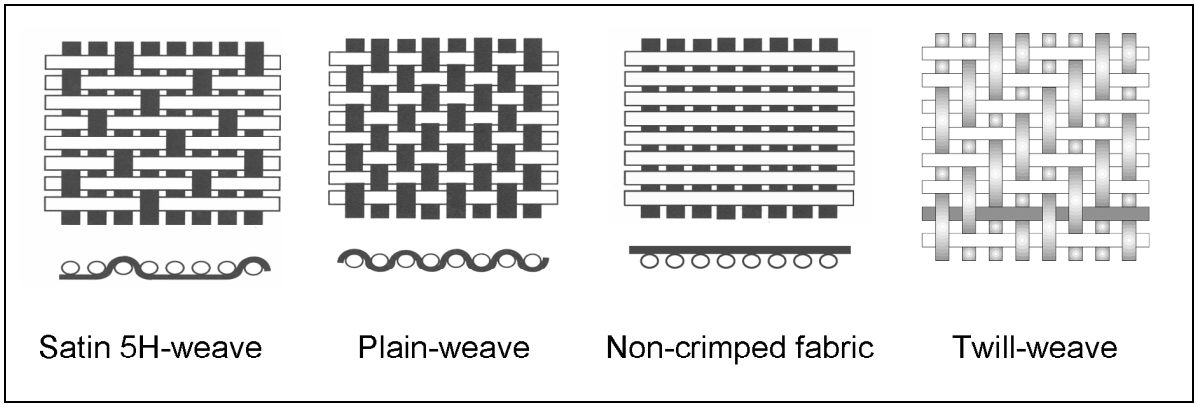

a)

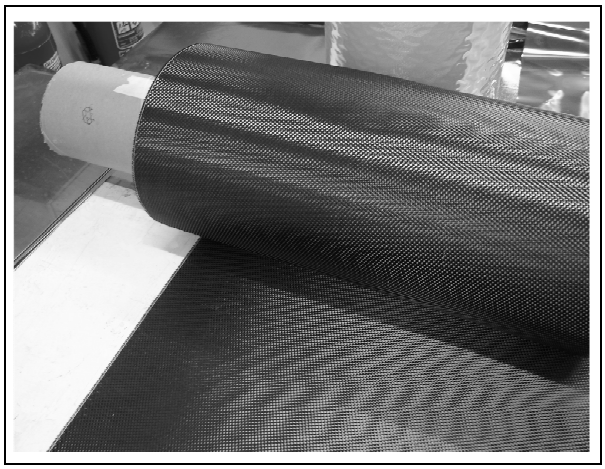

b)

Figure 3.13: a) Schematic set-up of the reinforcement structures b) Satin 5H-fabric in supply condition

Table 3.2 shows the polymer types used and their application.

Table 3.2: Designation and purpose of the used polymer

Parameters/Material	PA66	PEEK	PEEK
Designation	SF502	Victrex 150PF	LUVOCOM 1105 – 7373
Organic sheet	x	x	
Additional polymer for the joining area	x		x
Supplier	DuPont Liquid Packaging Systems	Victrex Europa GmbH	Lehmann & Voss & Co

The PEEK as additional polymer was compounded at the IVW and consists of 70 % PEEK, 10 % short carbon fibers, 10 % TiO_2, and 10 % PTFE. This PEEK compound is used for bearing applications and was also used in hot pressing experiments [70].

Table 3.3 shows an overview of the various material combinations and manufacturing process, and finally for which joining process the material is used for.

Table 3.3: Manufacturing processes for the material used

Reinforcement material and polymer type	Fabric	Manufacturing process	Joining process
CF/PA66	Satin 5H	Autoclave	Induction
	Plain weave	Continuous compression molding press (IHP)	Induction
	NCF	Autoclave	Induction
	Satin 5H	Autoclave	Adhesive bonding
GF/CF/PA66	Twill weave (GF)/ Satin 5H (CF)	Autoclave	Induction
CF/PEEK	Satin 5H	Autoclave	Induction
	Satin 5H	Autoclave	Adhesive bonding

Almost all induction welded samples were manufactured by means of the autoclave technology; therefore the manufacturing of these organic sheets is now explained.

To manufacture 2 mm thick organic sheets with a fiber volume fraction of 0.48, six layers of CF-fabric were used. The CF/PA66 laminates were manufactured by means of film stacking with PA66-sheets of 1000 µm thickness in total. The six layers of

fabric were put together with the polymer sheets (PA66) and placed between two coated stainless steel sheets, packed in a vacuum bag, and laminated with the standard autoclave process. For the CF/PEEK laminates an alternative way was chosen in which first a powder prepreg was made. A defined amount of powder is spread on the fabric by means of the IVW-build powder prepreg equipment (Figure 3.14). This PEEK-powder is heated above melting temperature by an infra-red heating field and finally cooled by a cooling drum.

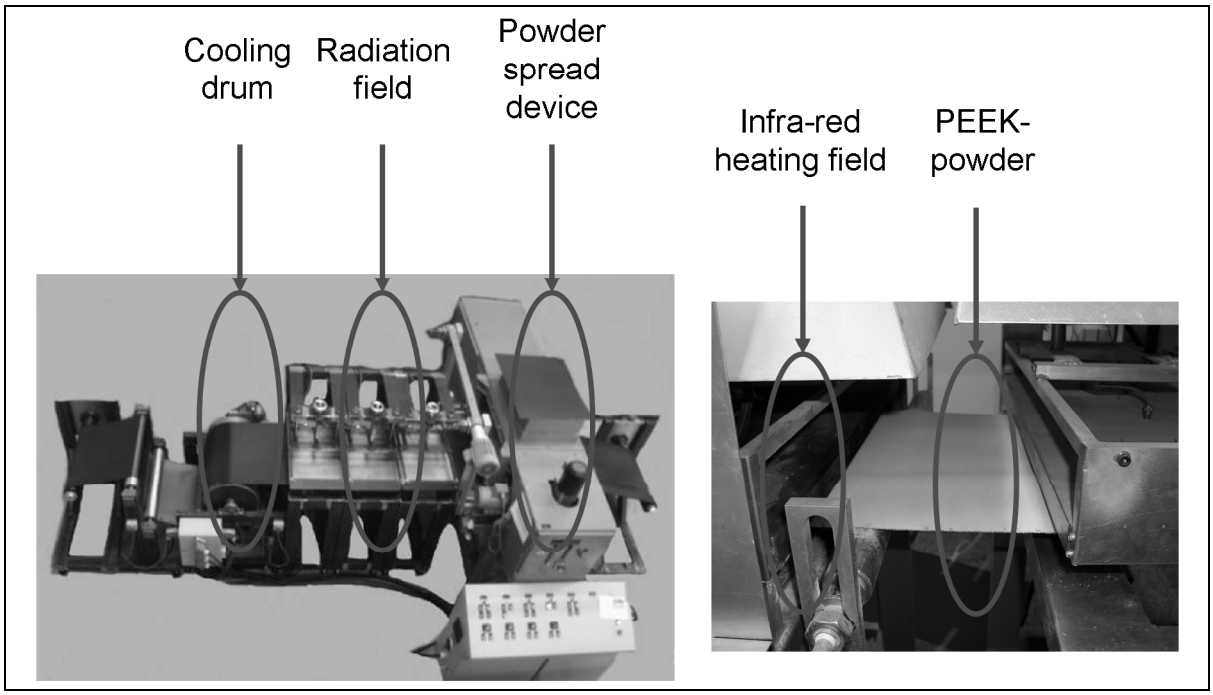

Figure 3.14: Used powder prepreg equipment

This way of working enables omitting the expensive step of sheets extrusion as only smaller amounts of polymer were manufactured. Figure 3.15 shows the manufactured CF/PEEK powder prepreg that was finally consolidated in an autoclave process.

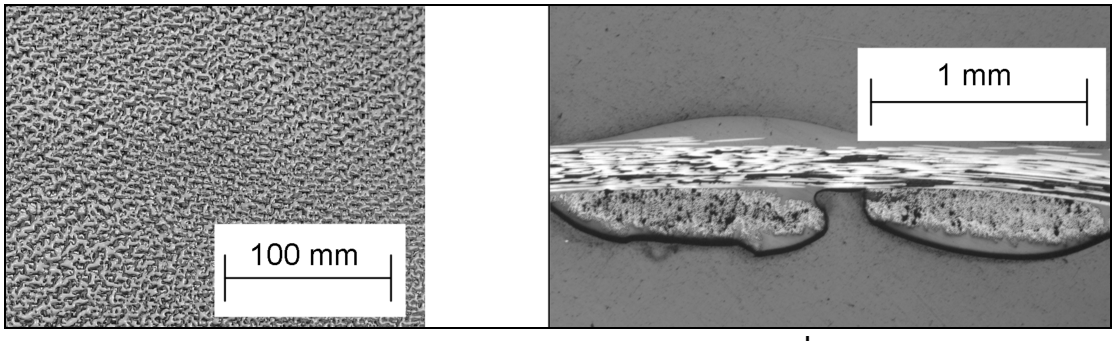

Figure 3.15: a) CF/PEEK powder prepreg; b) micrograph [13]

The process conditions used for the organic sheet manufacturing are illustrated in Table 3.4 and in Figure 3.16.

Table 3.4: Parameter for the autoclave cycle

Material Parameter		CF/PA66	CF/PEEK
Pressure	[bar]	25	8
Temperature	[°C]	280	380
Cycle duration	[min]	180	450
Heating time	[min]	80	120
Holding time	[min]	20	30
Cooling time	[min]	80	300

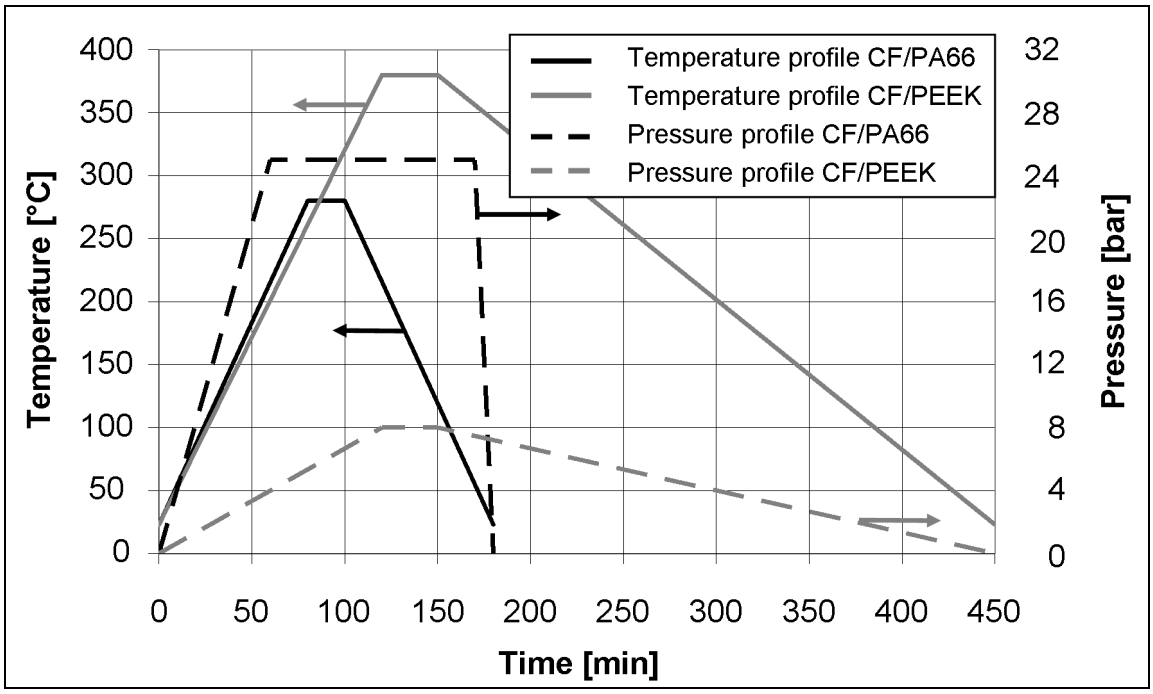

Figure 3.16: Temperature and pressure characteristics during an autoclave cycle

Figure 3.17 shows micrographs of the CF/PA66 and CF/PEEK laminates. The very good impregnation quality can be seen as every single carbon fiber is surrounded by polymer and no air entrapments were observed.

More detailed thermal and mechanical properties of the single components (fibers and polymer) and the manufactured organic sheets are given in the appendix (chapter 8.3).

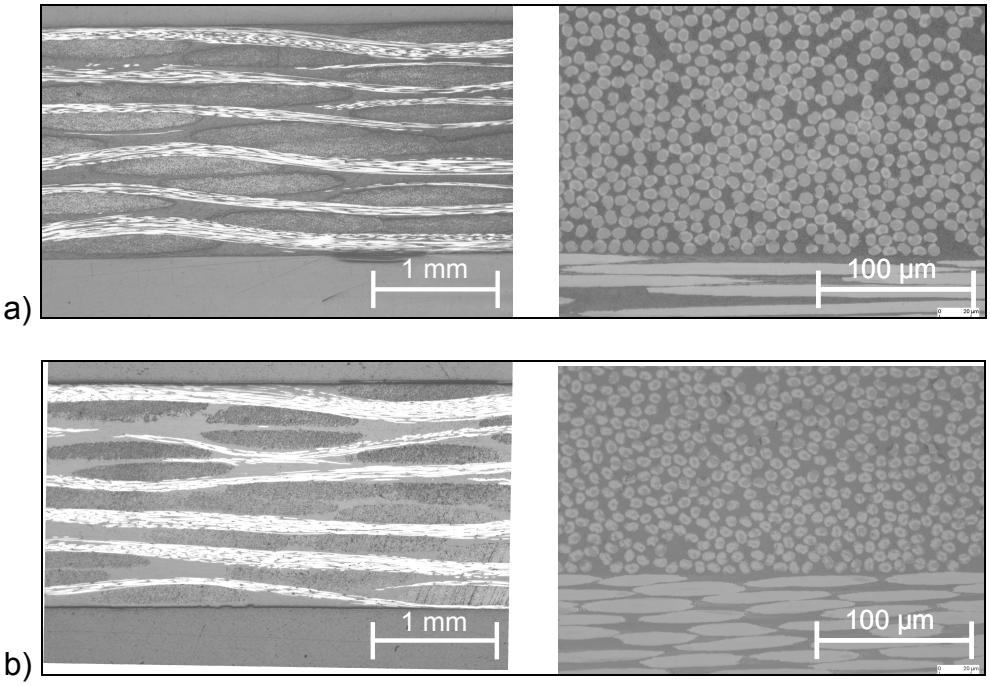

Figure 3.17: a) Micrographs of the used CF/PA66 (Fabric type: 5H Satin) and b) CF/PEEK (Fabric type: 5H Satin)

Furthermore, the non-woven fabric and the GF/CF/PA66, both manufactured in the autoclave, show a very good impregnation quality (Figure 3.18).

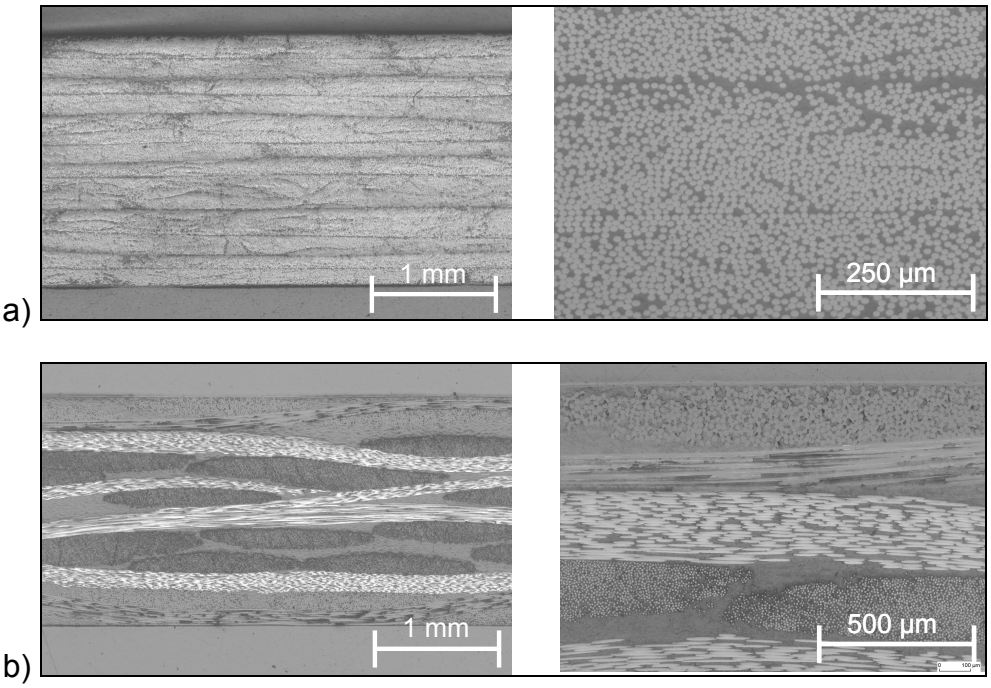

Figure 3.18: a) Micrographs of the used CF/PA66 (Fabric type: non-woven) and b) GF-4xCF-GF/PA66

Four types of metallic joining partners were used and they are presented in Table 3.5. The mechanical properties are given in chapter 8.1.

Table 3.5: Metallic joining partners and their composition in wt.%

AlMg3: (plate)

Designation			Composition					
Short form	DIN 1725-1	Int.Reg. Nr.	Al	Si	Fe	Mn	Mg	other
AlMg3	3.3535	AN5754	96	0.4	0.4	0.5	3.0	rest

AlMg0.4Si1.2: (plate)

Designation			Composition					
Short form	DIN 1725-1	Int.Reg. Nr.	Al	Si	Fe	Mn	Mg	other
AlMg0.4Si1.2	-	AA6016	97.5	1.0 - 1.5	< 0.5	< 0.2	0.3 - 0.6	rest

AlMgSi0.5: (U-shaped profile)

Designation			Composition				
Short form	DIN 1725-1	Int.Reg. Nr.	Al	Si	Mn	Mg	other
AlMgSi0.5	3.3206	6060	98.5 - 99	0.3 - 0.6	0.35 - 0.6	0.1	rest

DC01: (plate)

Designation			Composition					
Short form	DIN 17163	DIN 1623, part 1	Fe	C	P	S	Mn	other
DC01	1.0330	St 12	97.5	0.12	0.045	0.045	0.6	rest

All metallic joining partners have a thickness of 1.0 mm.

3.3 Design of experiments

Initially, the suitability of the developed equipment was verified and partially improved. The metal/fiber reinforced composite joints were made of metal (AlMg3, AlMg0.4Si1.2, and DC01) and carbon fiber reinforced polymer (CF/PA66 or CF/PEEK). The process was already shown in Figure 3.2. The top joining partner is heated by induction and transported to the consolidation unit (pressing tool) where the joint is cooled down and consolidated under pressure (Figure 3.5). A flow chart of all experiments to be performed is given in Figure 3.20. Now, the various treatments and testing conditions are given. For the performed testing series the settings are also given in chapter 5 next to the shear tensile strength figure.

3.3.1 Surface treatment and fabric type

The joining partners receive several surface treatments before joining (Table 3.6).

Table 3.6: Performed surface treatments

Treatment	Description	Abbreviation
Cleaning with acetone	Metal: Cleaning for three minutes in an acetone beaker placed in an ultrasonic bath Polymer: Wiped with acetone	AT
Blasting with aluminum oxide (white corundum)	Metal: Cleaning for 15 minutes in an acetone beaker placed in an ultrasonic bath. Blasting with aluminum oxide at a pressure of 6 bar Polymer: Wiped with acetone	corundum - AT
Alkaline pickling	Metal: Alkalic in 1 M NaOH for (15 min.); rinsing; pickling in 20 % nitric acid (3 min); rinsing with water Polymer: Wiped with acetone	alk. pickling
Acidic pickling	Metal: Submersion pickling in 65 % nitric acid (15 min); rinsing in water Polymer: Wiped with acetone	acidic pickling
Polishing	Metal: Polishing with sand paper of size 4000 Polymer: Wiped with acetone	polishing
Plasma cleaning	Metal: Compressed air supported atmospheric plasma cleaning for 5 seconds Polymer: Compressed air supported atmospheric plasma cleaning for 5 seconds	plasma

The composition of the white corundum is mainly Al_2O_3 with traces of other components (Table 3.7).

Table 3.7: Chemical composition of the corundum used for blasting

Element	Weight fraction (%)
Al_2O_3	99
SiO_2	0.02
CaO	0.05
Fe_2O_3	0.02
Na_2O	0.25
TiO	0.08

The diameter of the corundum is between 149 and 210 µm. The corundum was applied perpendicular to the surface for 10 seconds.

For plasma cleaning the following equipment settings were used:

- Generator voltage: 290 kV
- Generator current: 7.3 A
- Gas: pressured air at 4.5 bar
- Plasma pressured air: 60 mbar
- Distance sample to rotating plasma nozzle: 50 mm
- Cleaning time: 5 seconds

Various fabric types (Satin 5H, Plain weave, and NCF) were tested, also in different testing directions. As process condition the pressure was varied between 0.5 MPa and 3.0 MPa. Furthermore, the amount of additional polymer in the welding zone was varied between 0 µm and up to 300 µm.

3.3.2 Consolidation and cooling

In the state of the art section (chapter 2.2.3) already useful parameters for bonding materials with PA66 and PEEK are given. Therefore for AlMg3-CF/PA66 and DC01-CF/PEEK the following settings (Table 3.8) were used:

Table 3.8: Setting for consolidation and cooling

	AlMg3-CF/PA66	**DC01-CF/PEEK**
Pre-treamtent metal	Corundum blasting	Corundum blasting
Pre-treatment polymer	Acetone wiping	Acetone wiping
Holding temperature [°C]	280	370
Holding time [min]	7	7
Cooling rate [°C/min]	6	6

The experiments settings are schematically illustrated in Figure 3.19. By controlling the heating unit and by using the thermocouple in the pressing tool, the various holding temperatures (A), holding times (B), and cooling rates (C) can be adjusted and recorded.

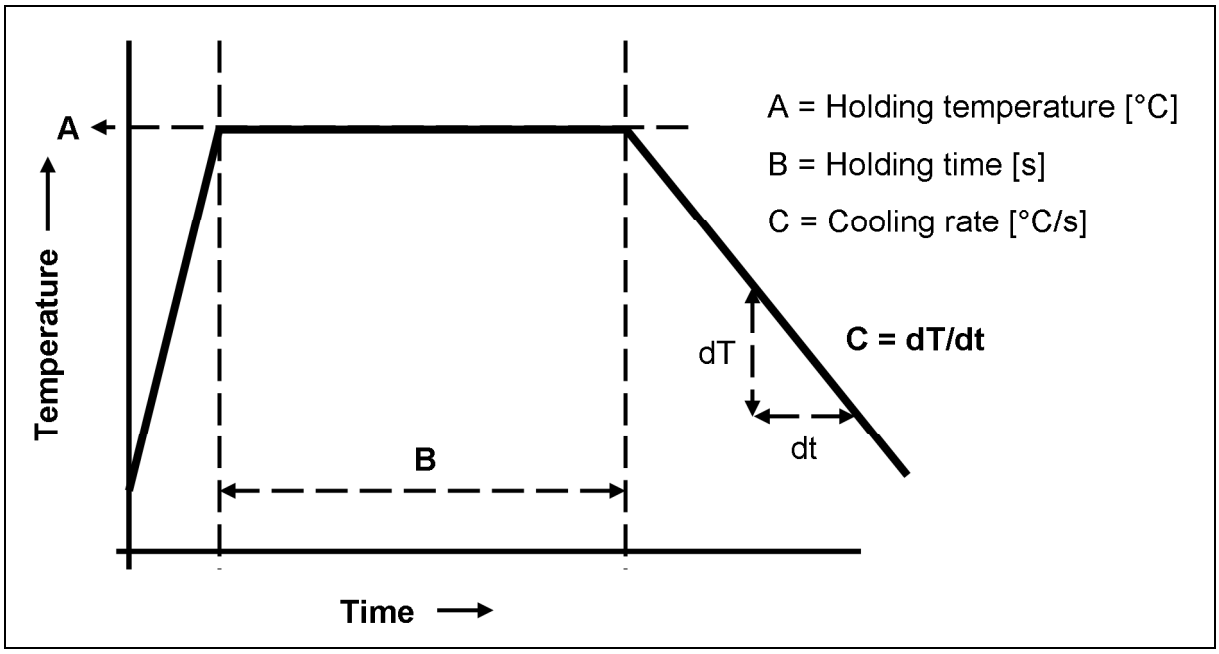

Figure 3.19: Definition of parameters for the consolidation and cooling rate experiments

3.3.3 Environmental conditions

The material compositions used for the galvanic corrosion investigations (chapter 3.1.5) are presented in Table 3.9.

Table 3.9: Material composition for the galvanic corrosion investigations

Material composition	Composite layout	Additional polymer layer thickness [µm]
1	CF/PA66	0
2	GF/CF/PA66	100
3	CF/PA66	100

Table 3.10 shows the various exploitation conditions of the samples.

Table 3.10: Material composition with various exposure conditions

Material composition			
	Exposure time [days]	7	21
	Environmental condition	Sea water	Demineralized water
1		X	X
2		X	X
3		X	X

For the environmental gas experiments two conditions were chosen, the standard one is normal air, and the second condition is nitrogen with a purity of 99.9 %.

Figure 3.20: Flow chart of different experimental settings and conditions

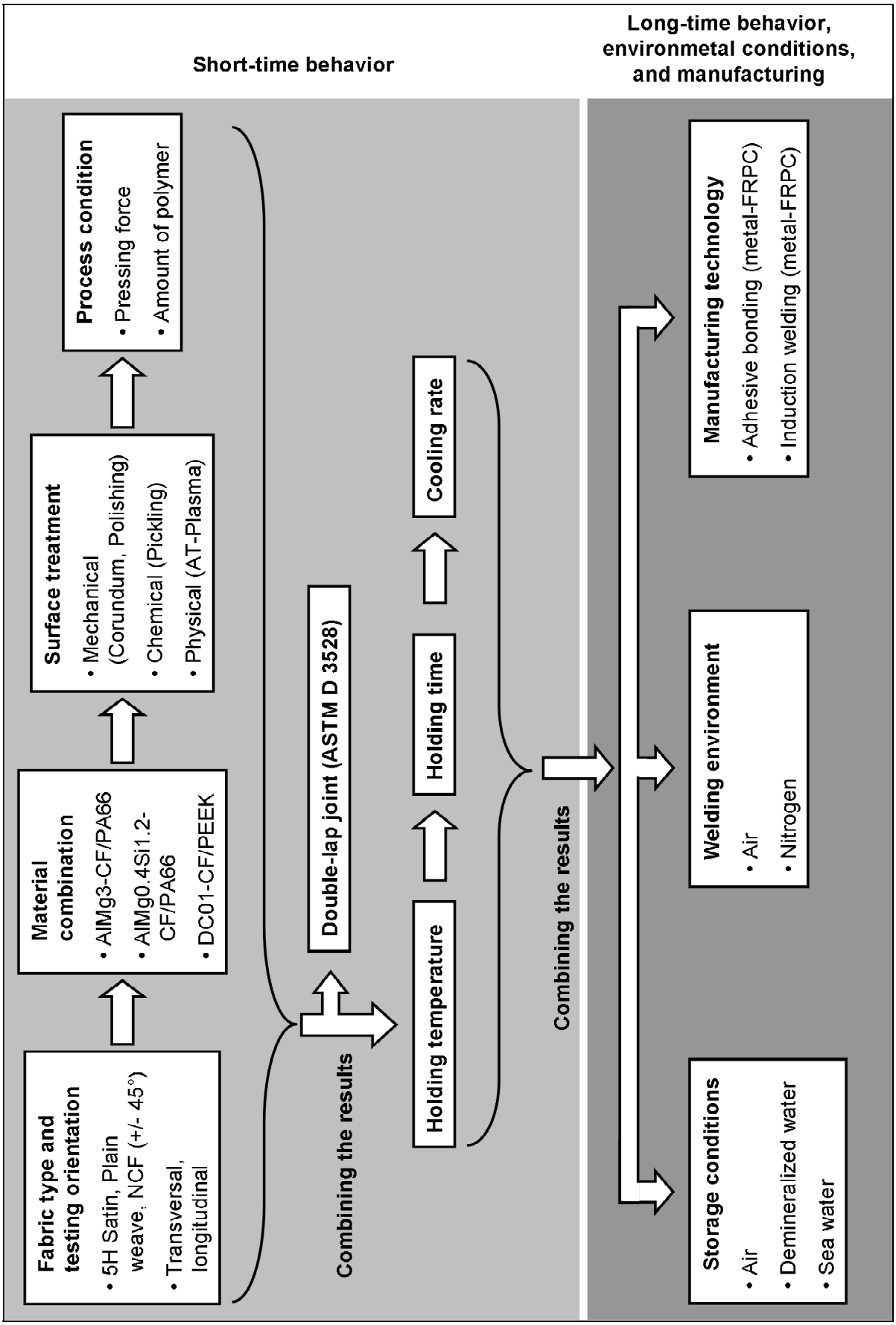

3.4 Protocol for manufacturing joints

The setting parameters required to perform the experiment and all relevant data of the welding materials (material type, manufacturing batch, geometry, etc.) are recorded and saved with their actual values in a measurement report (Figure 3.21).

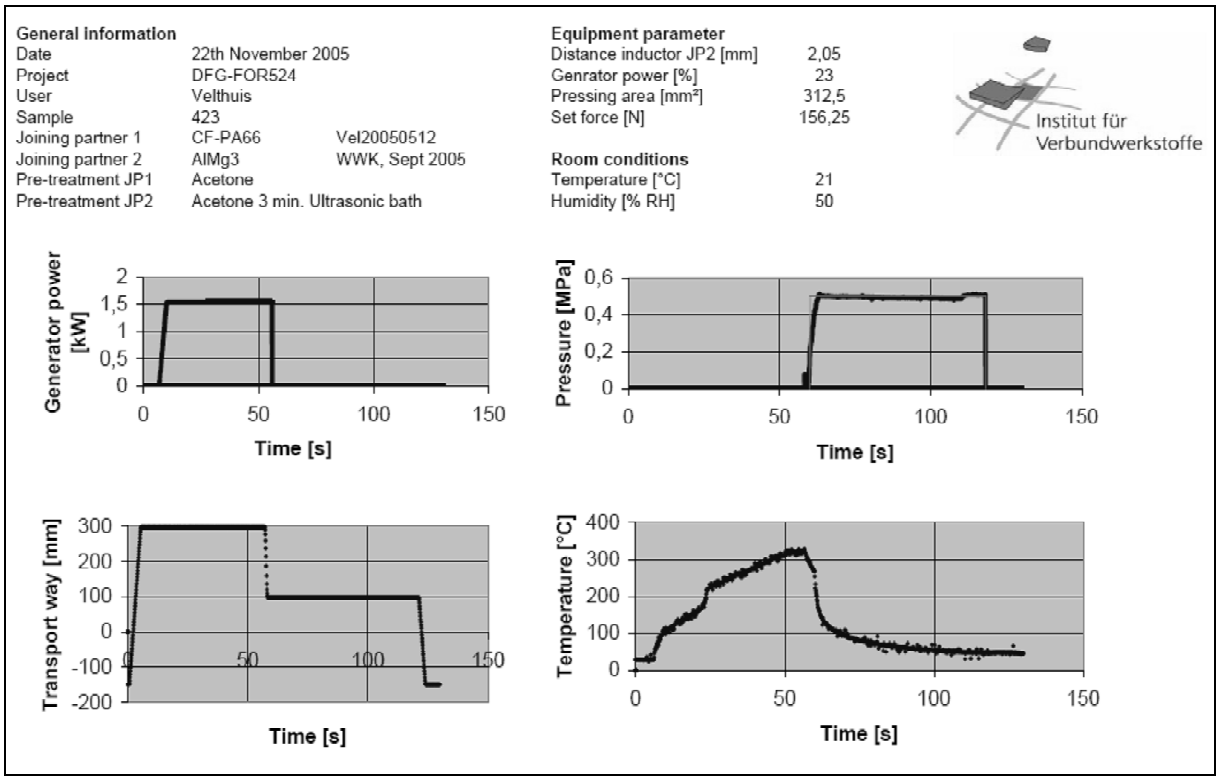

Figure 3.21: Measurement report for experiment documents

Each sample was marked, so the process conditions and the shear tensile strength could easily be assigned. Moreover, the micrographs of other samples in the test series can be compared.

3.5 Testing method and sample geometry

3.5.1 Single-lap joints in accordance with DIN EN 1465

To obtain the comparable testing results the experiments were performed according to norms (chapter 2.2.4). These norms clearly describe the requirement for the sample dimensions and the testing conditions for shear tensile strength testing. In some investigations in the literature the tests are performed in the style of the norm. Therefore, the sample geometry and the testing conditions need to be critically examined and taken into account before shear tensile strength values are compared and conclusions about the joining technique or the mechanical properties are drawn.

The sample geometry used with the characteristic dimensions is shown in Figure 3.22. This geometry is used for most of the experiments performed.

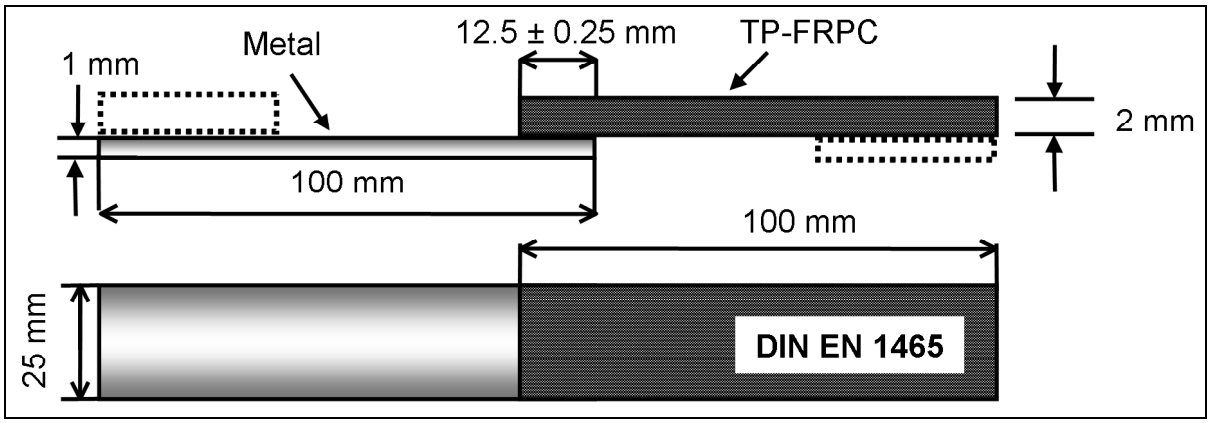

Figure 3.22: Single-lap joint in accordance with DIN EN 1465

Two plates with a length of 37.5 mm, a width of 25 mm, and a thickness of 1 and 2 mm were attached on both ends of the sample to ensure a parallel load introduction. The free clamping length therefore is 112.5 mm. The testing takes place at a speed of 1 mm/min.

The mechanical tests of welded samples were performed on a standard universal testing machine (1485, Zwick). Figure 3.23 shows a typical characteristic of the load-displacement diagram during the testing. The tensile force is determined in correspondence with the testing standard on the entire overlap area and so the bonding strength is determined according to DIN EN 1465.

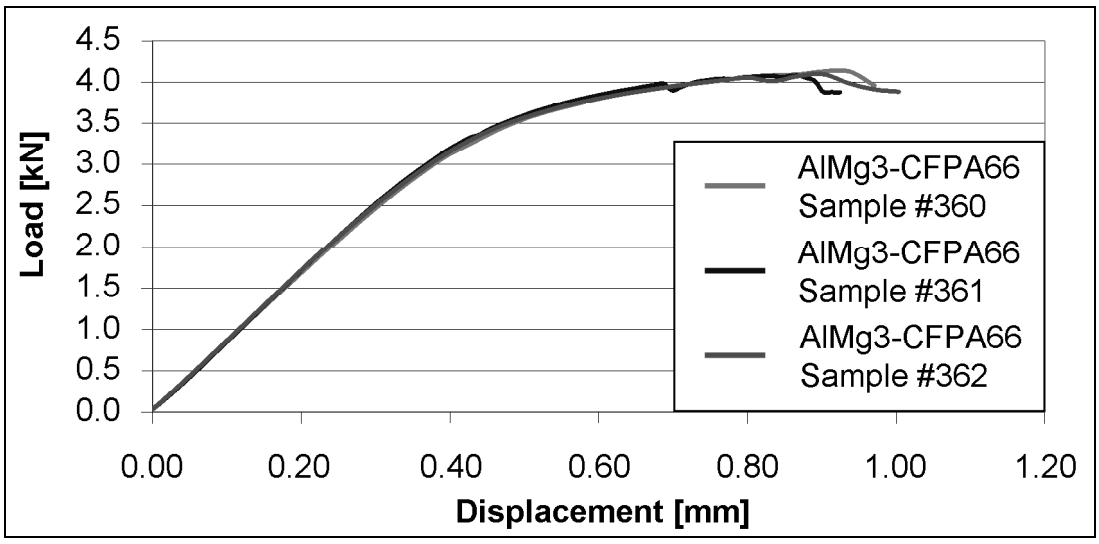

Figure 3.23: Load-displacement diagram of corundum blasted AlMg3 with an additional PA66-polymer sheet of 100 µm (sample #360, 361, and 362)

After applying loads on the sample it can be seen that at first a linear progress takes place, which is afterwards followed by deformation and brittle break of the joint. The given samples also show a high reproducibility. Besides the uneven stress distribution in the width of the sample (see Figure 2.9), the sample is deformed during the lap-shear testing. Once the sample starts bending peeling forces are introduced which reduce the measured shear tensile strength.

The surface fracture is validated in accordance with DIN EN ISO 10365 [134]. The typical failure modes of the adhesive are presented in Table 3.11.

Table 3.11: Designation of the main failure patterns

Failure pattern	Designation	Abbreviation
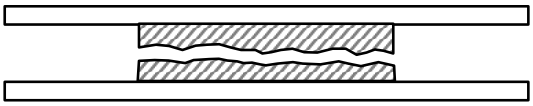	Cohesion failure	CoF
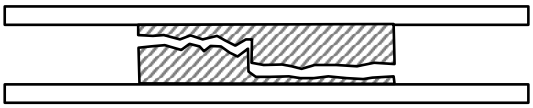	Near substrate cohesion failure (Weak boundary layer)	WBL
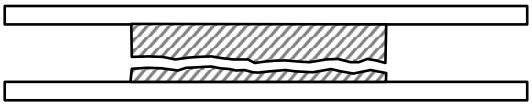	Near substrate cohesion failure (Weak boundary layer)	WBL
	Adhesion failure	AF
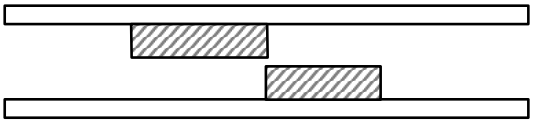	Adhesion failure	AF

If a mixed mode of pattern occurs, every sample should be validated with an estimated amount of failure pattern.

In the case of submerged samples, DIN 54456 is applied. Here four modes of failure are given:

- **Co**hesion **f**ailure (abbr. CoF)
- **A**dhesion **f**ailure (abbr. AF)
- Corrosion underneath of the adhesive or **b**ond line **c**orrosion (abbr. BC)
- **J**oining partner **b**reakage (abbr. JB)

To observe a change in the failure pattern, each tested sample is validated.

3.5.2 Double-lap joints in accordance with ASTM D 3528

During shear tensile testing of single-lap joints bending of the sample occurs. One way to prevent this bending is to bond two single-lap joints to obtain a double-lap joint (Figure 3.24). As no DIN-norm is available for the double-lap joints the ASTM D 3528 was used with the characteristic dimensions of the DIN EN 1465.

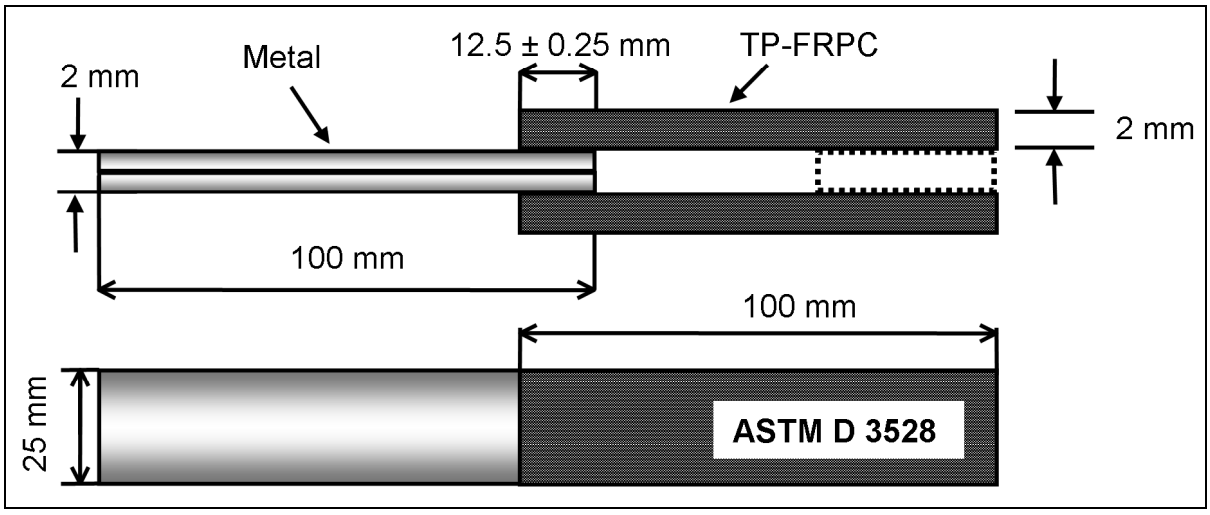

Figure 3.24: Double-lap joint in accordance with ASTM D 3528 [135]

One plate with a length of 37.5 mm, a width of 25 mm, and a thickness of 2 mm was positioned between both ends of the polymer sample to ensure a parallel load introduction after closing the hydraulic clamps of the testing machine. The free clamping length therefore is 112.5 mm. The testing took place at a speed of 1 mm/min. The adhesive used was Uhu Liquid Instant Adhesive.

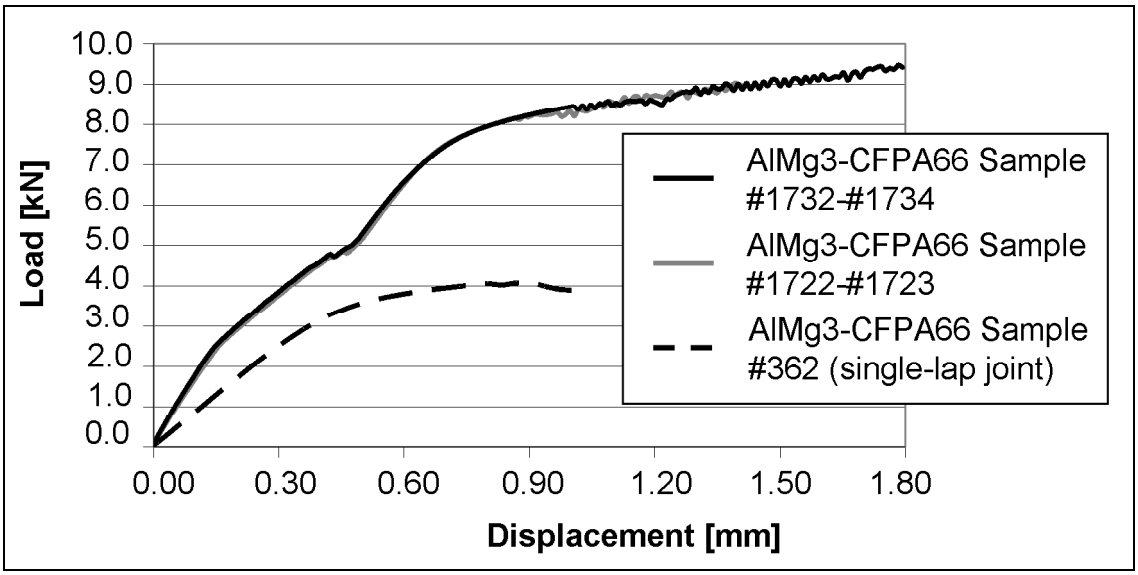

Figure 3.25: Load-displacement diagram of corundum blasted double-lap samples with an additional polymer sheet of 100 µm

As can be seen the linear-elastic section is increased, as the bending of the sample is reduced. The load at breakage of the double-lap joint is about two times higher than for the single-lap joints. After breakage also here bending can be observed.

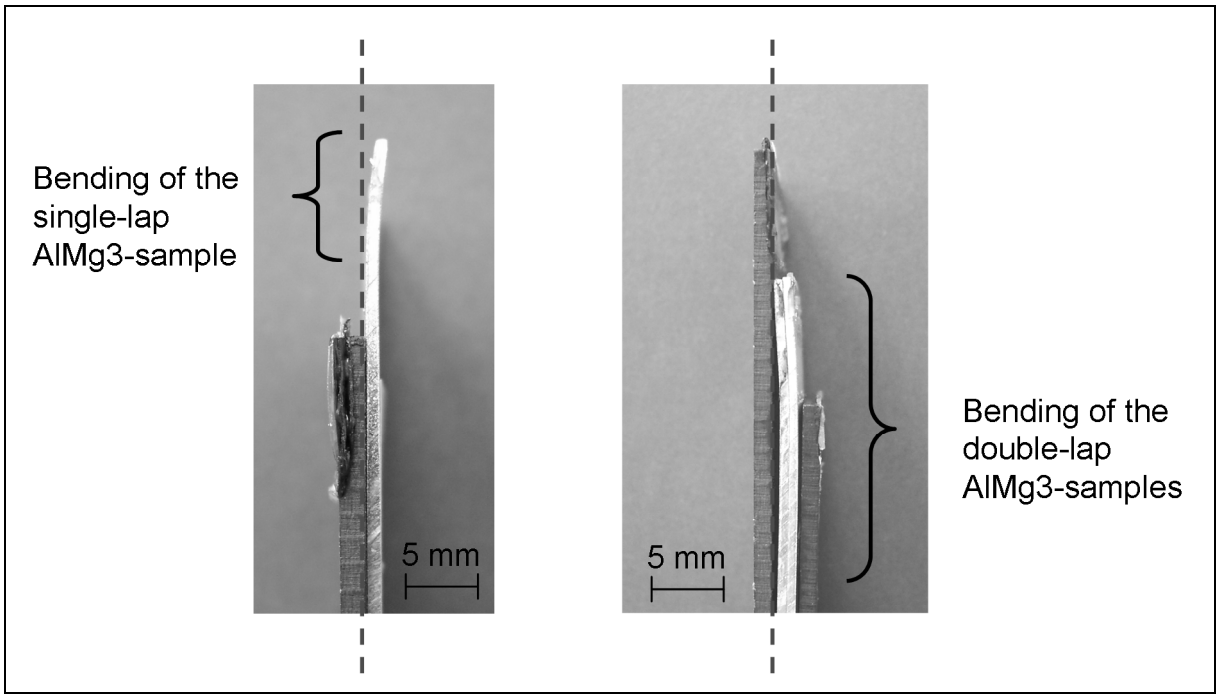

Figure 3.26: Bending in single and double-lap corundum blasted AlMg3-CF/PA66 samples after shear tensile testing

For this kind of materials the double-lap joint did not reduce the bending and did not increase the shear tensile strength.

3.6 Statistical analyses

A statistical analysis was performed with the standard deviation calculated according to formulas (3.1) and (3.2):

$$\sigma_{n-1} = \sqrt{\frac{\Sigma(x^2_{measurement} - x^2_{average})}{n-1}} \tag{3.1}$$

σ_{n-1} = the standard deviation

$x_{measurement}$ = measured value

$x_{average}$ = mean average

n = the amount of measured points

Now the 95 % confidence interval can be calculated according:

$$x = x_{average} \pm \frac{\sigma_{n-1} \cdot z}{\sqrt{n}} \tag{3.2}$$

z = random variable, which is 2.57 for 95 % confidence intervals with 6 samples (z = 2.26 for 10 samples)

4 Surface characterization, pre-treatments, and sample quality

Now the surfaces of both the metal and the polymer need to be characterized by topographical methods like scanning electron microscopy (SEM) and laser profilometer. The contact angle measurement method enables determining the disperse and polar contribution to wet an AlMg3-surface. Finally the chemical surface changes due to the surface treatments are analyzed and discussed.

4.1 Surface topography by scanning electron microscopy and laser profilometer

A laser profilometer (UBM) and a scanning electron microscope (JSM-6400, Jeol Inc.) were used for the surface characterization of the joining partners. These devices enable the generation of a topographical view of the surface structure and determination of the roughness parameter (R_a). This parameter is determined by the distance between the actual peak heights to the mean peak level over the length L_m (Figure 4.1).

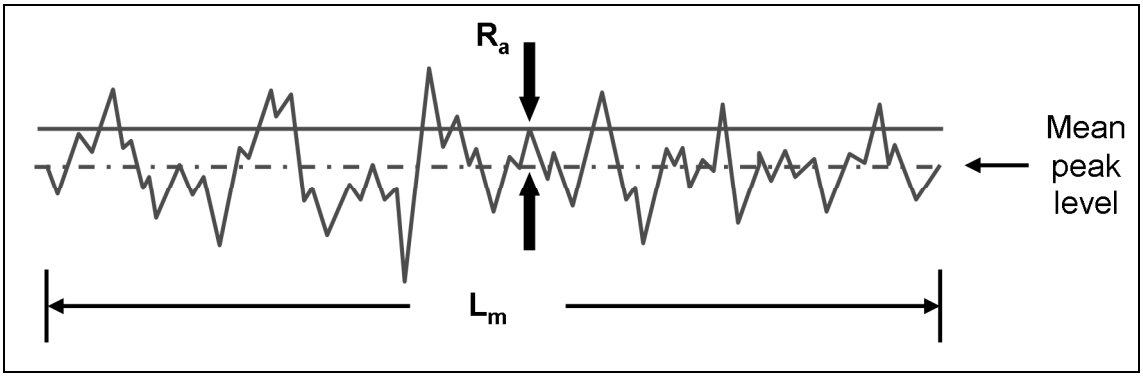

Figure 4.1: Schematic view of the roughness parameter R_a

Figure 4.2 to Figure 4.8 show the SEM micrographs and the surface topographies for the AlMg3 and DC01 surface treatments used [96, 136].

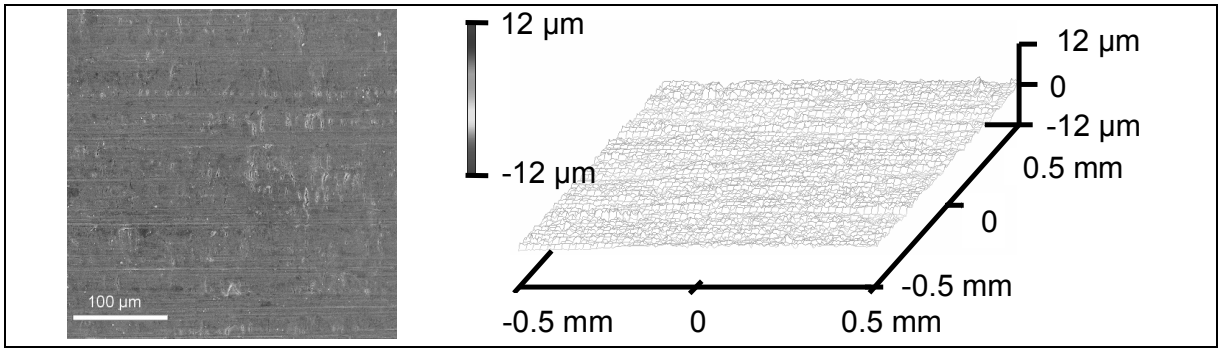

Figure 4.2: Topographical view of acetone treated AlMg3 with a R_a value of 0.35 µm

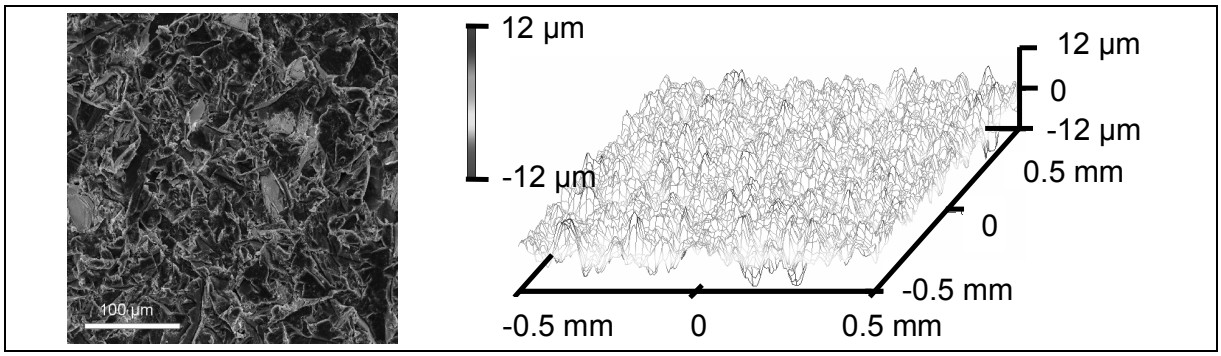

Figure 4.3: Topographical view of corundum blasted AlMg3 before joining with a R_a value of 2.17 µm

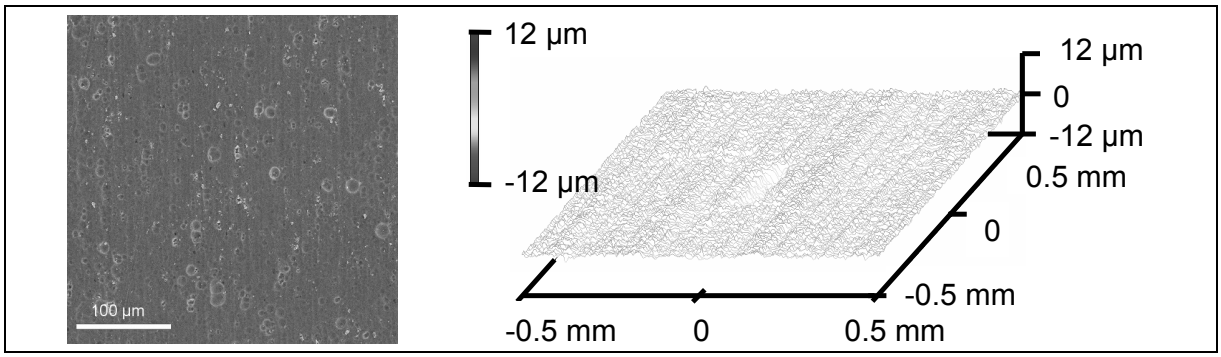

Figure 4.4: Topographical view of alkaline pickled AlMg3 before joining with a R_a value of 0.36 µm

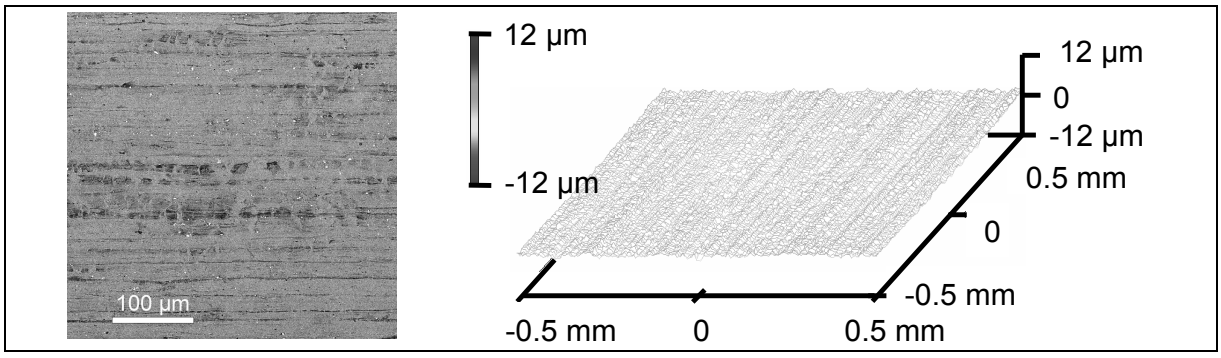

Figure 4.5: Topographical view of acidic pickled AlMg3 before joining with a R_a value of 0.37 µm

The surface of the corundum blasted sample (Figure 4.3) presents a uniform rough surface with height differences up to 20 µm. The AlMg3 with a R_a value of 2.17 µm has a clearly rougher surface than the acetone treated one (Figure 4.2).

Pickling leads to opening of holes on the surface due to the chemical reactions that take place (Figure 4.4, Figure 4.5). As can be seen the pickling does not influence the surface roughness of the AlMg3 if compared to the acetone treated samples.

Similar observations are made for the treated DC01-samples (Figure 4.6 - 4.8) [137].

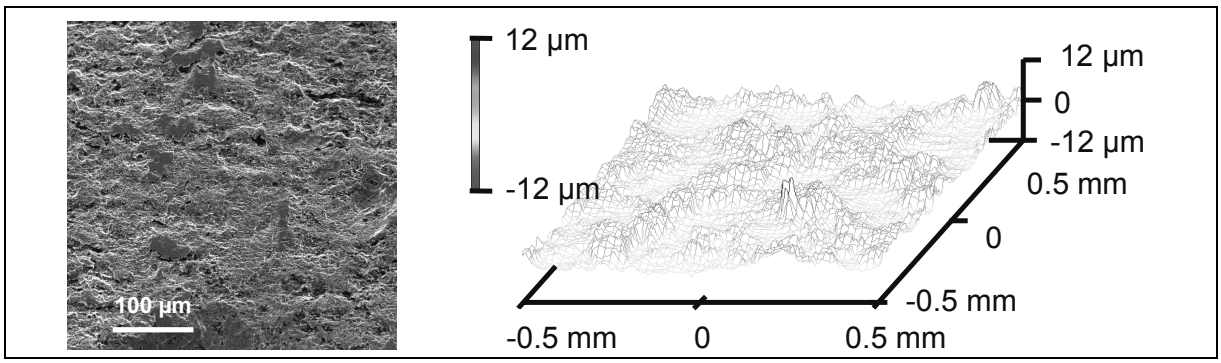

Figure 4.6: Topographical view of acetone treated DC01 before joining with a R_a value of 1.02 µm

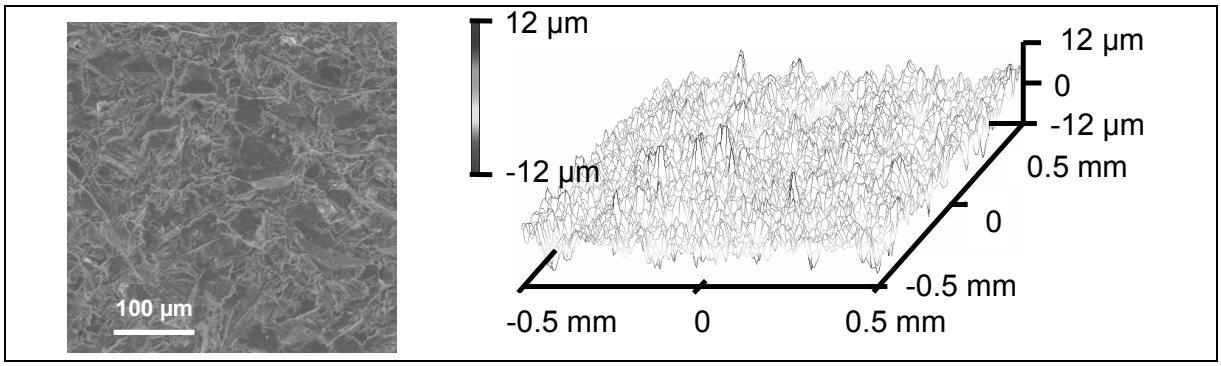

Figure 4.7: Topographical view of corundum blasted DC01 before joining with a R_a value of 2.14 µm

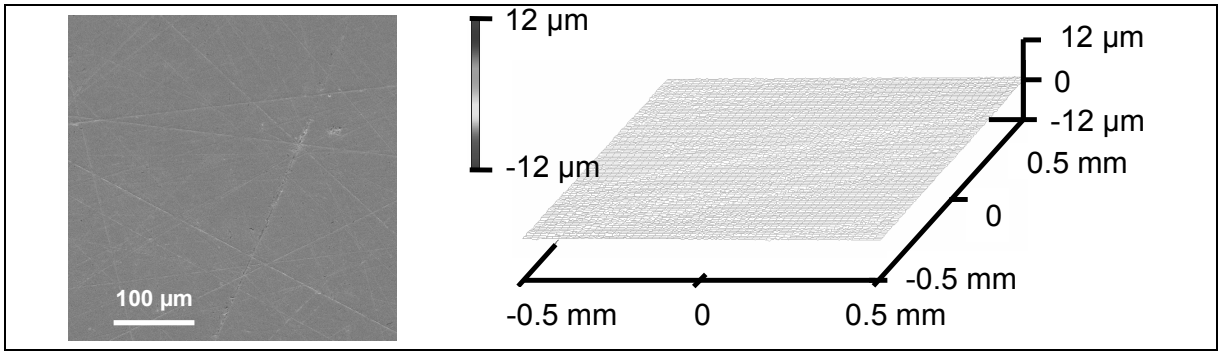

Figure 4.8: Topographical view of polished DC01 before joining with a R_a value of 0.07 µm

Transmission electron microscopic observations show that the pre-treatment methods for AlMg3-surfaces in adhesively bonded joints also have a large influence on the nano-structure in the bonding zone [96]. Acetone cleaned and corundum blasted samples show a sharp well-defined transition between the solid surface and the polymer. On the contrary the alkaline treated samples show a non-uniform thin filigree oxidized structure and the acidic pickled sample show a more uniform aluminum oxide layer of approx. 80 nm thick.

4.2 Contact angle measurements

Figure 4.9 illustrates a comparison of the surface tension resulting from the contact angle measurements [96, 136]. Here, the necessity of the surface treatment can be clearly seen, as the acetone treated AlMg3 with a comparable low surface energy is only partially able to be wetted by PA66. Moreover, the wetting behavior is a necessary but not the sole criterion for obtaining a good adhesion. This is illustrated by the alkaline pickled AlMg3-samples and the resulting low shear tensile strength.

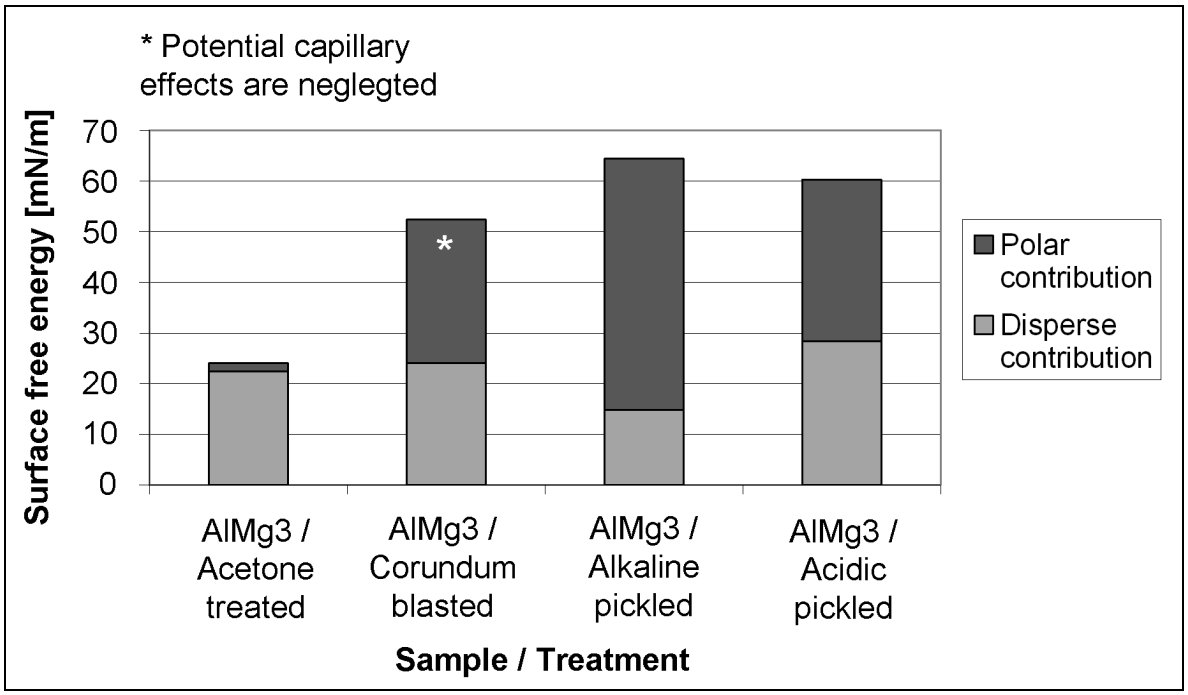

Figure 4.9: Comparison of the surface free energies of the AlMg3 in dependence of the surface treatment (according to Owens-Wendt-Rabel-Kaelble)

Also for the polymeric joining partner the contact angle was measured. From acetone wiped and atmospheric plasma treated samples the surface energies were determined (Figure 4.10).

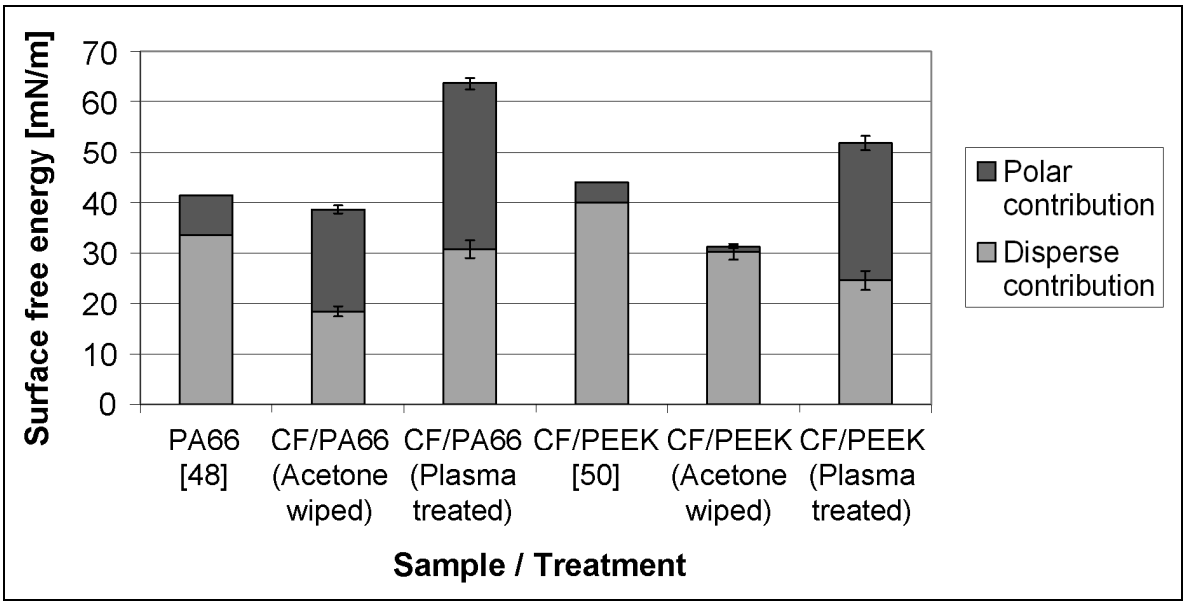

Figure 4.10: Comparison of the surface free energies of CF/PA66 and CF/PEEK in dependence of the surface treatment (according to Owens-Wendt-Rabel-Kaelble)

Due to the carbon fiber reinforcing slightly deformed drops of liquid on the surface of the CF/PA66 and CF/PEEK appeared. This explains the deviation of the measured value compared to those given in the state of the art. For PA66 the entire surface energy equals the literature value of 41 mN/m [48], the single components however (polar contribution: 33.6 mN/m, disperse contribution: 7.8 mN/m) are slightly different. For CF/PEEK the difference to the literature values in [50] (polar contribution: 40 mN/m, disperse contribution: 4 mN/m) is larger.

In general, the atmospheric plasma treatment tends to result in a large increase of the polar contribution on the surface free energy. The influence of this effect on the shear tensile strength is given in chapter 5.3.

4.3 X-ray photoelectron spectroscopy (XPS) recordings

The adhesive properties of a metal surface respectively oxide-layer is determined by the molecular and atomic interactions with functional groups of the used polymer. By applying mechanical or chemical treatments the metal surface is activated as the chemical reactivity is increased. The amount of carbon on the surface is frequently used as an indicator for the amount of organic contamination. A method to determine the element concentration is by means of X-ray Photoelectron Spectroscopy (XPS). With the XPS soft X-rays bring electrons out of the inner shells of the atoms due to

excitation. Electrons out of the outer shells can therefore leave their orbit without energy losses. The kinetic energy of these electrons depends on the bonding energy of their specific shell and is therefore characteristic of the emitting atom. Figure 4.11 show the XPS measured surface concentrations in dependence of the surface treatment [96, 136].

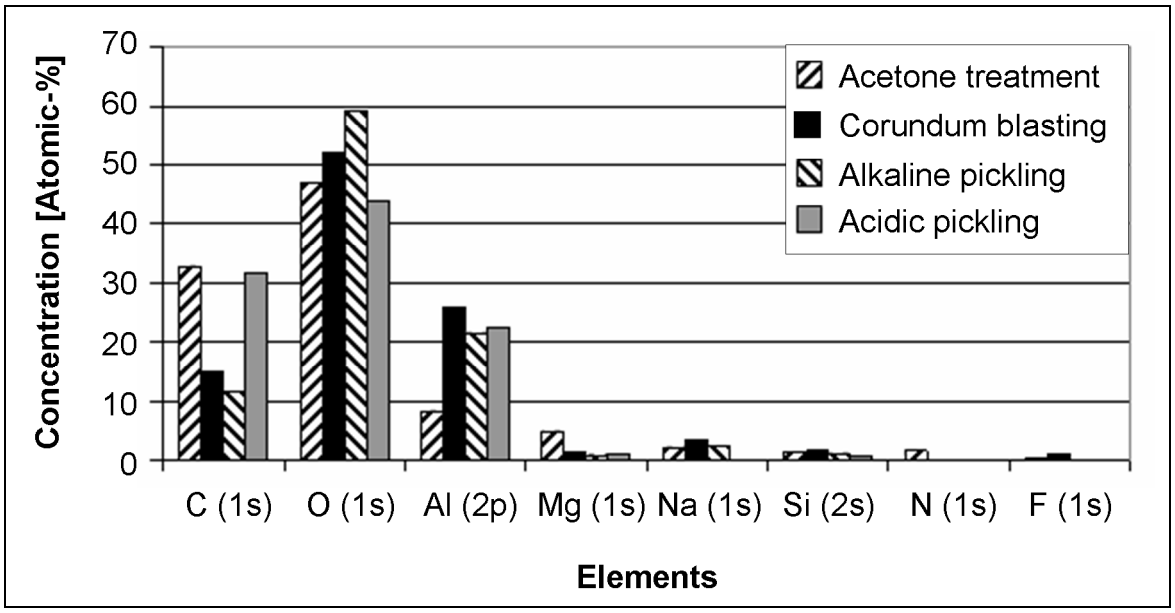

Figure 4.11: Surface concentrations on the treated AlMg3-surfaces, measured with XPS

A higher surface concentration of aluminum is achieved by both the abrasive effect of the corundum blasting and the chemical removal of the alkaline pickling. This means that by these methods relative clean, and therefore active, surfaces are generated.

4.4 Thermal elastic load analysis (TSA) recordings

The thermal elastic load analysis uses the Kelvin-effect and is based on the highly accurate temperature measurement during cyclic loads [138]. In the linear elastic load area and in adiabatic conditions the surface temperature during dynamic load cycles is determined. Now, the main loads and the main elongation differences can be determined. In the case of metal/composite joints the TSA-measurements can be used to determine the load introduction and distribution in the joining partners. The induction welded sample (#257, corundum blasted AlMg3) shows in Figure 4.12 that the elongation is homogenous over the sample width, which means that loads are homogenously introduced into the sample [81]. The experiment was performed by Bos and Renz.

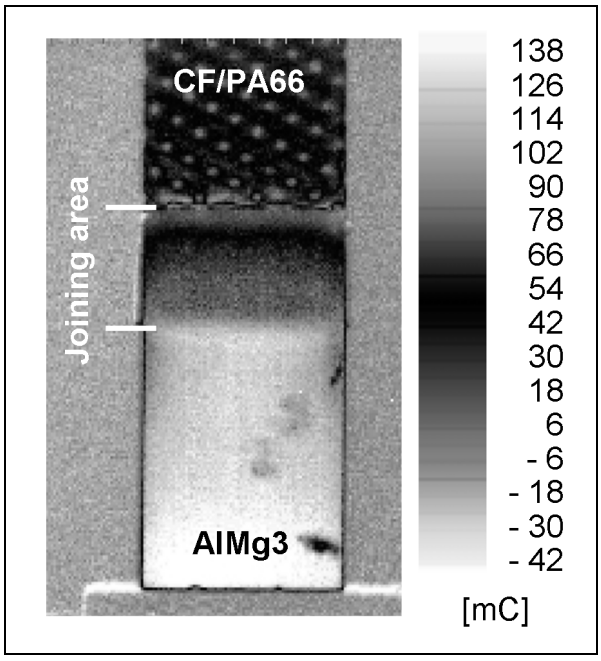

Figure 4.12: Homogeneous load distribution in the induction welded sample (#257) This analytic method can also be used as a non-destructive testing method to detect the damaged area [138].

5 Results

In this chapter the results are given for the various experiments performed. Figure 5.1 shows an example of a manufactured induction welded sample.

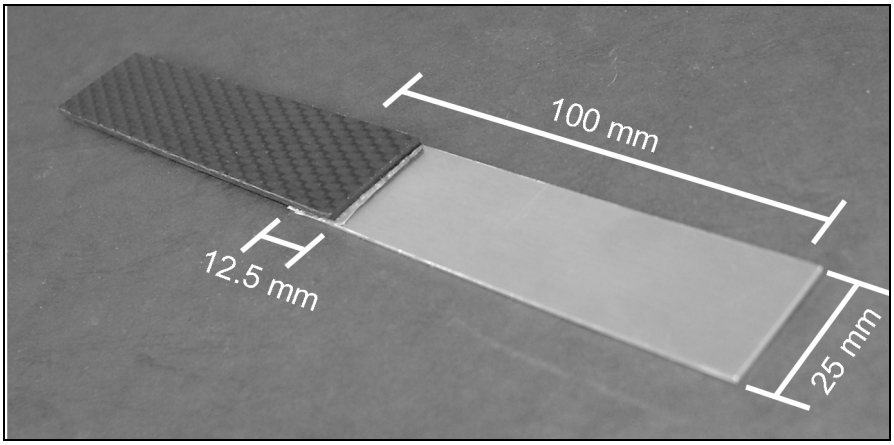

Figure 5.1: Sample made out of AlMg3-CF/PA66 with a polymer sheet of 100 µm between both joining partners

To determine the temperature in the joining area, a thermal wire was positioned between both joining partners. Figure 5.2 shows the temperature evolution in the joining area during the process time.

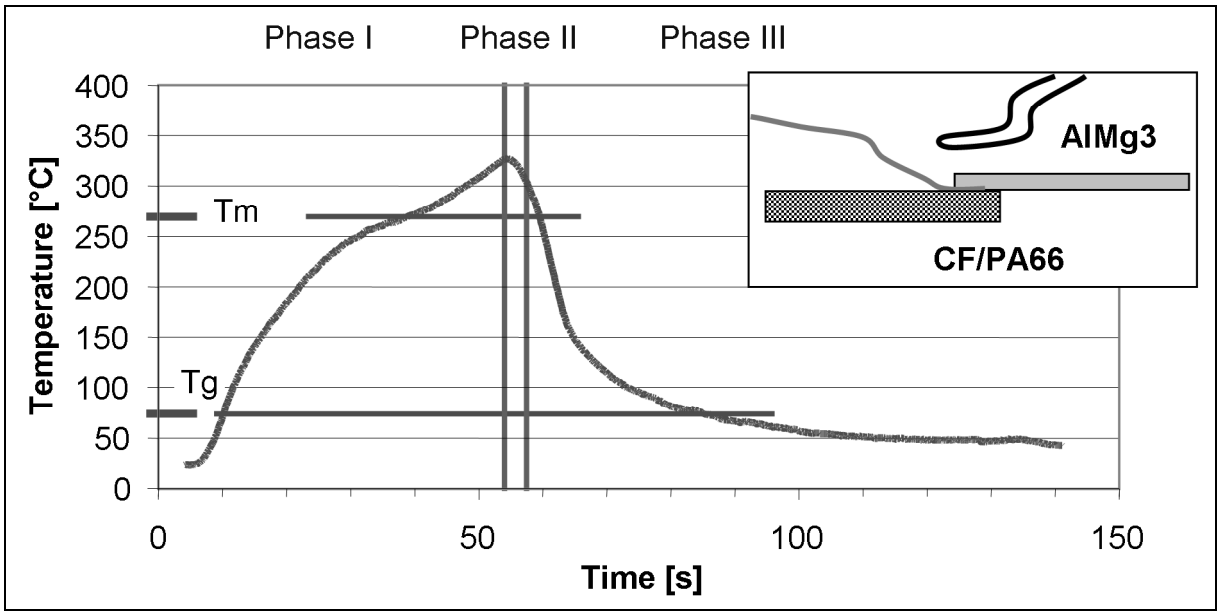

Figure 5.2: Measured temperature evolution in the joining area (AlMg3-CF/PA66)

Also shown are the melting point (T_m) of the polymer used and its glass transition point (T_g). With the set equipment parameters, of generator power: 1.2 kW and inductor distance to the laminate: 2 mm, the heating was performed in 52 s.

5.1 Influence of the testing orientation and the type of fabric

Fundamental tests with CFRPC-samples, using a different testing orientation, were performed to determine the possible influence of dissimilar forces of the weft and warp rovings, which are induced during the fabric manufacturing.

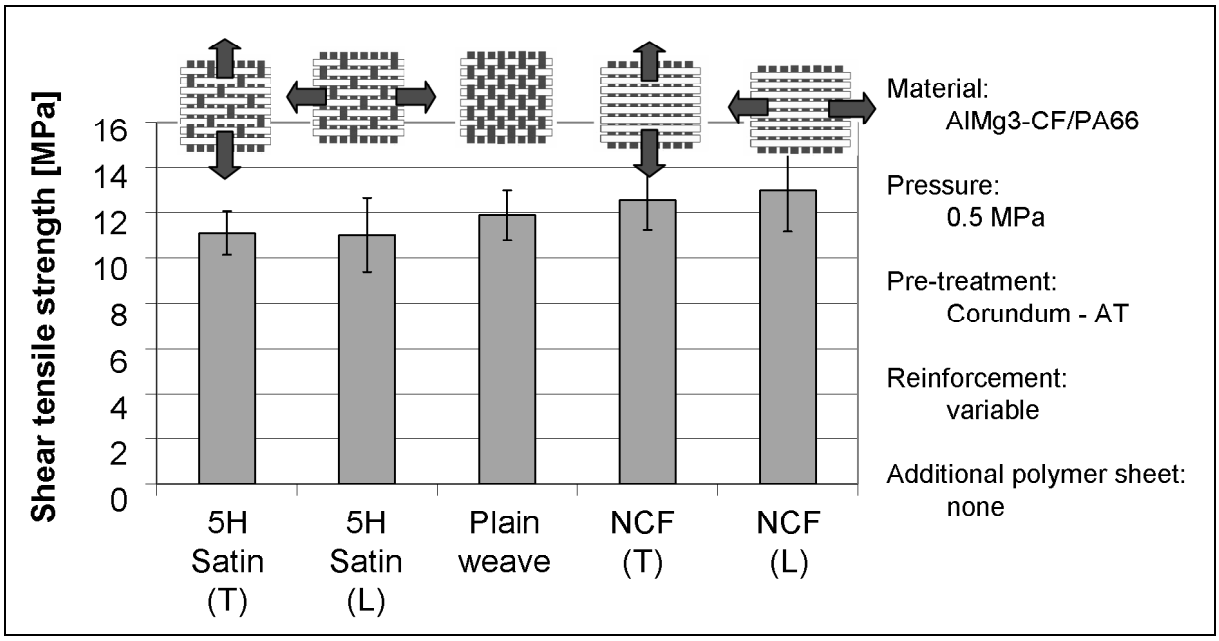

Figure 5.3: Influence of the testing orientation and the type of fabric on the shear tensile strength

The fabric used is orthogonal balanced. This means that the fiber amount in both weft and warp direction is equal. The amount of knots is also identical in both directions. Figure 5.3 summarizes the corresponding results. It shows no dependence of the fiber orientation relative to the testing force. By using two different types of fabrics (5H Satin and plain weave) the influence of the matrix rich areas between the knots in the fabric can be examined more closely. Figure 5.3 schematically shows the difference between these two fabrics. It can be seen that the plain weave has more intersections and, therefore, a higher amount of matrix rich areas. It is to be expected that with the same process conditions, the shear tensile strength increases when the amount of intersections increases. Also the NCF shows similar shear tensile strength values, although no polymer rich knots are available. Here the carbon fibers are more easily moved out of the joining area and a weak boundary layer is formed.

5.2 Influence of the mechanical and chemical surface pre-treatment of the metallic joining partner

The shear tensile strength resulting from the various surface pre-treatments is shown in Figure 5.4. The error bars show 95 % confidence intervals. The diagram is based on 6 measurements per adjustment.

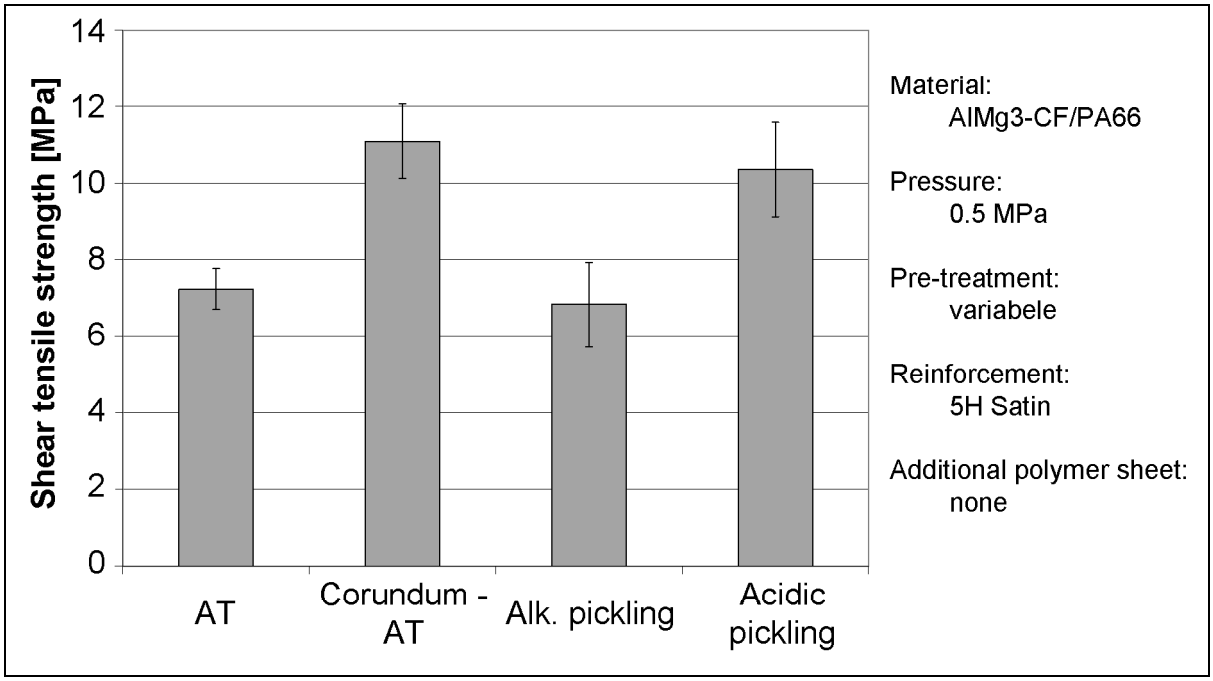

Figure 5.4: Influence of the surface pre-treatment on the shear tensile strength (AlMg3-CF/PA66)

It can be seen that corundum blasting and acidic pickling leads to an increase of the shear tensile strength. An acetone treatment, with or without alkaline pickling, clearly results in lower values. It was shown that a higher surface roughness and a chemical acidic pickling with HNO_3 (see Table 3.6, page 59) leads to an increase of the shear tensile strength.

With the help of this observation, it can be concluded that several bonding mechanisms have a contribution to the shear tensile strength. This difference in the mechanical load capacity of the joints has a direct correspondence to the photographical analyses. Meaningful photos are shown in Figure 5.5.

Process conditions	Photographs	Fracture type
Pre-treatment: 3 min. AT Pressure: 0.5 MPa Shear tensile strength: 7.2 MPa	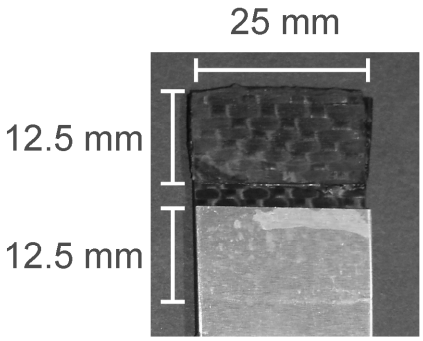	AF (100 %)
Pre-treatment: Corundum – AT Pressure: 0.5 MPa Shear tensile strength: 11.0 MPa	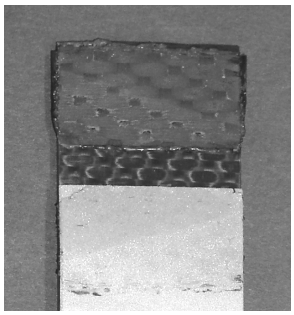	AF (95 %) WBL (5 %)
Pre-treatment: Alk. Pickling Pressure: 0.5 MPa Shear tensile strength: 6.2 MPa	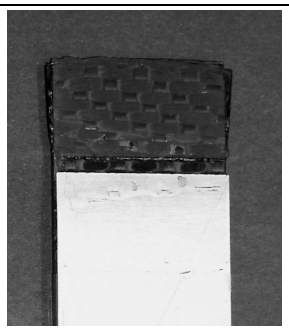	AF (100 %)
Pre-treatment: Acid pickling Pressure: 0.5 MPa Shear tensile strength: 9.6 MPa	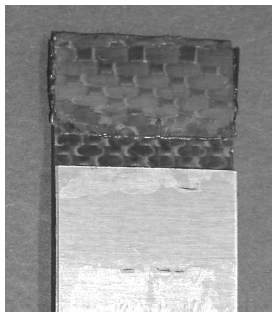	AF (97 %) WBL (3 %)

Figure 5.5: Surface fracture of samples with different pre-treatments

It can be seen how pre-treatment (see Table 3.6, page 59) has an influence on the welding zone formation. The more polymer remains on the metal surface, the higher is the shear tensile strength. This illustrates the need for a high enough amount of polymer in the welding zone.

Comparable surface treatment investigations were also performed with the DC01 and CF/PEEK combination. The influence of the treatment on the shear tensile strength is presented in Figure 5.6.

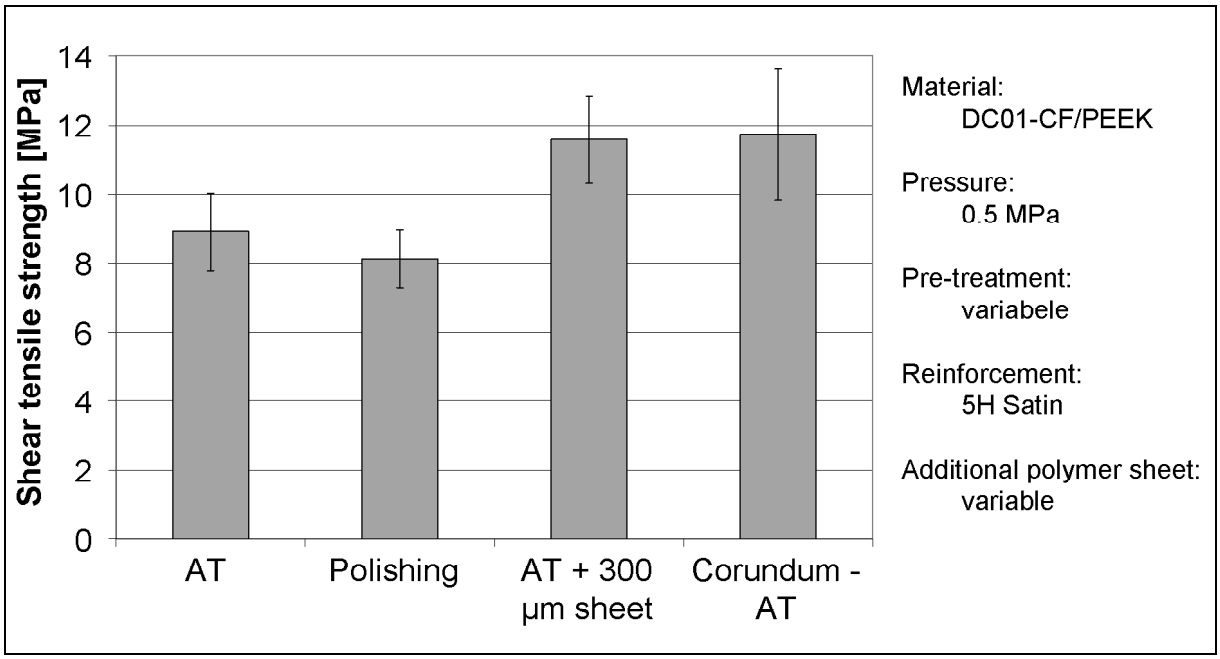

Figure 5.6: Influence of the surface pre-treatment on the shear tensile strength (DC01-CF/PEEK)

Here it is also observed that the various bonding mechanisms contribute to the steel/PEEK bonding. Through polishing a very flat and shinny surface is created (R_a-value is 0.1 µm), the shear tensile strength is the same as the acetone treated one (R_a value is 0.3), but less than for the corundum blasted one (R_a value is 2.2). Pickling could also be performed for DC01, but corundum blasting was chosen to be comparable to the AlMg3-treatments.

The topographical and chemical analyses of AlMg3 (see chapter 4) are summarized in Table 5.1 to analyse the influence of the surface treatment on the shear tensile strength.

Table 5.1: Summary of the topographical and chemical analyses of AlMg3 after surface treatment

Treatment	Surface roughness R_a [µm]	Surface energy (disperse amount) [mN/m]	Surface energy (polar amount) [mN/m]	Element concentration [atomic-%]				Shear tensile strength [MPa]
				C (1s)	O (1s)	Al (2p)	Mg (1s)	
Acetone	0.35	22.4	1.6	33	47	8	5	7.2
Corundum blasting	2.2	24.0	28.4	15	52	26	1	11.1
Alkaline pickling	0.36	14.8	49.5	11	59	22	1	6.8
Acidic pickling	0.37	28.4	31.8	32	44	22	1	10.3

First of all, it can be concluded from corundum blasting and acidic pickling that increasing the surface roughness plays a minor role on the shear tensile strength. The chemical and physical changes due to the treatment are more important. Apparently, also the disperse amount of the surface energy does not influence the bonding properties; the polar amount however is measured between 1.6 and 50 mN/m. The polar amount of the CF/PA66 is approx. 20 mN/m and equals more or less the value of the corundum blasting and the acidic pickling treatment. For the elemental analyses no exact conclusion can be drawn. Neither the carbon, oxygen aluminum, and magnesium atoms show a tendency that fits to the obtained shear tensile strength values. From these observations, it can be concluded, that besides the mechanical interlocking in the holes and pores on the surface also the physical bonding mechanisms appear.

The influence of the polar contribution on the shear tensile strength is also illustrated by welding glass fiber reinforced polypropylene on corundum blasted AlMg3 (Table 5.2).

As a result from the corundum blasting treatment the same surface conditions for both samples are available. As can be seen the disperse amount of polypropylene equals the amount of the PA66, the main difference is the polar contribution.

Table 5.2: Comparison of surface parameter of polypropylene and CF/PA66 and shear tensile strength of welding GF/PP to AlMg3

	Surface energy (disperse amount) [mN/m]	Surface energy (polar amount) [mN/m]	Surface roughness [µm]	Shear tensile strength after bonding to AlMg3 [MPa]
Polypropylene GF/PP	30.5	0.7	2.2	2.8 ± 0.5
PA66 CF/PA66	33.6	7.8	2.2	11.1 ± 1.0

The physical bonding mechanisms can be influenced by treating the polymer with atmospheric plasma and by the processing conditions (pressure, temperature, and time).

5.3 Influence of the physical surface pre-treatment of CFRPC and metal

To influence the surface structure of CFRPC preliminary experiments with plasma-activation were performed. The AlMg3 and DC01 were also pretreated with the plasma activation. The results are shown in Figure 5.7.

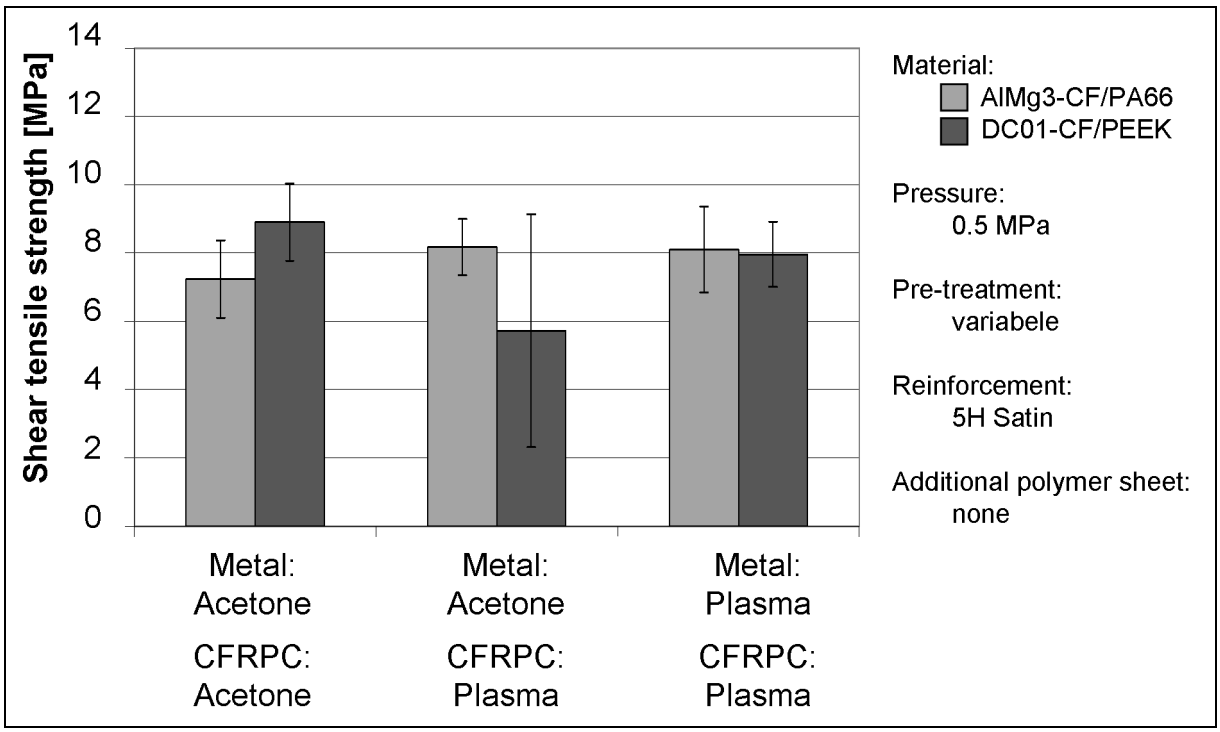

Figure 5.7: Influence of the plasma activation on the shear tensile strength (AlMg3-CF/PA66 and DC01-CF/PEEK

It can be seen that atmospheric plasma treatment leads to a higher shear tensile strength for AlMg3-CF/PA66, although this effect is less than that given in the state of the art section. The improved shear tensile strength is explained by surface cleaning and creation of active groups on the polymer (activation). The plasma treatment of the AlMg3 did not result in an increase of the shear tensile strength. For the DC01-CF/PEEK-bonding no improvement after the plasma cleaning is observed. The confidence intervals got larger for the acetone treated DC01 in combination with the plasma cleaned CF/PEEK; after plasma cleaning of both the DC01 and CF/PEEK the confidence interval for the measured shear tensile strength are in a normal range again.

5.4 Influence of the pressing force

As shown in [139], the thickness of the polymer in the joining area has a significant influence on the achievable bonding strength. Increasing the adhesive thickness leads to an increase of the tensile and shear modulus, which results in a higher bonding strength. As the polymer is melted during welding, external forces easily influence the polymeric layer thickness. Correspondingly, a change in the joining pressure results in a change in the polymeric layer thickness, and therefore affects the shear tensile strength (Figure 5.8).

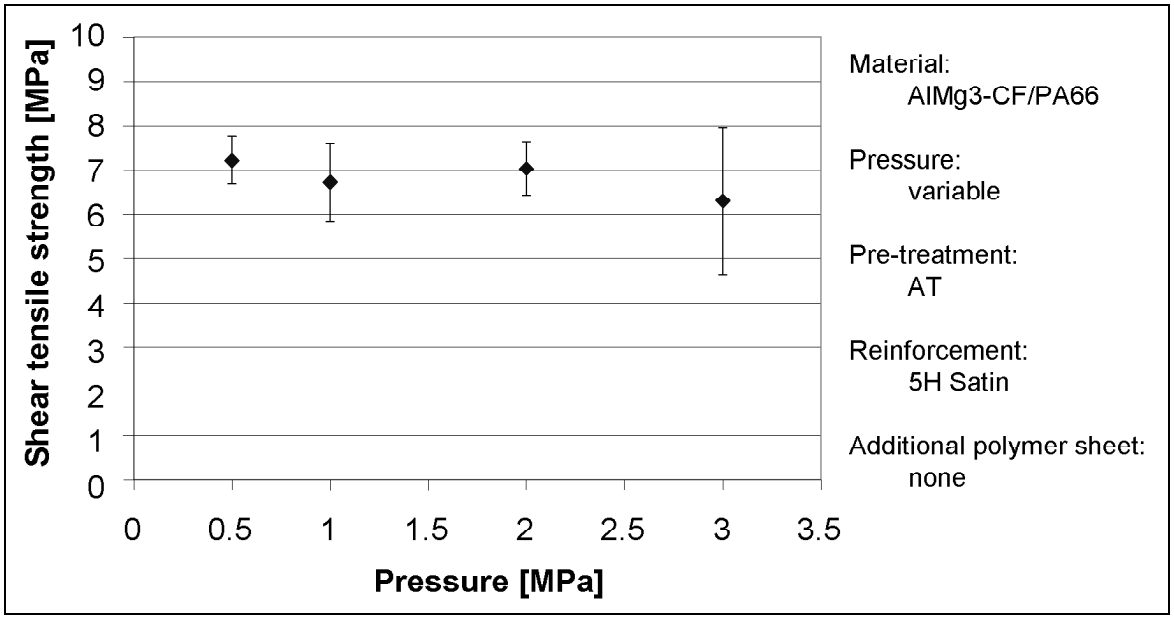

Figure 5.8: Influence of the pressure on the shear tensile strength of acetone treated samples

A reduced pressure leads to slightly higher shear tensile strength. Due to the higher pressure the polymer flows towards the edges and, therefore, is not able to bond to the metal.

5.5 Influence of the aluminum type

Aluminum is available in many alloys. In Europe AlMg3 is common; in North-America the common aluminum alloy type is AlMg0.4Si1.2. This type was also used to perform shear tensile strength measurements. The results are given in Figure 5.9.

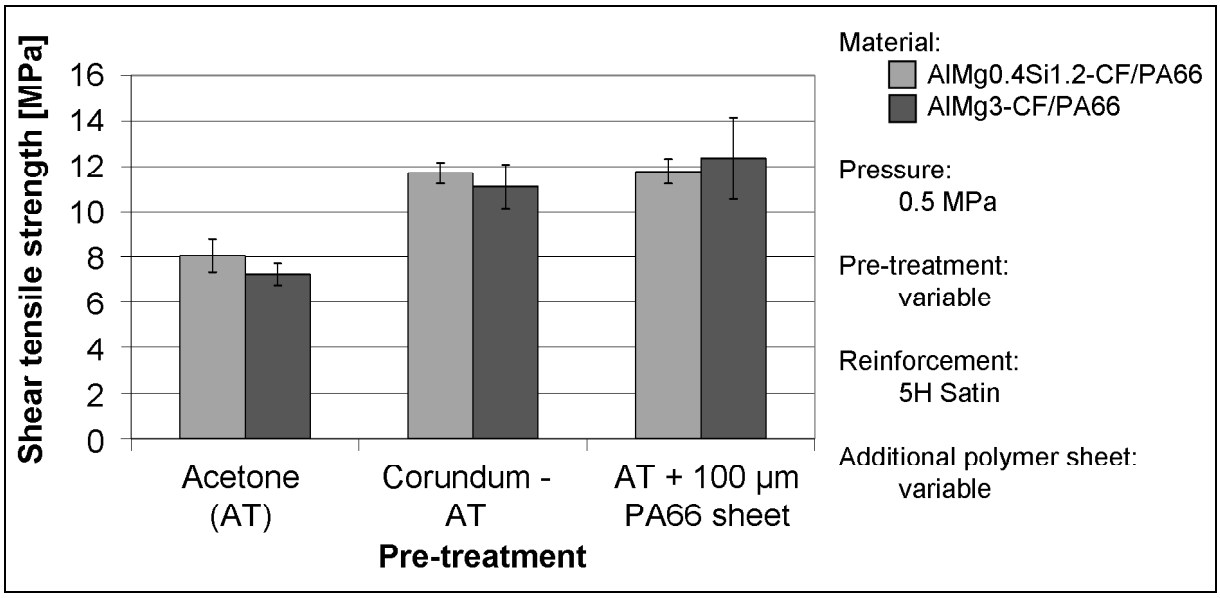

Figure 5.9: Shear tensile strength of AlMg0.4Si1.2-CF/PA66 in dependence of the pre-treatment

In the case of AlMg0.4Si1.2 the shear tensile strength is similar to that of AlMg3, although the mechanical properties (see chapter 8.1) of the AlMg0.4Si1.2-samples are lower. Apparently, the alloy composition has no influence on the shear tensile. An explanation is that the aluminum amount of in both cases above 97%.

5.6 Polymer intermediate layer

To determine the influence of a polymer in the joining area, additional polymer in form of a PA66-film was inserted between the joining partners. The investigated configurations are summarized in Table 5.3.

Table 5.3: Experimental configurations with a polymer intermediate layer of PA66

Joining pressure [MPa]	Additional sheet thickness [µm]	Micrograph of the joining area	Average layer thickness [µm]
0.5	50	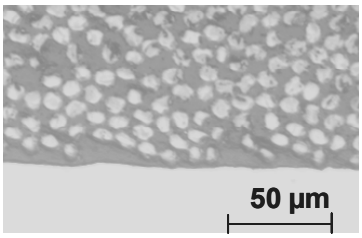	0 - 5
0.5	75	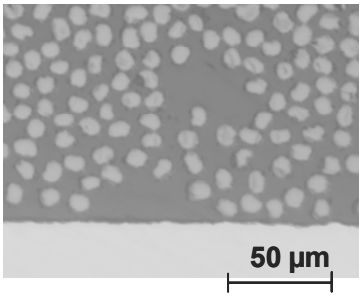	0 - 10
0.5	100	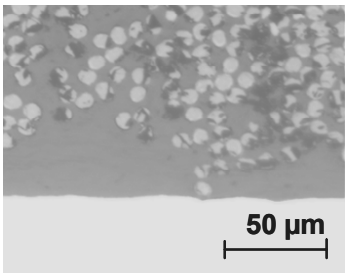	5 - 20
0.5	200	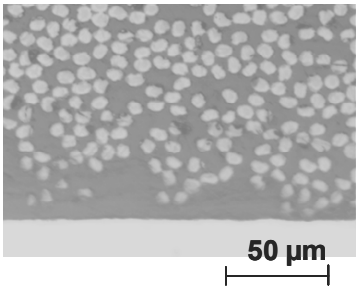	5 - 20

Table 5.3 shows that due to the higher amount of polymer in the joining zone less carbon fibers are close to the metal surface and, therefore, the entire contact area can be used for the adhesion. The influence on the shear tensile strength is shown in Figure 5.10.

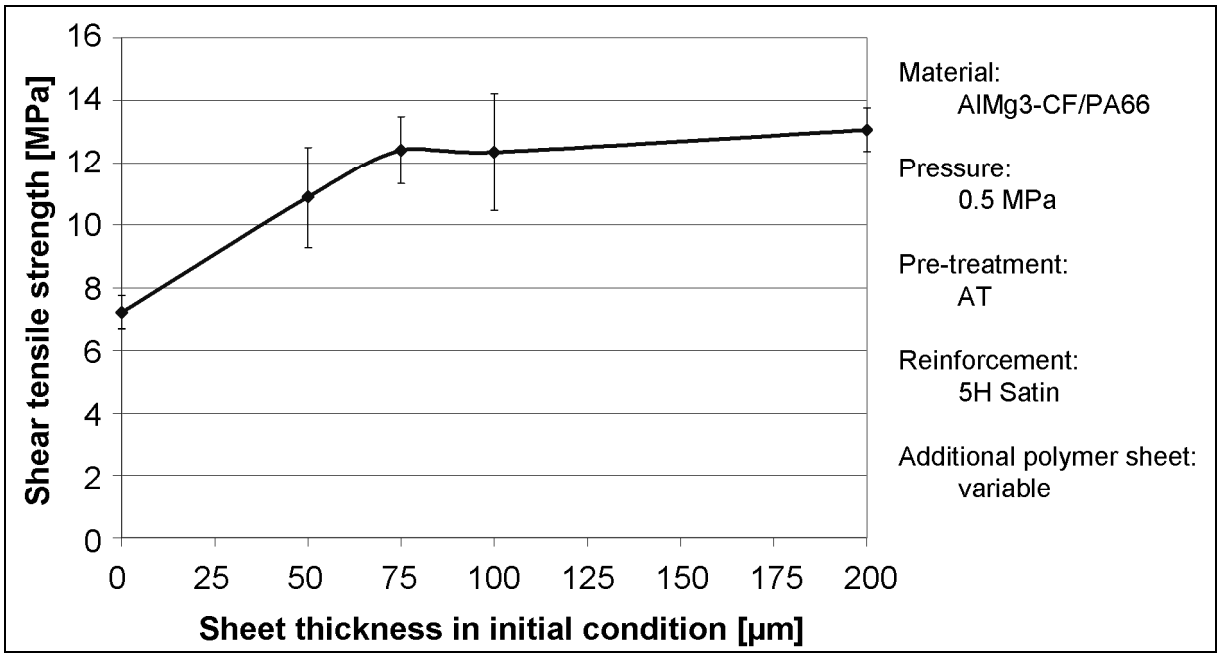

Figure 5.10: Influence of the sheet's thickness in the welding zone on the shear tensile strength

As was expected from the influence of the welding pressure, the shear tensile strength increases with a thicker polymer intermediate layer. A boundary layer of about 5 - 20 µm thick PA66 is formed. This layer thickness is be achieved by using an additional polymer sheet of 100 µm thickness that is placed between both joining partners before welding. A further increase of the PA66-polymer amount (here up to 200 µm) does not lead to further increase of the shear tensile strength as a large amount of the polymer is pressed out of the welding zone. For this reason in the further experiments an additional polymer layer of 100 µm before welding was used to ensure a polymer rich welding zone.

5.7 Combining the results

The previous described test series mainly showed that the pre-treatment of the metallic joining partner by corundum blasting and the application of additional polymer in the welding zone have a positive influence on the shear tensile strength. If the combination of these settings also leads to a superposition of the effects, it will be verified in further experiments. Therefore, samples with combined process parameters were manufactured and tested (Figure 5.11).

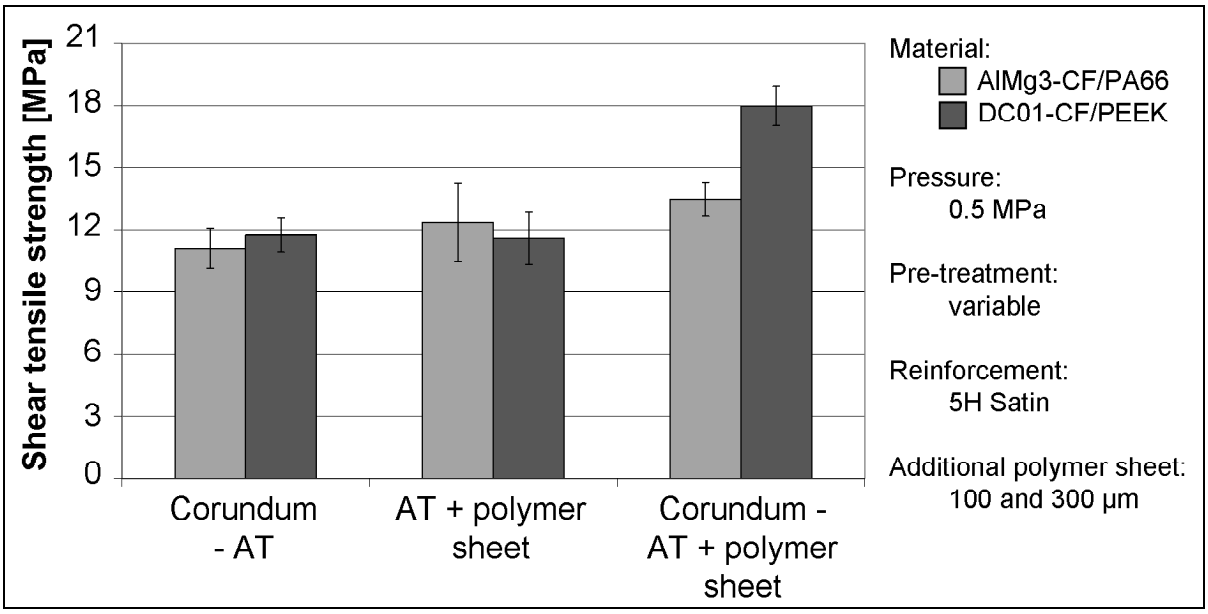

Figure 5.11: Influence of the combined process parameters on the shear tensile strength

Figure 5.11 shows that by combining the best pre-treatment methods further significant increase of the shear tensile strength can be achieved. Compared to acetone treated samples (AT) the application of corundum blasting and additional polymer nearly doubles the shear tensile strength for both the AlMg3-CF/PA66 and the DC01-CF/PEEK.

Figure 5.12 shows a micrograph of the cross section of a sample, which was corundum blasted and had additional polymer. The formed polymer intermediate layer in the joining zone is recognizably smaller than the additional polymer sheet of 100 µm thickness before welding.

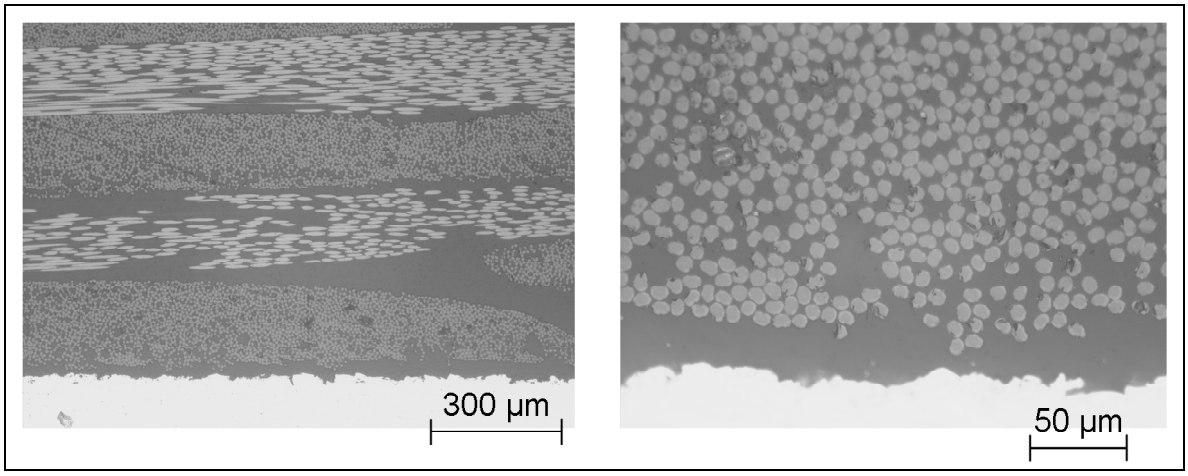

Figure 5.12: Micrograph of the joining area of a corundum blasted AlMg3 with an additional PA66-sheet (initial thickness: 100 µm)

One possibility to see how the polymer flows after applying pressure is by using a red colored PA66 sheet 200 µm thick in the joining area. The mixing of polymer from the joining partner and the red PA66 can be observed. Moreover, it can be seen that all pores and holes introduced by the corundum blasting are filled with the red colored polymer (Figure 5.13).

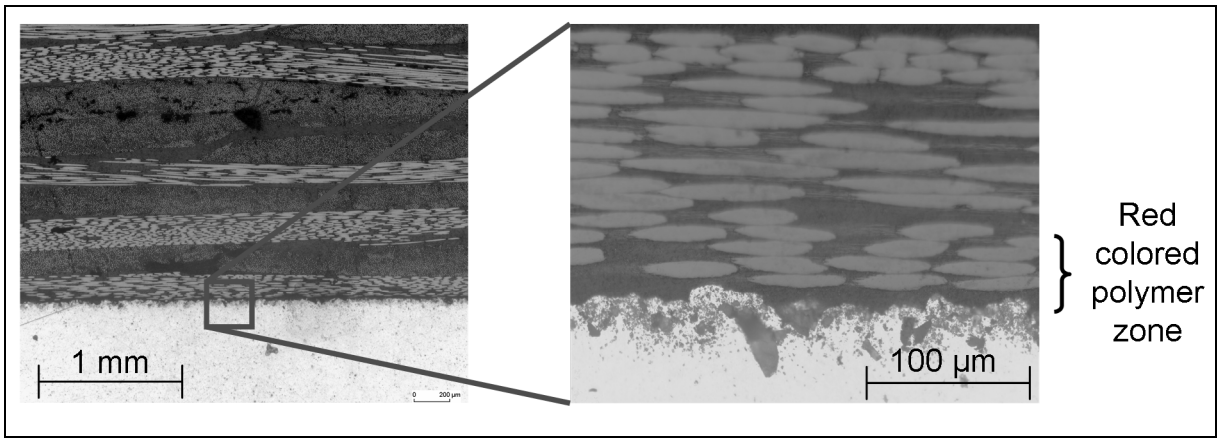

Figure 5.13: Observation of the mixing behaviour of red colorized PA66 thickness from the joining area and the joining partner

The red colored polymer only penetrates the joining partner in a small amount.

For DC01-CF/PEEK-joint a thicker polymer layer (up to approx. 250 µm) is observed (Figure 5.14). In this layer also the carbon fiber reinforcement from the PEEK based additional polymer can be seen.

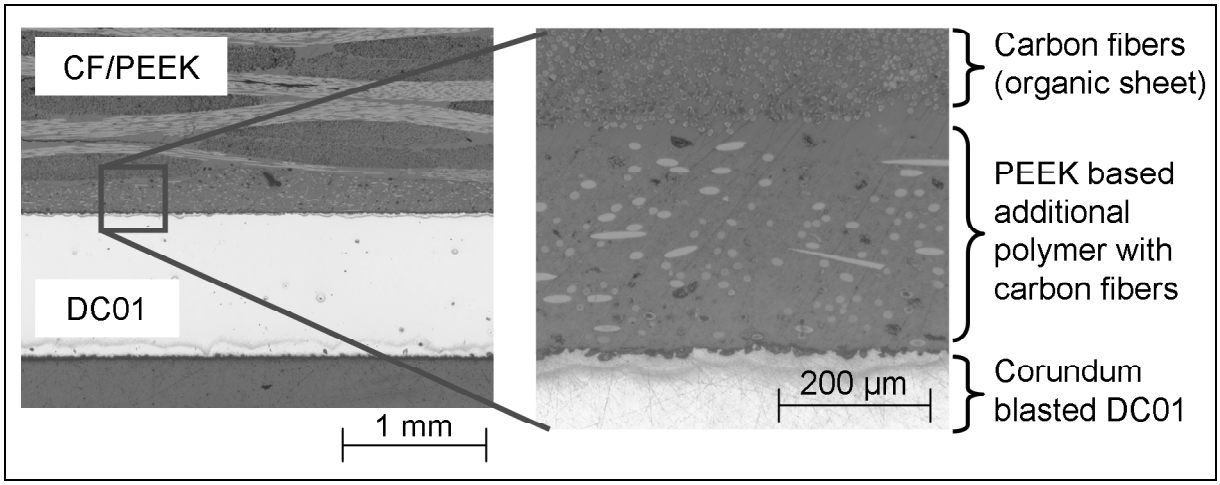

Figure 5.14: Micrograph of the joining area of a corundum basted DC01 with an additional PEEK-sheet (initial thickness: 300 µm)

Important for the determination of the bonding mechanisms are surface fracture analyses (Figure 5.15 and Figure 5.16).

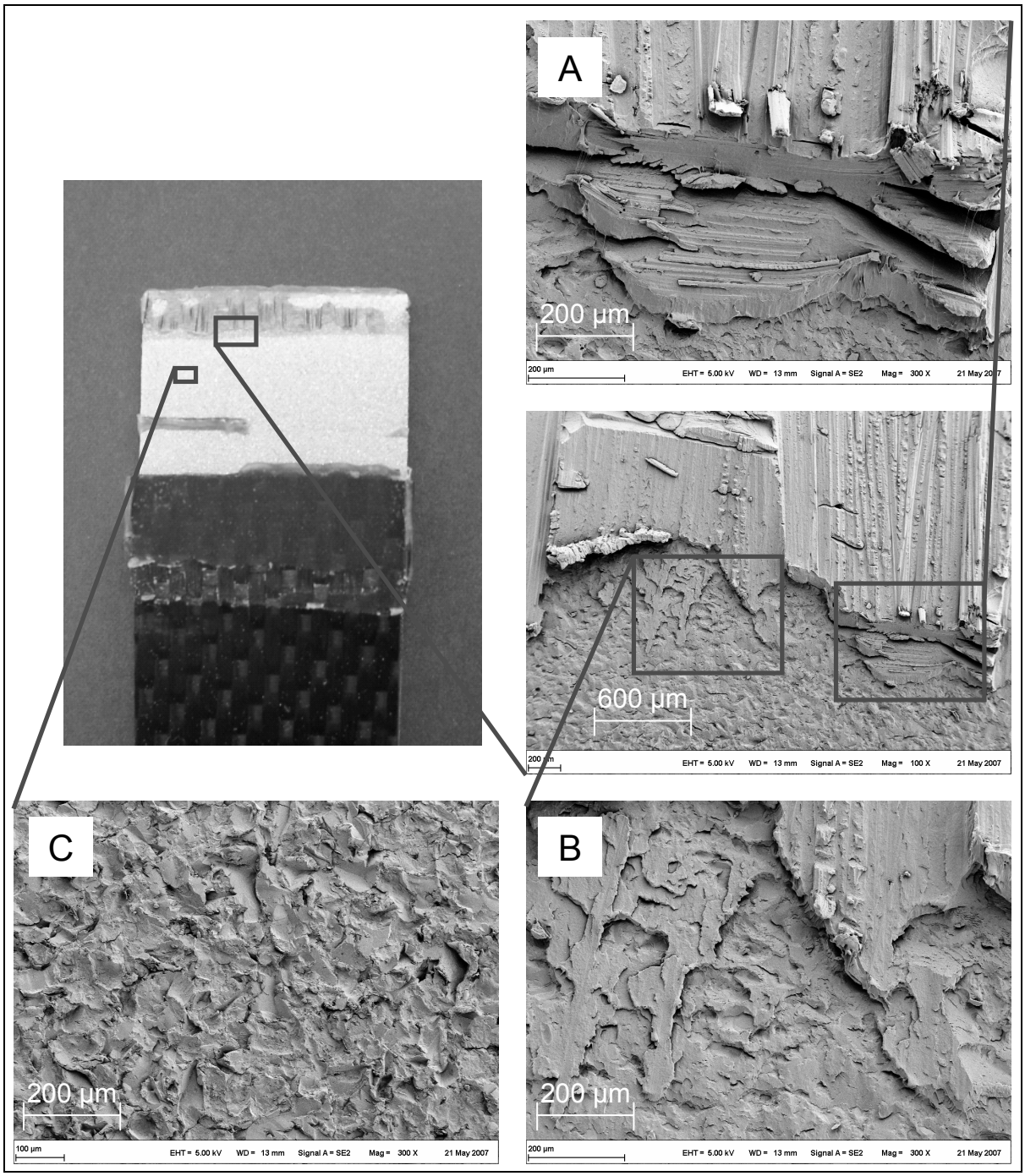

Figure 5.15: SEM-Micrograph of the AlMg3-joining partner after shear tensile testing. Pre-treatment: corundum + 100 µm PA66-sheet, shear tensile strength: 14.2 MPa)

In case of induction welded metal/composite joints, the surface fracture can be divided into three areas:

- In area A polymer remains and carbon fibers pulled out of the composite are found on the surface (cohesion failure).

- In area B a very thin polymer layer is found on the surface (weak boundary layer).
- In area C no polymer is found on the surface (adhesion failure).

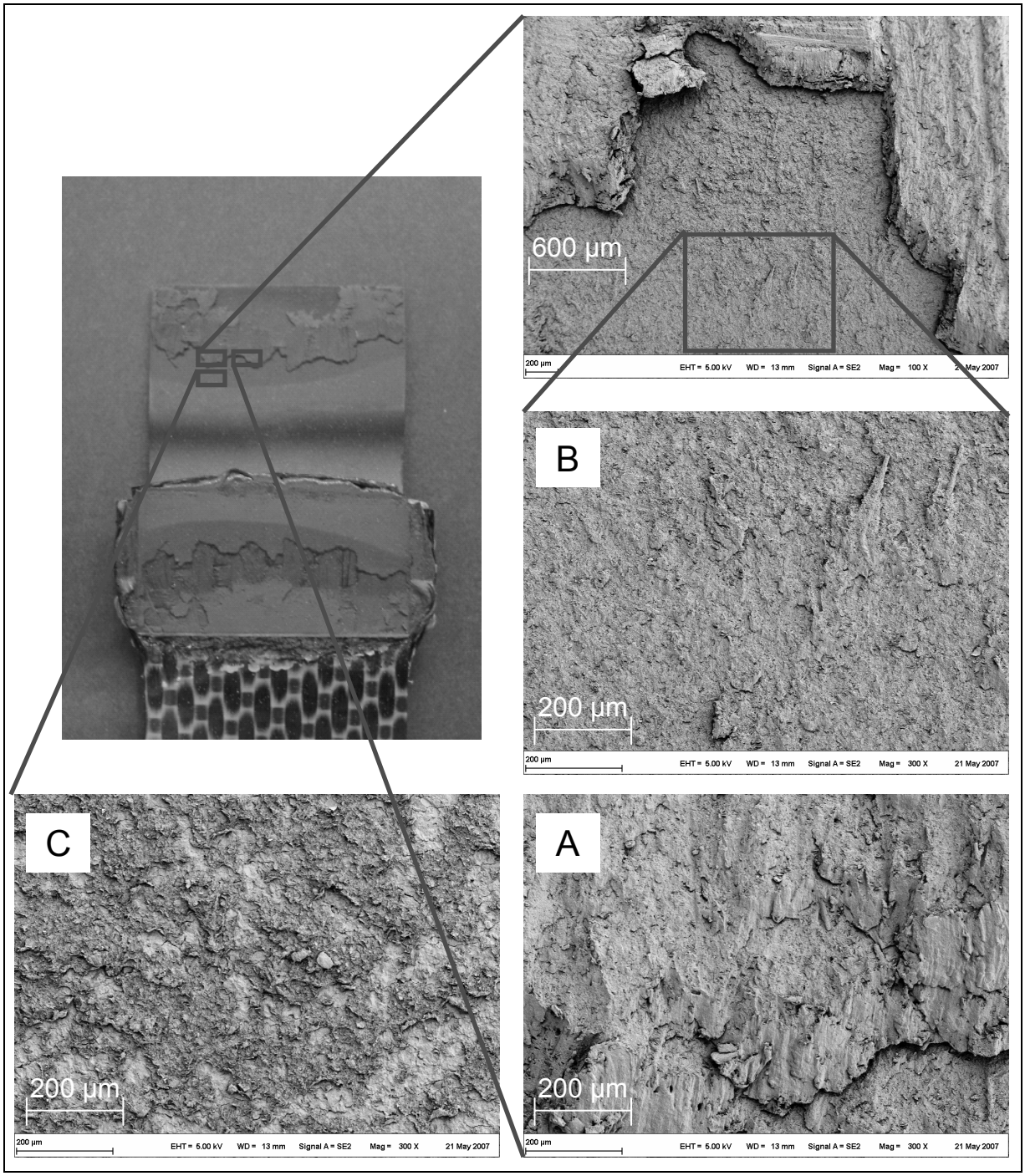

Figure 5.16: SEM-Micrograph of the DC01-joining partner after shear tensile testing. Pre-treatment: corundum + 300 µm PEEK-sheet, shear tensile strength: 20.7 MPa)

A similar division of surface fracture types can also be made for the DC01-CF/PEEK-joints. Here the amount of cohesion failure is slightly higher (Figure 5.16). The surface fracture analyses show that some polymer remains on the surface and even single carbon fibers are pulled out of the organic sheet. The areas with adhesion failure (no polymer remains on the surface) are explained by the bending of the samples during shear tensile testing (peel forces) and the relative thin polymer layer.

So far mainly the influence of the surface treatment has been investigated in this thesis. Now detailed investigations about the influence of thermal properties of the semi-crystalline polymers and environmental conditions are presented.

5.8 Holding temperature, holding time, and cooling rate

The tempered pressing tool enables pressing at a given temperature, during a certain pressing time, and cooling with a given cooling rate. These three settings are investigated in this sub-chapter.

In the state of art (see page 21) seem to imply that the following settings should increase the shear tensile strength of both AlMg3-CF/PA66 and DC01-CF/PEEK:

Parameter		**AlMg3-CF/PA66**	**DC01-CF/PEEK**
Holding temperature [°C]	A	280	370
Holding time [min]	B	7	7
Cooling rate [°C/min]	C	6	6

Experiments with the above given conditions were performed to verify these observations.

In the case of CF/PA66 the high temperature even at the relative low pressure of 0.5 MPa presses the polymer out of the joining area and carbon fibers are in direct contact to the AlMg3. Here no adhesion can take place so the shear tensile strength is very low (average 7 MPa). Then experiments were performed where the pressing temperature was hold at a constant temperature of 10 °C and 140 °C. The polymer was quickly cooled down below melting point T_M (see Figure 5.17).

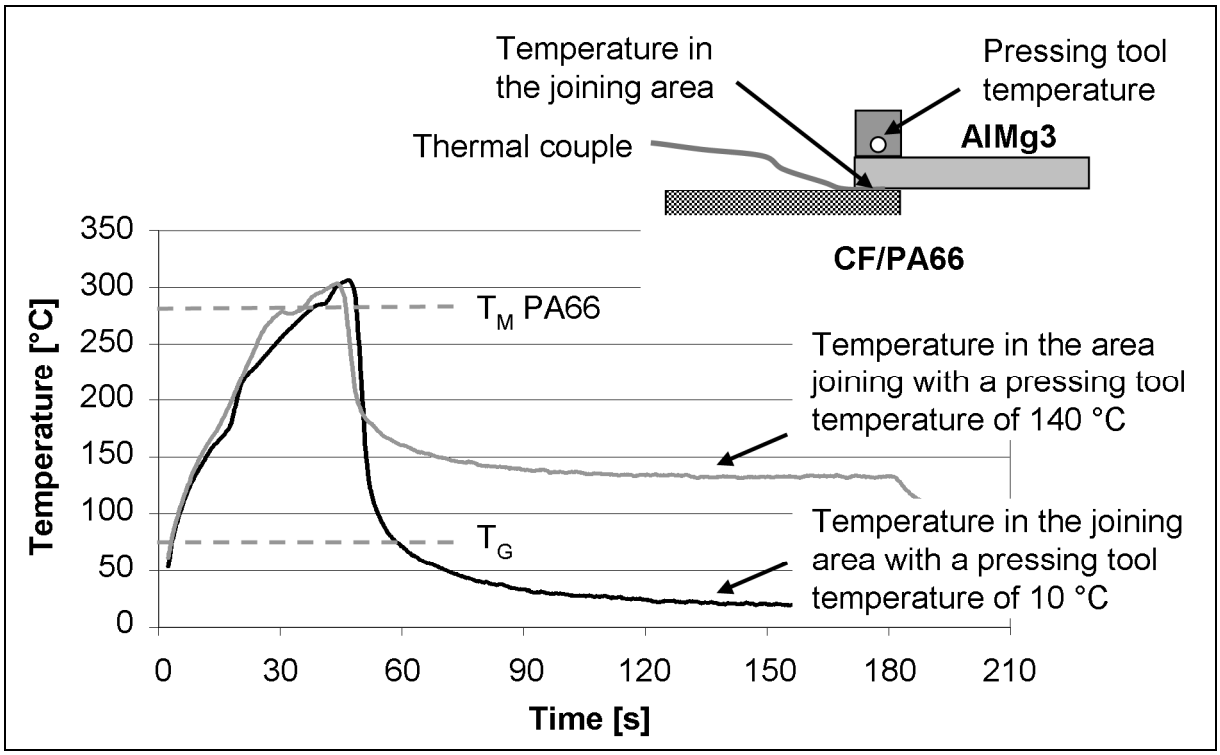

Figure 5.17: Temperature evolution in the joining area for corundum blasted AlMg3-CF/PA66 with additional polymer

These two pressing temperatures did result in slightly different shear tensile strength values (up to 14.5 MPa) that correlate to the crystallinity in the joining area (Figure 5.18). The highest crystallinity and shear tensile strength was obtained for the samples pressed at 10 °C.

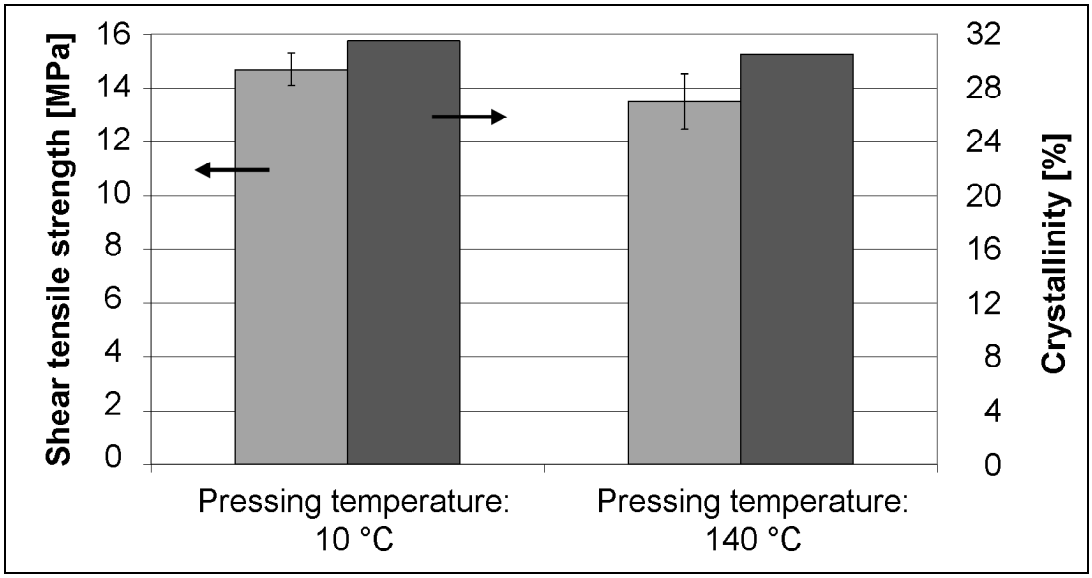

Figure 5.18: Shear tensile strength and crystallinity of corundum blasted AlMg3 and CF/PA66 with additional polymer pressed at 10 °C and 140 °C

The cold pressing temperature leads apparently to many quickly grown small crystals instead of slowly grown large crystals.

For PEEK the temperature control increases the shear tensile strength up to 20 MPa. On the surface fracture is observed that a high amount of polymer remains on the surface (Figure 5.16). A part from that polymer is used to determine the crystallinity and is compared to the polymer from pressing at 23 °C and the original PEEK compound.

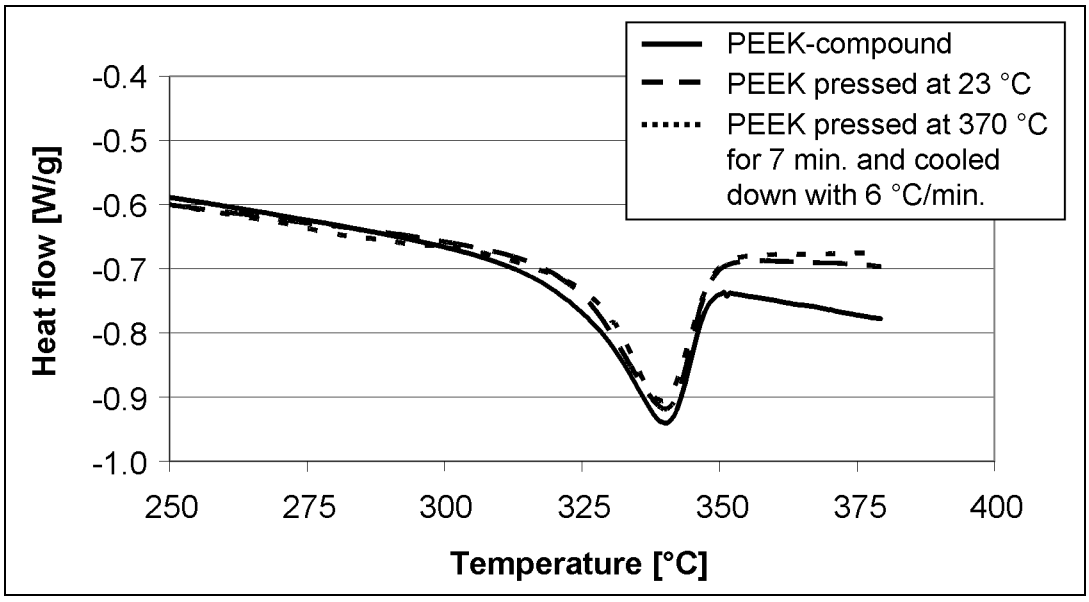

Figure 5.19: DSC-plots from the original PEEK-compound and the polymer pressed at 23 °C and 370 °C

Figure 5.19 and Figure 5.20 illustrate the same tendency as for AlMg3-CF/PA66.

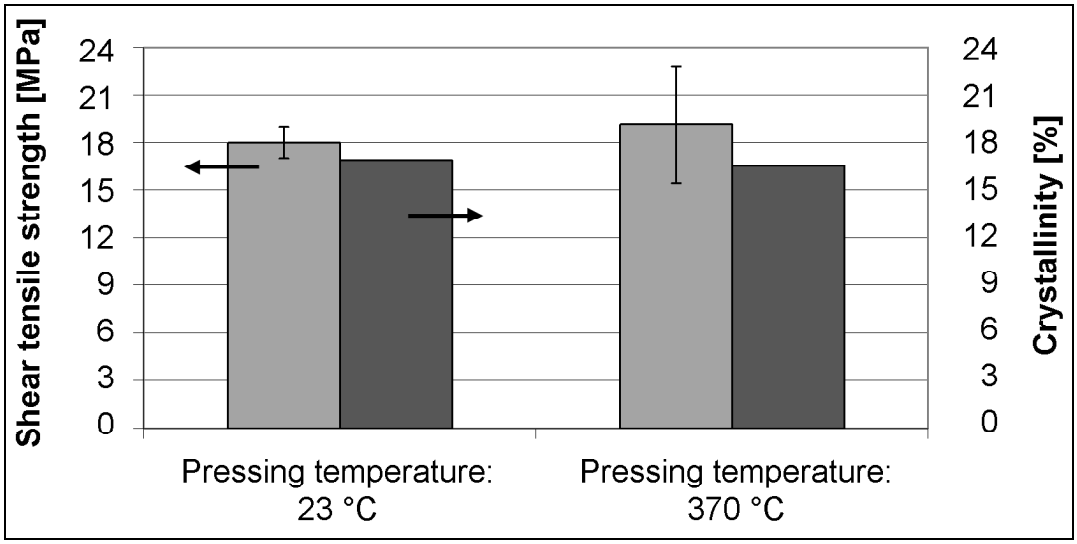

Figure 5.20: Shear tensile strength and crystallinity of corundum blasted DC01 and CF/PEEK with additional polymer pressed at 23 °C and 370 °C

The crystallinity of the sample pressed at 370 °C and cooled down at 6 °C/min is 3 % lower than the sample pressed at RT (16.5 % compared to 16.9 %). The highest crystallinity was obtained by the original compound (17.3 %). As reference for the crystallinity PEEK with a melt enthalpy of 130 J/g was used. Also the melting points of the samples show a similar tendency. The sample pressed at 370 °C and cooled down at 6 °C/min has a melting point of 339.8 °C, the one pressed at room temperature has 340.0 °C, and the original compound has a melting point of 340.2 °C.

These experiments illustrate that choosing the appropriate processing conditions can increase the shear tensile strength. As the differences in crystallinity are very small no general explanation is found and further large scale investigations are needed.

So far only the short-time behavior of the joints has been presented. Next, in chapter 5.9, the influence of environmental conditions is illustrated as these conditions play a role on the long-time behavior of the joints.

5.9 Influence of corrosion on the shear tensile strength

In the case of contact between the aluminum and the carbon fibers resistance can be measured when the copper clamps (see chapter 3.1.5) are used. The results of measuring the resistance through the overlap area thickness after various pre-treatments are given in Figure 5.21.

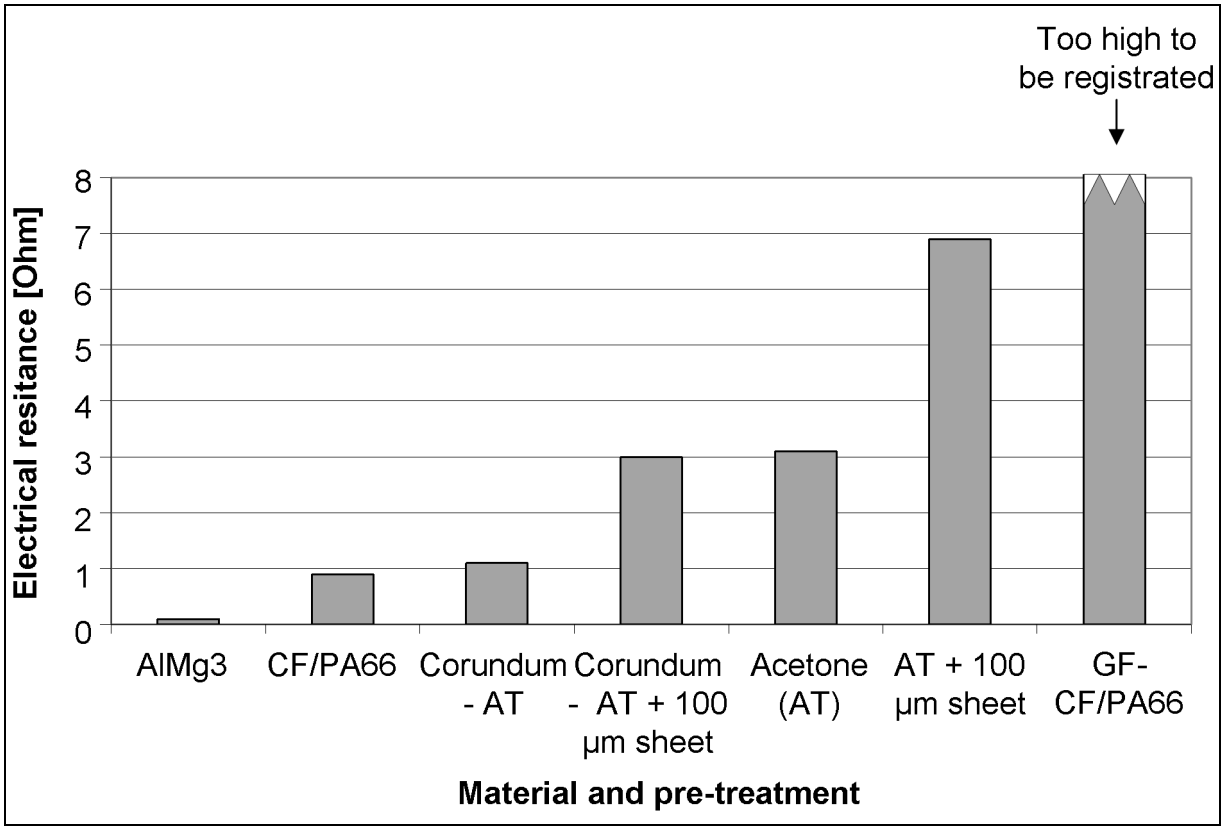

Figure 5.21: Electrical resistance measurements on samples with various pre-treatments

The corundum blasted samples with or without additional polymer show the lowest resistance, indicating that on many positions a direct fiber contact is given and the galvanic corrosion can take place. The acetone cleaned samples with an additional polymer layer show the highest resistance, which means that little contact is given. This contact between carbon and AlMg3 influences the galvanic corrosion as it is one of the requirements for corrosion as was stated in chapter 2.2.5.

The corrosion on the metallic as well as on the polymeric joining partner leads to the formation of a white corrosion product (Figure 5.22). On this sample an elemental analysis with Energy Dispersive X-Ray (EDX) was performed on the given four locations.

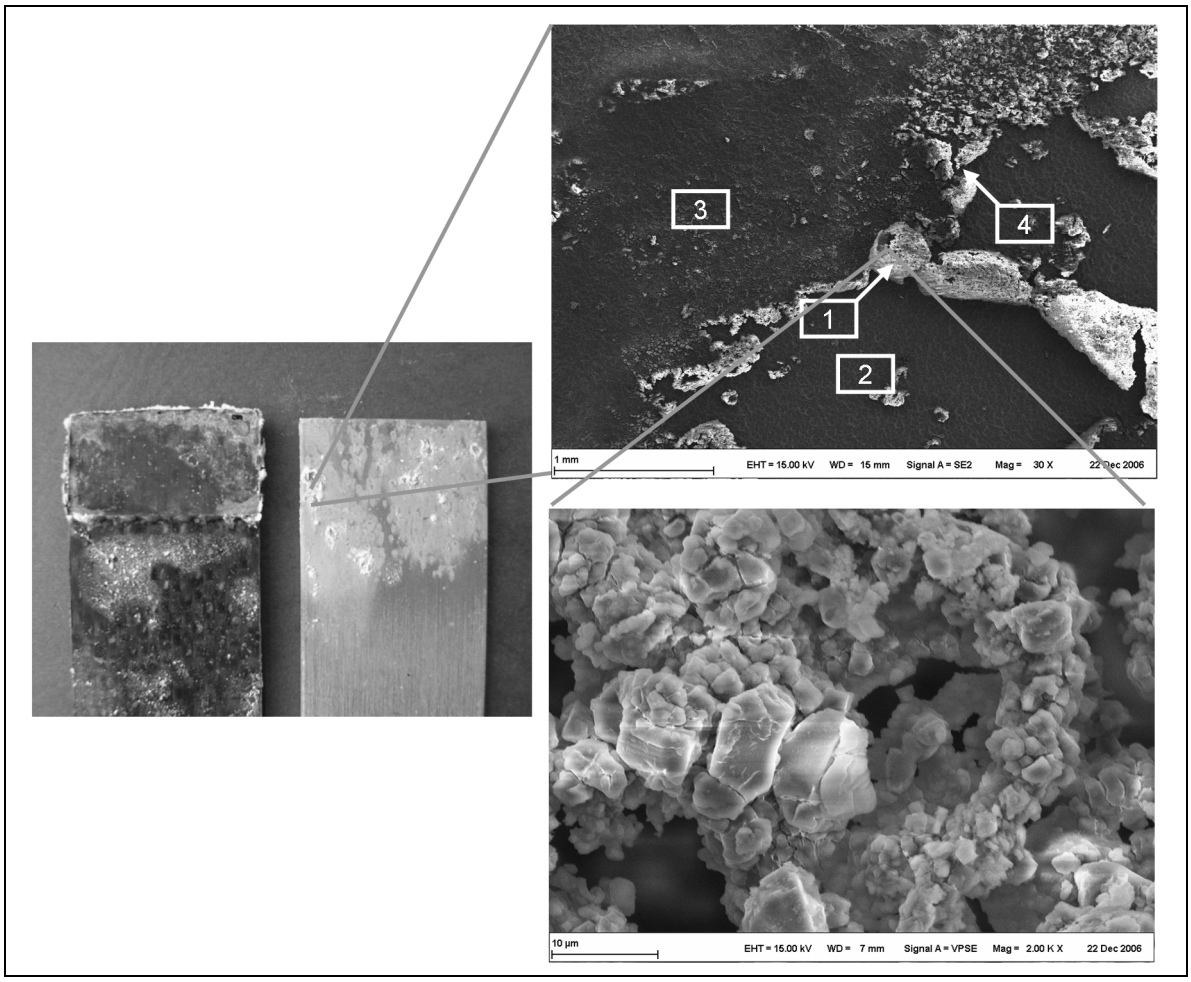

Figure 5.22: Surface fracture of a corundum blasted induction welded joint after submerging in water for four weeks and SEM-micrograph of the AlMg3-joining partners after breakage with four marked locations where a EDX-measurement was performed

The results from these measurements on location 1 and 2 are shown in Figure 5.23. At position 1 the white corrosion product contains mainly aluminum (Al) and oxygen (O). The atomic amount is 72.2 % of oxygen and 25.8 % of aluminum. This is a ratio of nearly three to one and indicates that $Al(OH)_3$ is formed on the surface. Position 2 is the corundum blasted surface without any sort of disposition. Here no oxygen is detected so the surface is mainly aluminum. This indicates that the $Al(OH)_3$-salt on location 1 results from the galvanic corrosion and proves that the equations number 2.4 and 2.5 in chapter 2.2.5 are correct. The formation of $AlCl_3$ and NaOH as was given by Boyd in [84] is therefore not observed. Position 3 and 4 confirmed the obtained results.

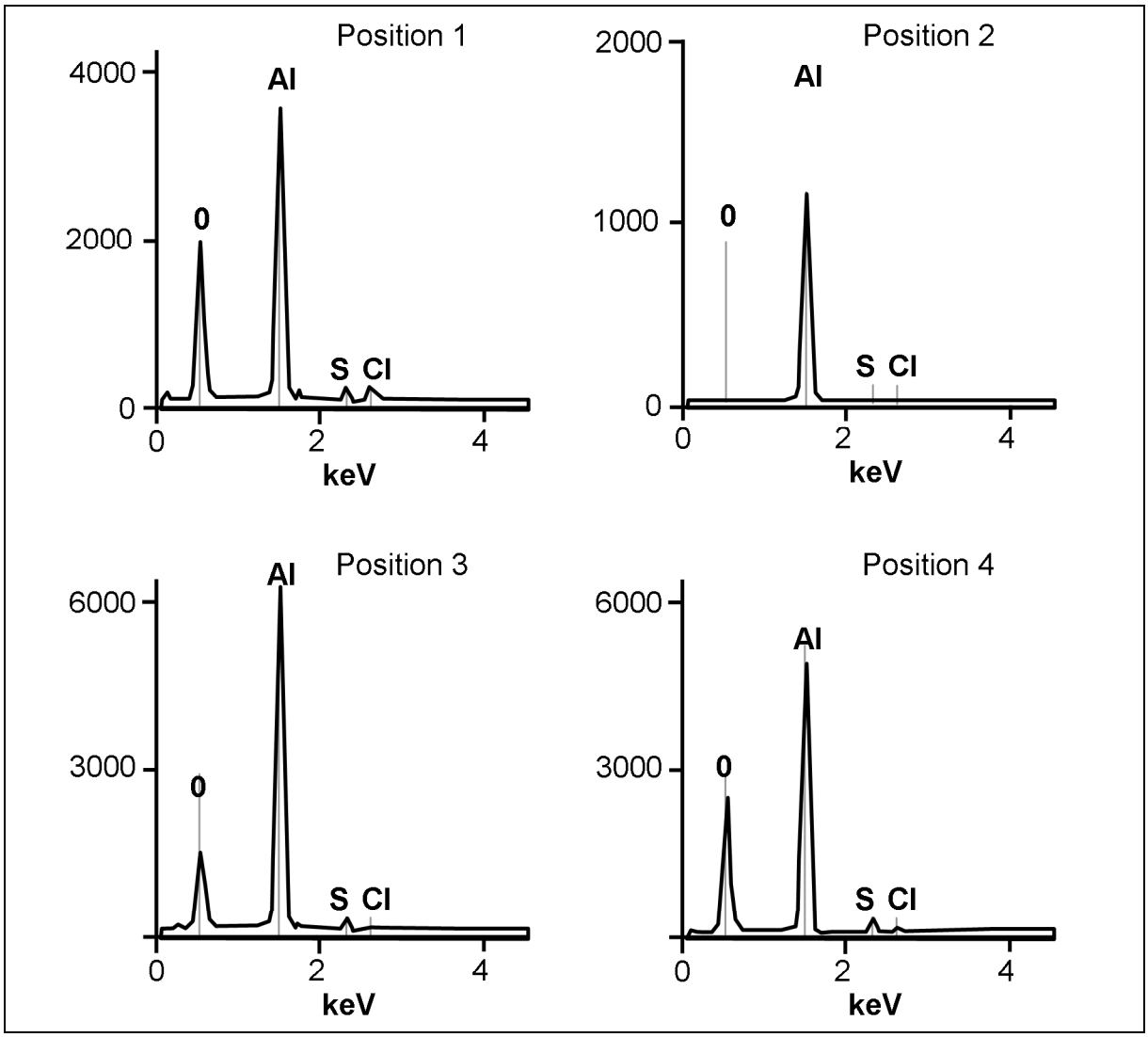

Figure 5.23: Energies obtained from EDX with the characteristic energies from some atoms

The exposure of AlMg3-CF/PA66-joints during three weeks in water shows a large influence on the shear tensile strength. Three kinds of samples were made:

- Corundum blasted AlMg3-CF/PA66
- Acetone treated AlMg3-CF/PA66 with additional polymer
- Corundum blasted AlMg3-GF/CF/PA66 with additional polymer

In the case contact corrosion occurs, a decrease of shear tensile strength is observed for both the corundum blasted AlMg3-CF/PA66-joints and for the acetone treated AlMg3-CF/PA66 with additional polymer (Figure 5.24).

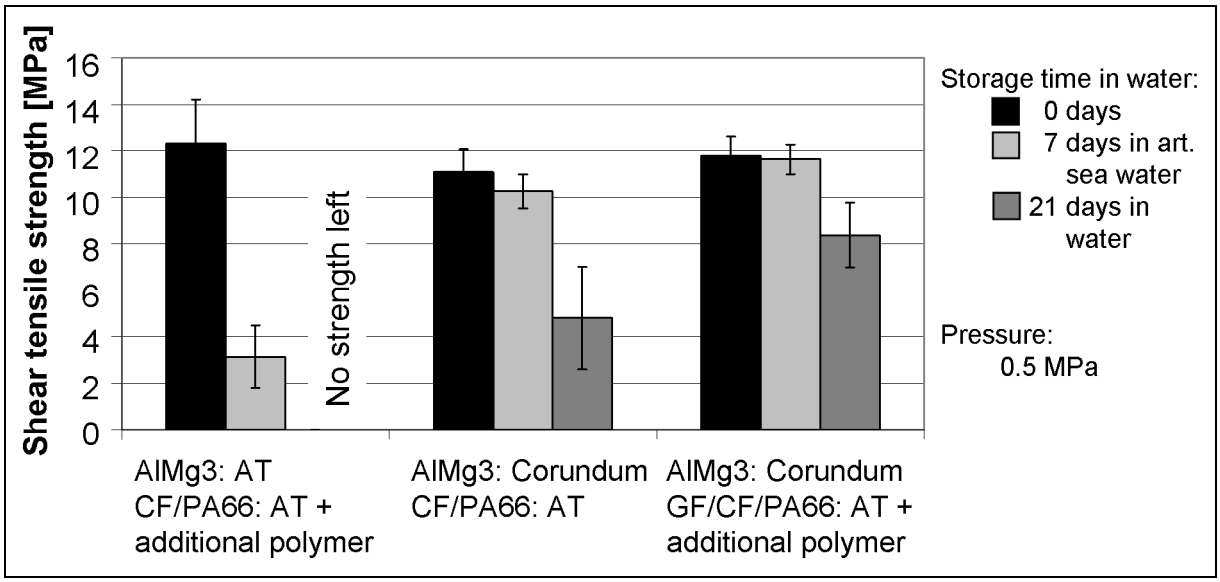

Figure 5.24: Shear tensile strength after storage of samples for 7 days in an artificial sea water solution and 21 days in water

Figure 5.24 show that not only corrosion takes place, but also a reduction of the physical bonding properties for the acetone treated AlMg3-CF/PA66 with additional polymer. Here the samples were carefully removed from the sample holder, but no residual strength was left. The surface fracture shows 50 % of bondline corrosion and 50 % of adhesion failure (Table 5.4). The other samples were taken out of the water and dried for 2 days in air before testing.

Interesting to observe is that the corundum blasted AlMg3-CF/PA66-joints show more or less the same shear tensile strength of 3 MPa as the corundum blasted AlMg3-GF/PP-joints. The contribution of the physical bonding forces seems to be reduced, but due to the interlocking of polymer (mechanical adhesion) also shear tensile strength values of 3 – 5 MPa are observed. In the case of GF/CF/PA66 a reduction of only 30 % was noticed even though PA66 is known to be water sensitive.

Table 5.4: Surface fracture analyses of selected samples after 21 days in water

	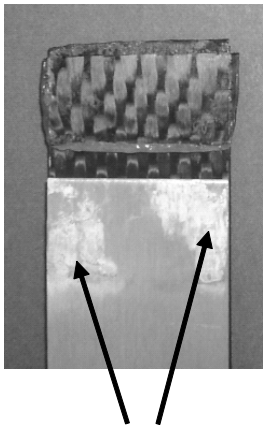 Corroded areas	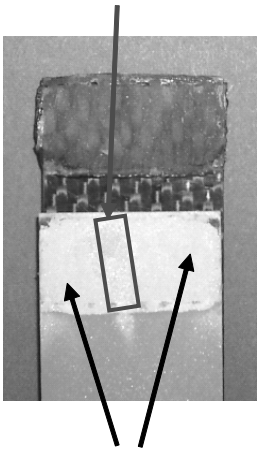 Small band showing optically no change in the surface condition Corroded areas	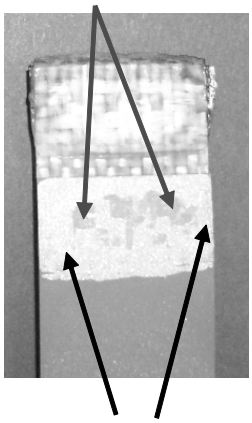 Polymer remains Optically no change in the surface condition
Material	AlMg3; CF/PA66	AlMg3; CF/PA66	AlMg3; GF/CF/PA66
Pre-treatment	Metal: AT Polymer: AT with additional polymer	Metal: Corundum Polymer: AT	Metal: Corundum Polymer: AT with additional polymer
Shear tensile strength [MPa]	0 (could not be determined)	3.2	9.7
Surface fracture analyses	BC: 50 % AF: 50 % CoF: 0 %	BC: 83 % AF: 17 % CoF: 0 %	BC: 0 % AF: 84 % CoF: 16 %

In the case of submerging sample in water no additional electrolyte is included. A sea water solution mainly based on NaCl and water (for the exact composition see page 50) was made to accelerate the corrosion and was used for submerging samples. Here the same materials were used as for the water submerging; only the storage time was reduced to 7 days. The sea water solution clearly accelerated the galvanic corrosion as is illustrated in Table 5.5.

The direct contact of AlMg3 and carbon fibers leads to the formation of the white $Al(OH)_3$ salt; on the glass fiber fabric no salt is visible.

Table 5.5: Surface fracture analyses of selected samples after 7 days in a sea water solution

	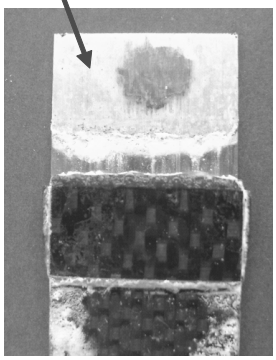	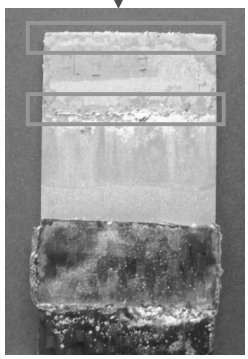	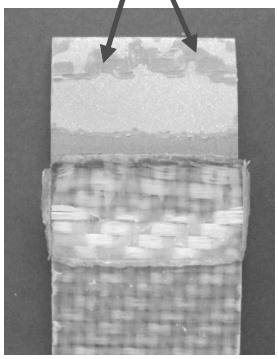
Material	AlMg3; CF/PA66	AlMg3; CF/PA66	AlMg3; GF/CF/PA66
Pre-treatment	Metal: AT Polymer: AT with additional polymer	Metal: Corundum Polymer: AT	Metal: Corundum Polymer: AT with additional polymer
Shear tensile strength [MPa]	2.9	9.5	11.8
Surface fracture analyses	BC: 83 % AF: 17 % CoF: 0 %	BC: 34 % AF: 43 % CoF: 23 %	BC: 0 % AF: 80 % CoF: 20 %

From these experiments the following conclusions can be drawn:

- An acetone treatment even with additional polymer has little or no residual shear tensile strength as the physical bonding forces are disappeared due to corrosion and no interlocking took place.
- Corundum blasted AlMg3-CF/PA66-joints have a residual shear tensile strength of 3 – 5 MPa, which is comparable to corundum blasted AlMg3-GF/PP-joints and indicates that the physical bonding forces have disappeared

and that due to the mechanical interlocking a shear tensile strength of 3 – 5 MPa remains.

- In the case of corundum blasted AlMg3-CF/PA66 and acetone treated AlMg3-CF/PA66 with additional polymer contact corrosion took place and led to shear tensile strength values between 0 and 5 MPa. The glass fiber layer in GF/CF/PA66 prevented the corrosion and a reduction of the shear tensile strength of only 30 % took place. Similar tendencies are made for the samples submerged in the artificial sea water solution. Here the corundum blasted samples still had an average shear tensile strength of 9 MPa, but the corrosion product deposition in the joining area already started and quickly the shear tensile strength is reduced.
- The observation above indicate that the induction welded AlMg3-CF/PA66 joints are bonded by physical bonding mechanisms and in the case of corundum blasting an additional contribution in the height of approx. 3 MPa is achieved.

5.10 Degradation temperature and influence on the shear tensile strength

Figure 2.11 (in chapter 2.2.6) shows the dynamic thermogravimetric analysis (TGA) of PA66 with a heating rate of 10 °C/min in oxygen, argon, and helium. In order to observe a similar behavior for the reinforced PA66 and PEEK used, TGA-experiments with various environmental gases were performed (Figure 5.25).

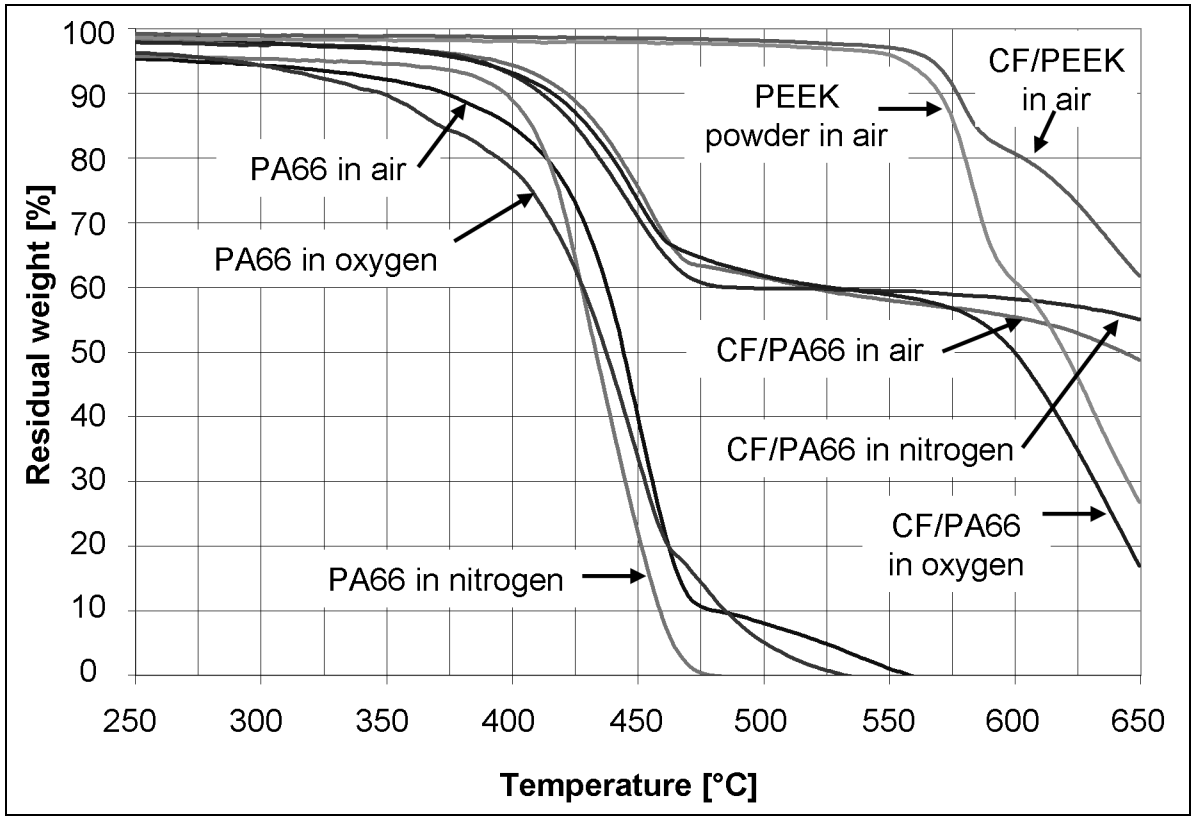

Figure 5.25: Thermogram of PA66, CF/PA66, PEEK powder, and CF/PEEK at 10 °C/min in various environmental gases (oxygen, air, and nitrogen). Specimen mass: 11-17 mg

Figure 5.25 shows an unexpected result for PA66. Although in [92] a large increase of the decomposition temperature for PA66 was observed, this behavior is not confirmed by the performed experiments. A closer look at the PA66-sheet thermogram illustrates that the oxygen influences the decomposition only to a low extent. The decomposition is therefore supposed to be mainly dominated by thermal degradation instead of thermal oxidative degradation. In the case of carbon fiber reinforced PA66 this effect is even smaller compared to the PA66-sheets. It should be noted that although between 300 and 400 °C a weight loss of only 5 % for CF/PA66 in oxygen, air, and nitrogen was observed, the molecular structure would be significantly changed, but this cannot be determined by the TGA.

Moreover, at low heating rates (e.g. 0.1 or 1.0 °C/min) a larger influence of the gases on the polymer is expected. On the opposite, heating rates of 300 °C/min for welding are normal (see Figure 5.2) and will even reduce the small effect of the environmental gas on the PA66.

In case of PEEK powder and CF/PEEK in air the decomposition temperature is around 550 °C, which is about 200 °C higher than the melting point of PEEK. For welding of PEEK this results in a large process window.

Also interesting is the oxidative behavior of the carbon fiber PA66-fabrics above 500 °C. In nitrogen no weight loss was observed but in the pure oxygen environment a weight loss of 80 % was obtained. This indicates that carbon fibers are also oxidized at higher temperatures.

Although the thermogram in the case of carbon fiber reinforced PA66 and PEEK does not show an increase in the process window, several welding experiments with PA66 were performed in a nitrogen environment to observe a change in structural influences. The equipment used was already presented in Figure 3.12. The influence of the oxygen exclusion on the shear tensile strength of the single-lap joints is illustrated in Figure 5.26.

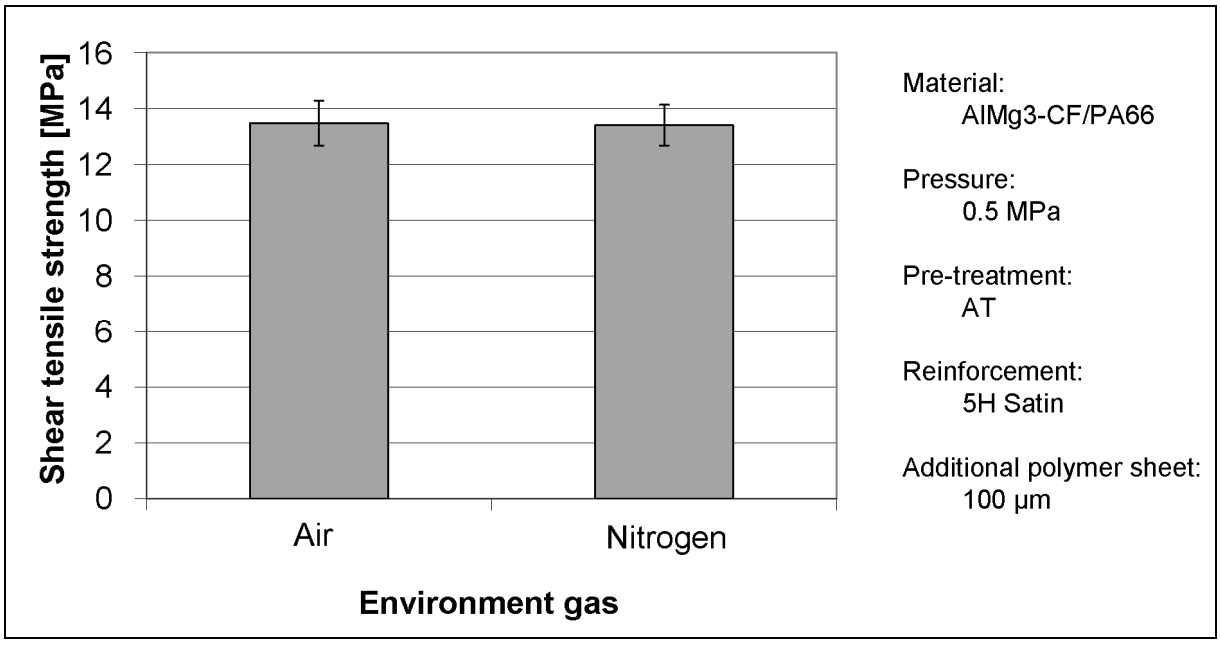

Figure 5.26: Shear tensile strength of samples welded in an air and a nitrogen environment

The exclusion of oxygen leads to the same shear tensile strength for welding of AlMg3-CF/PA66 in air as the PA66 degradation is mainly thermally induced [91]. For other polymer types (like PP) the thermal degradation is oxidative. Especially when the CFRPC-joining partner is the top joining partner and heating of the entire thickness takes place, the exclusion of oxygen can lead to better results. Locally higher temperatures can be obtained when heating the CFRPC-joining partner in the carbon fiber rovings, because these rovings are heated inherently and transfer the generated heat to the polymer.

In the case of welding of other thermoplastic materials (e.g. GF/PP) large quality improvements are expected as the manufacturing window is increased as is shown by TGA-measurements (Figure 5.27). The material used was a GMT (GF/PP) named Symalite 100G30L09 manufactured by Quadrant Composites.

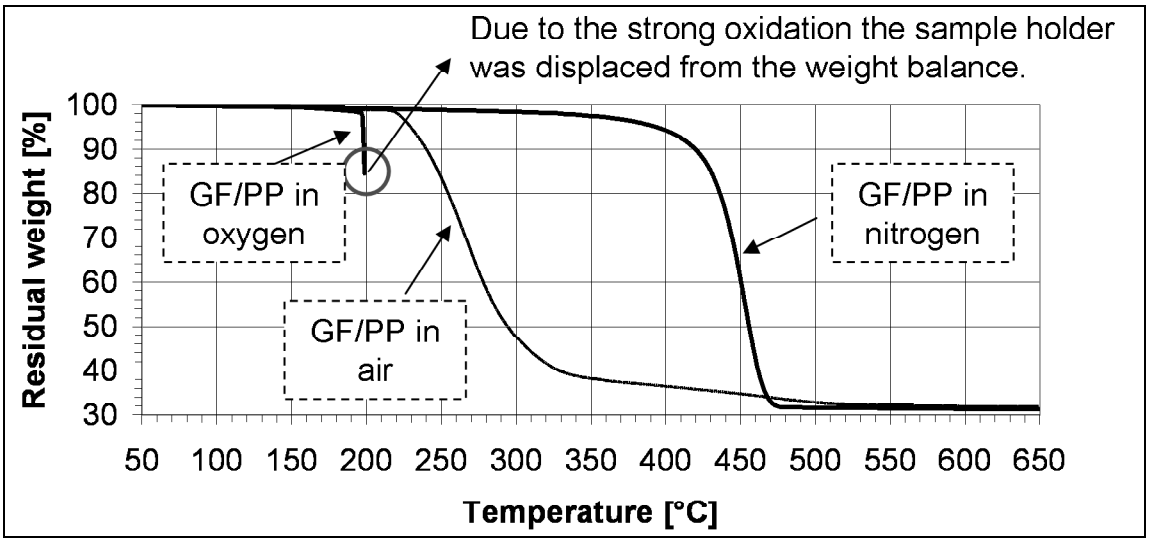

Figure 5.27: Thermogram of GF/PP in various environmental gases (oxygen, air, and nitrogen). Specimen mass: 12-16 mg

When GF/PP was heated in a nitrogen atmosphere up to 390 °C it shows a weight loss of 5 %, whereas for GF/PP in air the same weight loss of 5 % is observed at already 230 °C. The presence of pure oxygen even leads to displacing the sample holder from the weight balance, so the measurement was stopped at 200 °C. This phenomenon happened twice. This clearly shows that oxygen influences the polymer degradation. Oxygen exclusion by a shielding gas (like nitrogen) can be used to enlarge the process window for welding of GF/PP. The experiments show that the application of a non-oxygen environment creates new potential for welding. The gas nozzle can be located close to the welding zone and can also be used as a cooler.

5.11 Comparison of induction welding and adhesive bonding

In Table 2.4 many literature values of metal/composite bonding are already given, but to validate the obtained results a comparison with other joining techniques is made. To determine the maximum shear tensile strength that can be achieved with the materials used, various samples were adhesively bonded [140]. The pre-treatment of the AlMg3 was alkaline pickling (see Table 3.6); DC01 was corundum blasted. Both polymeric joining partners were acetone wiped. The applied adhesive was a 1k-epoxy resin and the results of the shear tensile testing are given in Figure 5.28.

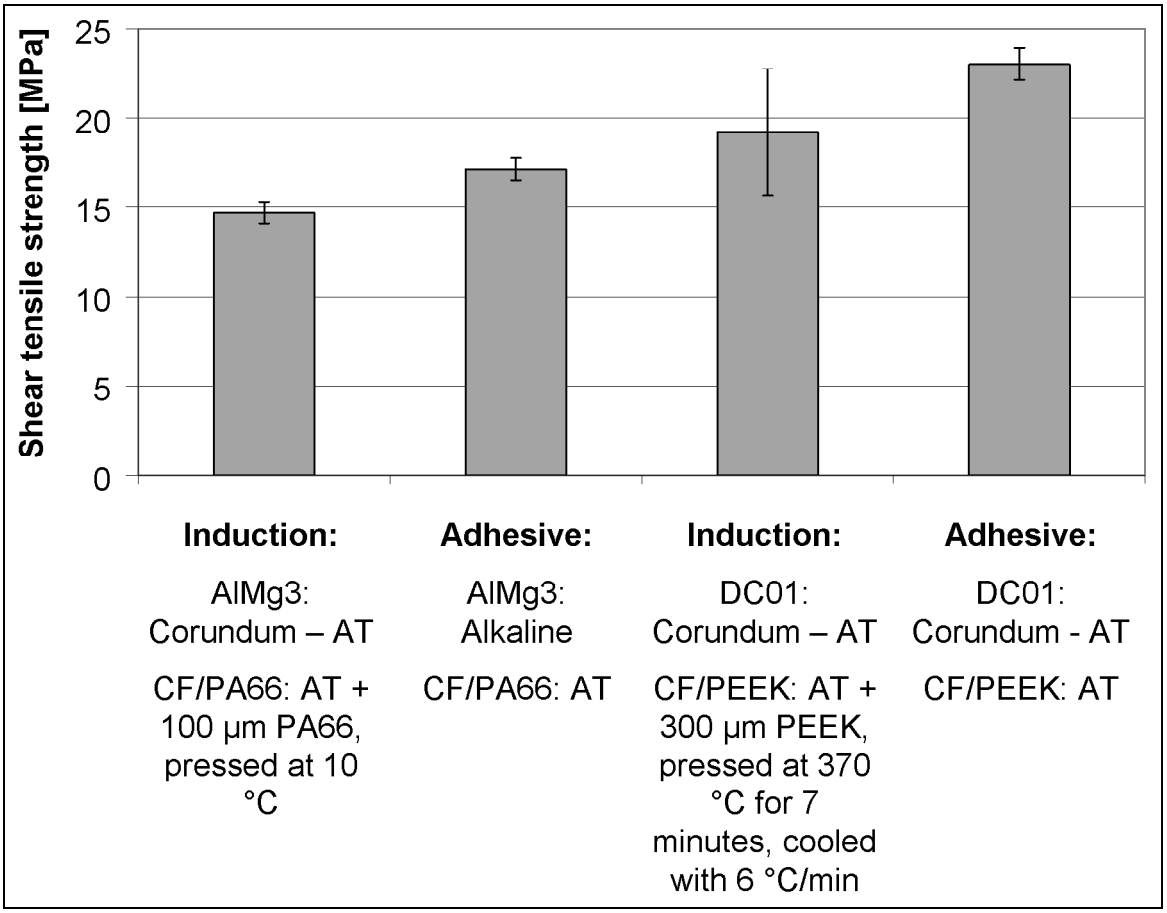

Figure 5.28: Comparison of induction welding and adhesive bonding of AlMg3-CF/PA66 and DC01-CF/PEEK

Figure 5.28 clearly shows that the adhesively bonded samples result in a higher shear tensile strength. During adhesive bonding a chemical reaction with the surface takes place and chemical bondings appear which are stronger than physical ones. The surface fracture mainly shows a cohesive failure and necking of the AlMg3-joining partner is also observed [140]. Compared to the induction welded joints, an increase of 15 % in shear tensile strength can be seen for the AlMg3-CF/PA66

combination. The adhesively bonded DC01-CF/PEEK samples have a maximum shear tensile strength that is 16 % higher than induction welded joints. In general it can be concluded that induction welding of metal/composite joining partners leads to a good bonding, as the shear tensile strength is just below adhesive bonded joints. The reduction of the shear tensile strength can be explained by the minor ability of the induction welded joints to take up bending of the sample as the polymer layer is only 5 – 25 µm thick. The adhesively bonded joints have an adhesively layer of approx. 1.0 mm (Figure 5.29).

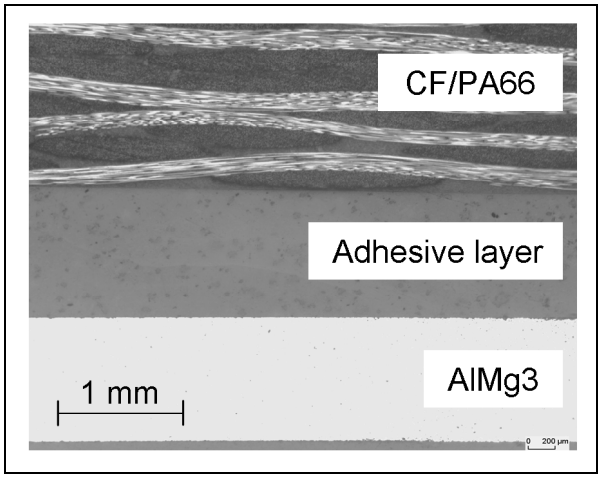

Figure 5.29: Micrograph of the adhesively bonded joint

The load displacement diagram shows that the induction welded joints are slightly stiffer, but can not be deformed to such a large extent as the adhesively bonded joints can (Figure 5.30).

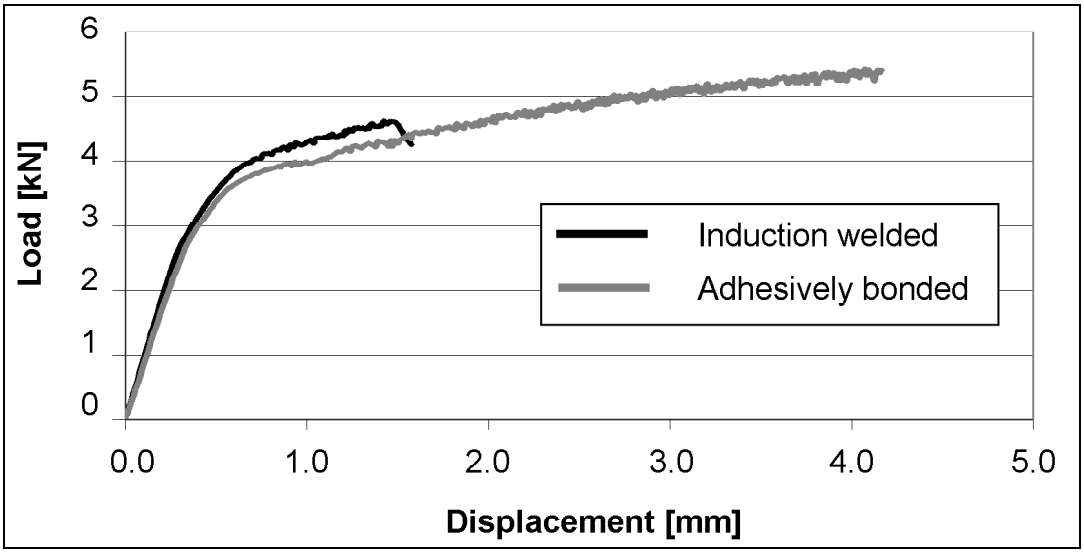

Figure 5.30: Comparison of the load displacement curves of induction welded and adhesively bonded joints

5.12 Transfer of the generated information

To transfer the generated information from the investigation a possible application of induction welded metal/composite joint is demonstrated by welding a U-shaped profile on a CF/PA66-plate (Figure 5.31). The metal was acetone cleaned, the polymer was acetone wiped.

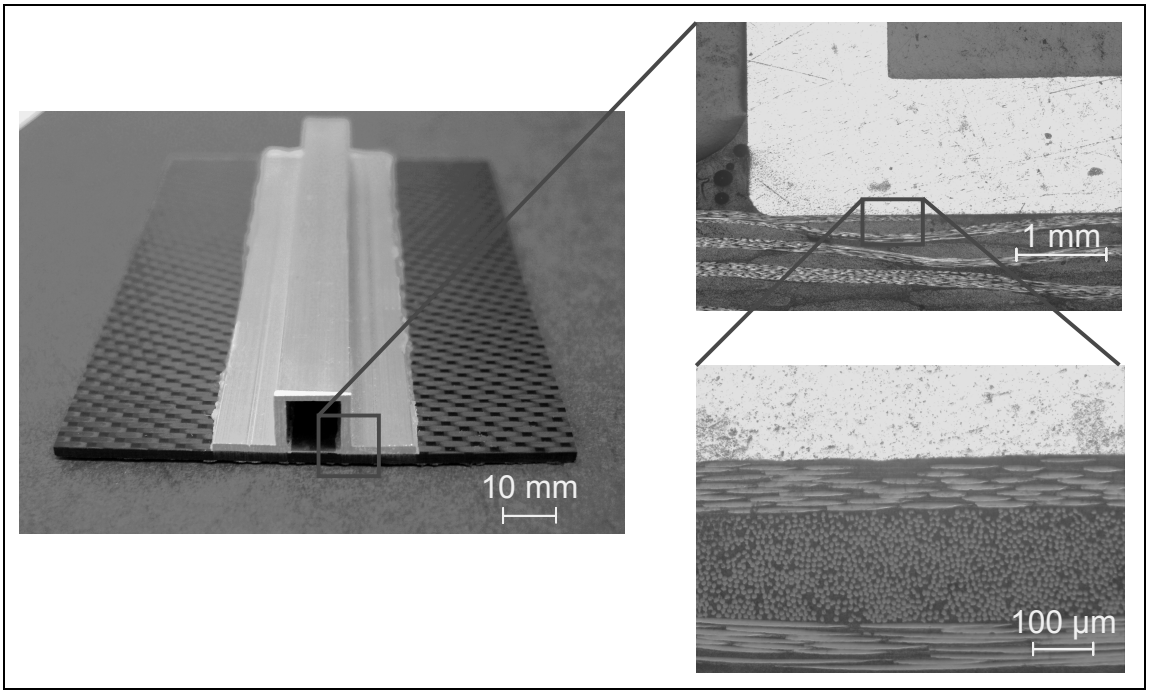

Figure 5.31: Induction welded profile and a micrograph of a U-shaped aluminum profile on CF/PA66

The micrographs show a thin polymer layer between the metal and the composite. This kind of stiffening profiles can of course also be made out of FRPC and then welded on metal plates. The results can also be used for continuous welding by means of robotic systems.

For that purpose, a new welding head was designed. This multitask tool enables continuous heating and applying pressure on the same position. The constructed tool consists of three bearings that support a glass fiber thermoset filament winded tube. Inside this tube an inductor is located, which enables heating of the joining partner under pressure without heating of the tube due to the alternating magnetic field (Figure 5.32).

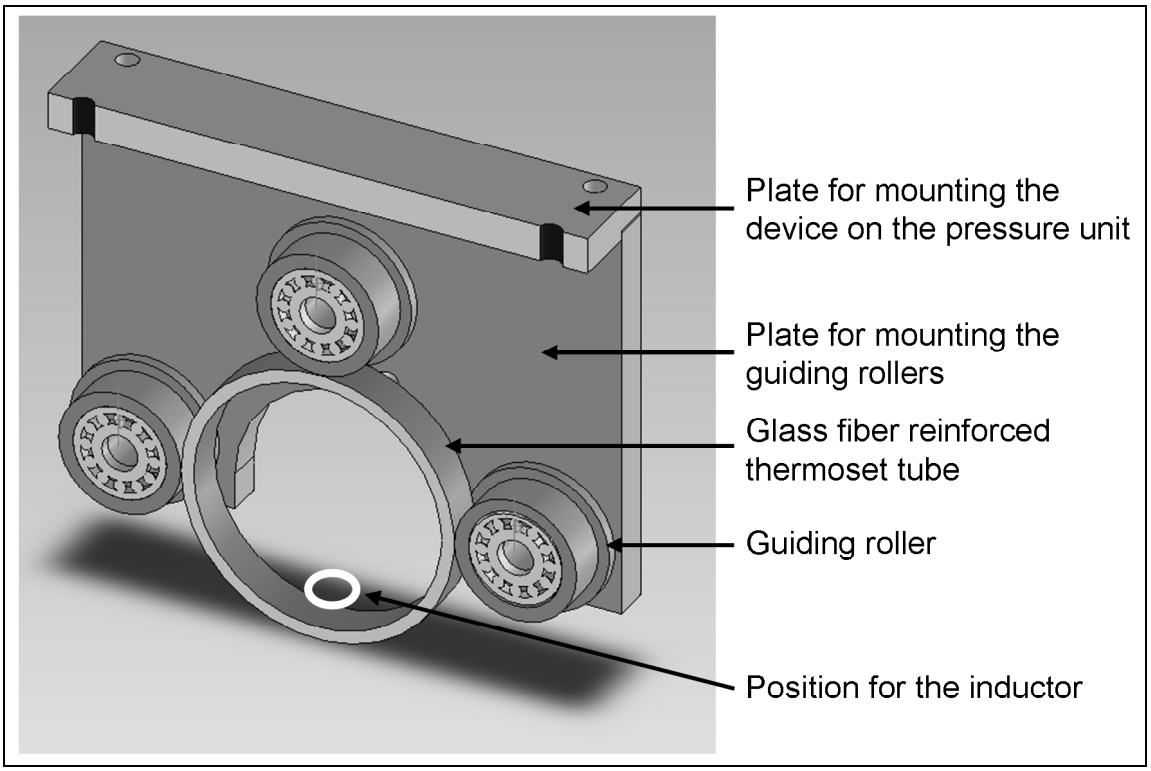

Figure 5.32: Designed compression and heating roller [141]

The glass fiber reinforced filament winded thermoset tube is electrically not conductive and retains its structure during pressing. The advantage (compared to the state of the art of continuous induction welding technique) of this compression and heating roller is the elimination of the area without pressure between the inductor and the compaction roller. A good contact between both joining partners is created, so a higher heat transfer takes place, which also leads to less polymer degradation. Moreover, the control needed to weld three-dimensional joints by means of a robot is much easier. A disadvantage is the increased distance between inductor and joining zone, but increasing the generator power can easily compensate this. The concept of the roller was used to build a modified welding tool for induction by means of a robot [142].

This welded aluminum/CFRPC structure clearly shows the possibilities of manufacturing metal-composite joints by using induction welding. Robotic systems with the appropriate welding head can weld many geometries. Also, integration of the oxygen-free environments can easily be implemented by using a gas nozzle pointing to the welding head. The high output of good metal-composite joints can then be guaranteed. Now an analytical and finite element model that enables describing and simulating the heating is needed. This is shown in the next chapter.

6 Building a model for predicting inductive heat generation

Analytical calculations and FE-simulations are useful to provide an insight into the equipment and process parameter that influence the induction heating. The obtained information enables the improvement of the process as the parameters are identified. Moreover, the calculations enable the application of a quality assurance using indirect measurements, e.g. measuring the temperature outside of the welding zone to obtain information about the temperature in the welding zone. First the material properties need to be determined to obtain reliable starting conditions for the calculations. Many of the needed parameters (e.g. thermal conductivity, and specific heat capacity) are not constant, but are temperature dependent, and therefore had to be determined experimentally. In the Appendix 8.2 thermal properties are given for both AlMg3 and CF/PA66. These values are used for calculations and FE-simulation with the Ansys Workbench 10.0 software. This chapter now describes the induction heating in three categories:

- Experimental measurements
- Analytical calculations
- FE-simulations

6.1 Experimental measurement of heating AlMg3-CF/PA66

The thermal conductivity of the AlMg3 is about 500 times higher than the thermal conductivity of the PA66 polymer and almost 90 times higher than the CF/PA66 in fiber direction [Appendix 8.2, 46]. This means that generated heat is quickly transferred to the entire AlMg3-sample and is therefore not available to heat the polymer in the composite. Experiments were performed with three thermal couples attached to various positions of the AlMg3-sample. The fourth thermal couple was attached to the bottom of the CF/PA66 sample. These positions are given in Figure 6.1.

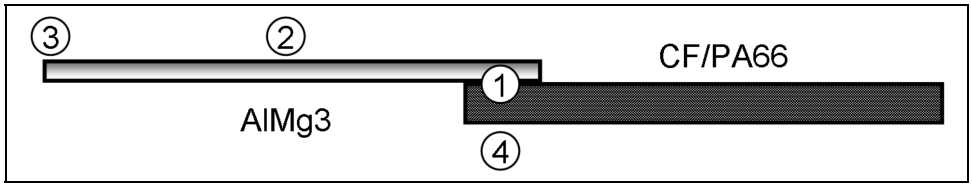

Figure 6.1: Positions of the measuring points of the temperature during induction heating of AlMg3 and CF/PA66

During the heating the temperature evolution of the various positions was recorded (Figure 6.2).

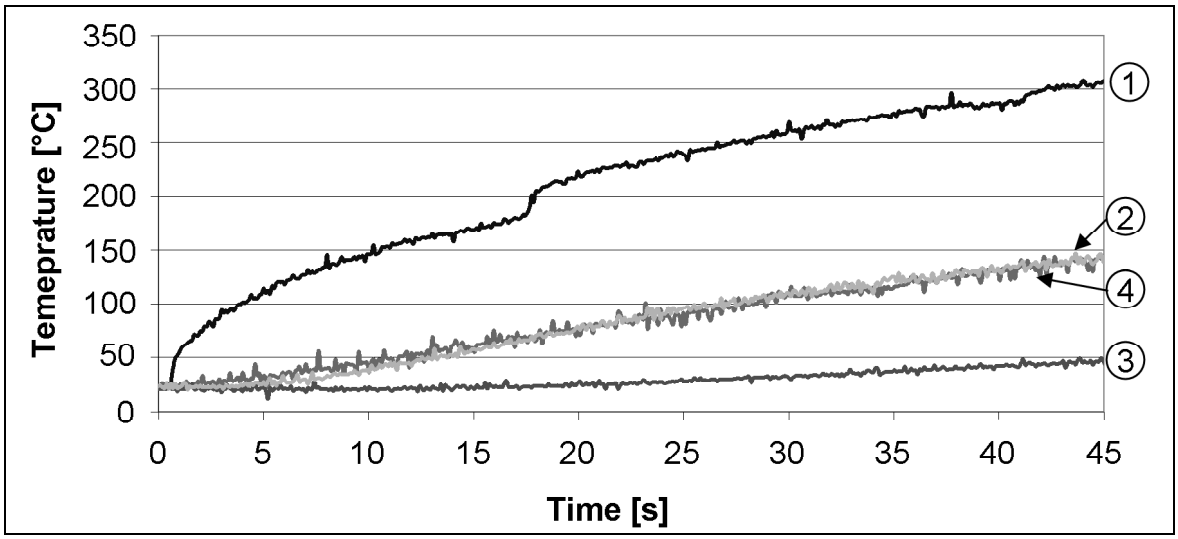

Figure 6.2: Induction heating of AlMg3-CF/PA66 measured on four positions

As can be observed the entire aluminum is heated up to a large extent (Pos. 1 to 3) and little heat was transferred into the CF/PA66 sample (Pos. 4).

6.2 Analytical model

Starting with the law of thermodynamics an analytical model for heating was developed [143]. The final equation after assuming that the entire Al-sample was homogenously heated was formulated by:

$$\frac{T_{Al}-T_R}{T_0-T_R}=\exp\left(\frac{-2\cdot\alpha_{heat}\cdot t}{\rho\cdot b\cdot c_p}\right)+\frac{Q_{in}}{2\cdot A\cdot\alpha_{heat}\cdot(T_0-T_R)}\left(1-\exp\left(\frac{-2\cdot\alpha_{heat}\cdot t}{\rho\cdot b\cdot c_p}\right)\right) \qquad (6.1)$$

The average aluminum temperature (T_{Al}) now depends on the following parameters:

- Heat transfer coefficient α_{heat} [W/(m²·K)]
- Time t [s]
- Density ρ [kg/m^3]
- Sample thickness b [m]
- Specific heat capacity c_p [J/g·K]
- Inserted heat Q_{in} [J]
- Surface area A [m^2]
- Starting temperature T_0 [K]
- Room temperature T_R [K]

The average aluminum temperature can be determined with equation 6.1 and is used to calculate indirectly the temperature in the joining zone (Figure 6.3).

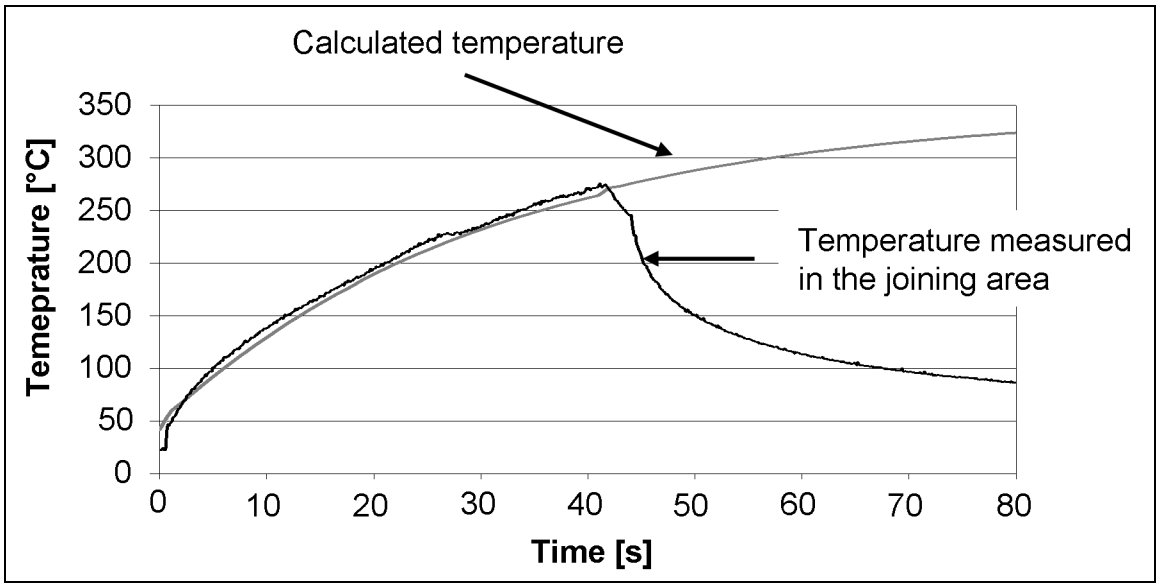

Figure 6.3: Calculation and measured temperature in the joining area

The calculated temperature evolution fits very well with the measured temperature evolution and indicates that the predicted temperatures are correct. The equation shows that mainly the heat transfer coefficient (α_{heat}), the sample thickness (b), and the specific heat capacity (c_p) influence the heating.

6.3 FE-Model

To compare the experimental results with an FE-model, CAD-models of the materials were created in SolidWorks 2005 and imported into Ansys Workbench 10.0. Here, an internal heat source can be assigned to the welding zone. By means of calorimetry the generated heat caused by induction heating can be determined (Figure 6.4) [144].

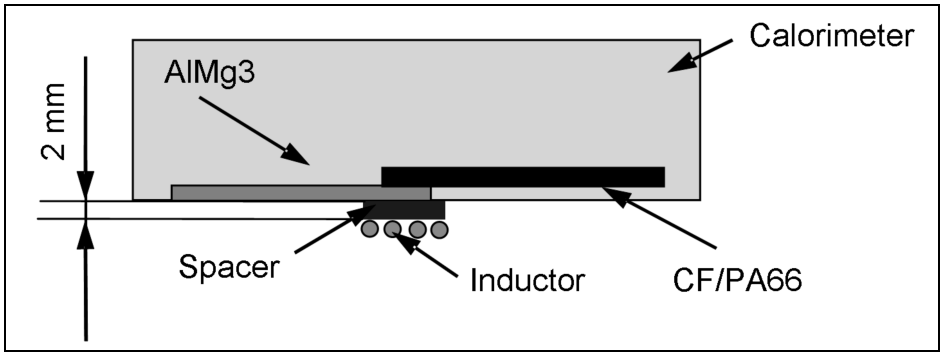

Figure 6.4: Experimental set-up for the calorimetry experiment

The samples are placed in a vessel containing a certain volume of water. Inductive heating is applied and the temperature change is measured. The generated heat can be measured by using equation 6.2.

$$Q = \Delta T \cdot (m_{Sample} \cdot c_{p,Sample} + m_{Water} \cdot c_{p,Water} + m_{Vessel} \cdot c_{p,Vessel}) \quad (6.2)$$

Q = Heat stored in water [J]

ΔT = Measured temperature difference in the calorimeter [K]

m_x = Mass of the sample, water or vessel [g]

$c_{p,x}$ = Specific heat capacity of the sample, water or vessel [J/(g·K)]

For the calculation of the generated heat the following conditions were used.

Heat capacity water: c_p = 4.18 J/(g·K)

Heat capacity aluminum: c_p = 0.90 J/(g·K)

Heat capacity vessel (PC): c_p = 1.3 J/(g·K)

The heat capacity of the water is regarded to be constant in the applied measuring range [145]. By recording water temperature in the vessel in respect to time, the heat transferred into the water is calculated thus the heat generation in the joining partner can be determined (Figure 6.5).

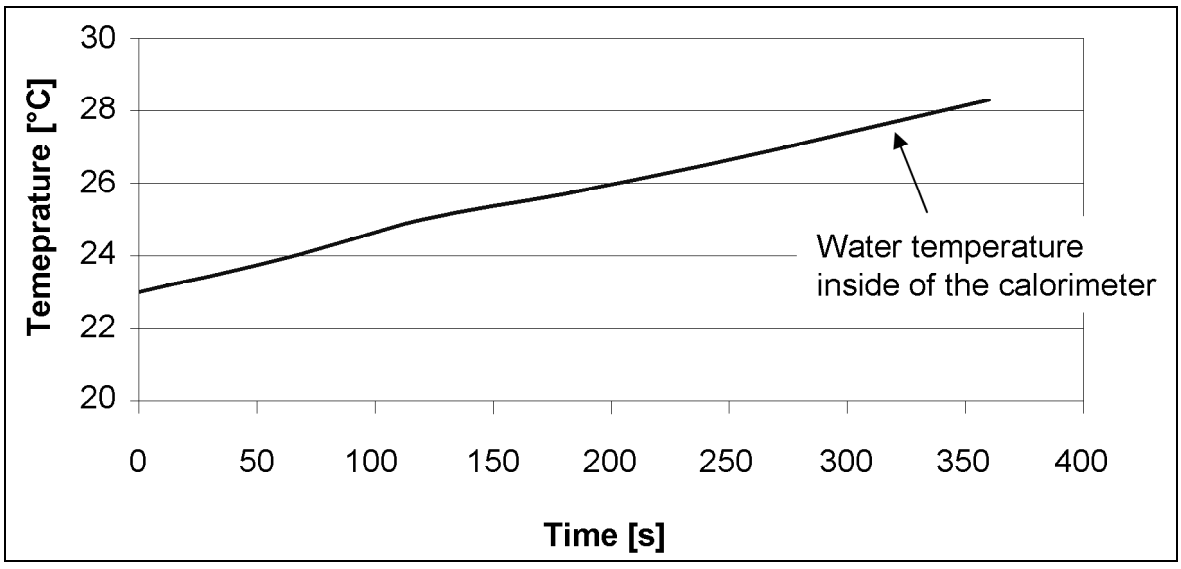

Figure 6.5: Water temperature evolution inside of the calorimeter in dependence of time

The generated heat was determined and its value of 8.0 x 10^7 W/m³ was used as internal heat source for the overlap area of the AlMg3 to simulate the induction heating (Figure 6.6).

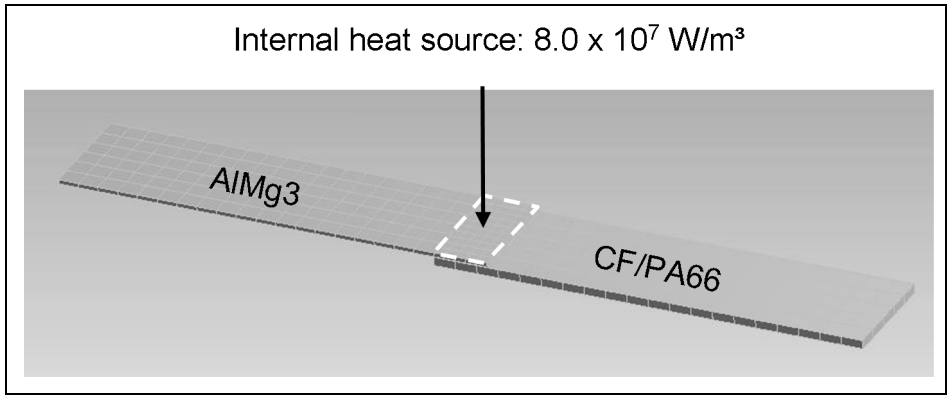

Figure 6.6: Mesh used for simulation of the heat transfer in AlMg3-CF/PA66-joint

The experimental and FE results from the sample heating are shown in Figure 6.7.

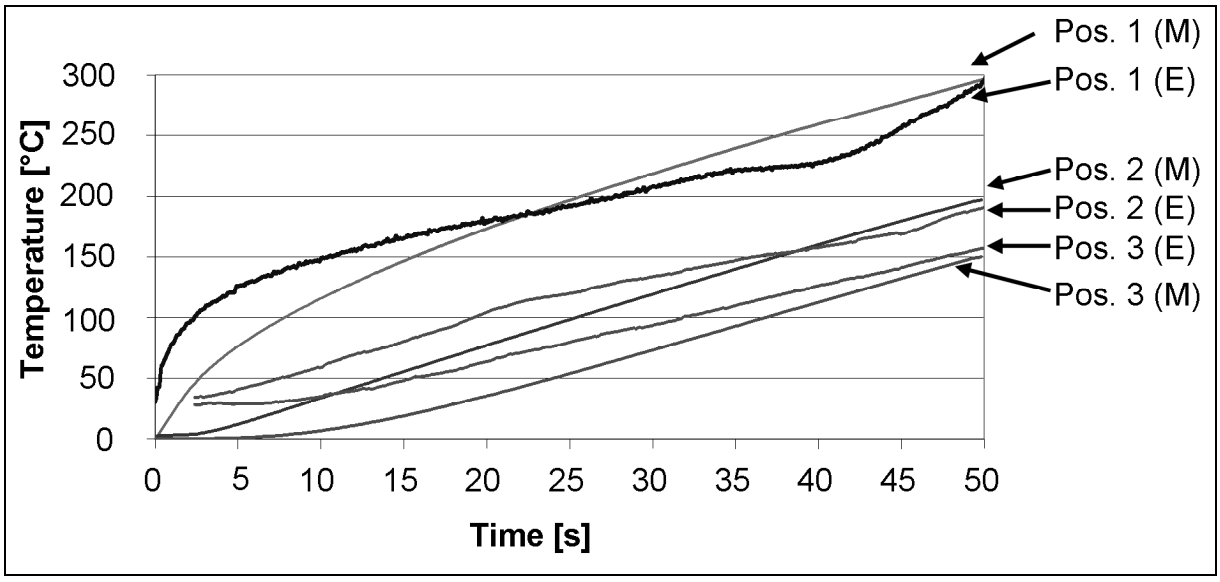

Figure 6.7: Temperatures at various positions recorded with thermal wires (E) and from the FE-model (M) after 50 seconds of heating

The values of the measuring points one to three correspond very well with the measured values indicating that the used FE-model is able to predict the temperature distribution after applying an internal heat source. For the developed model the sample holder was also integrated. Figure 6.8 shows the temperature distribution after 50 seconds of heating and a view of the sample cross section.

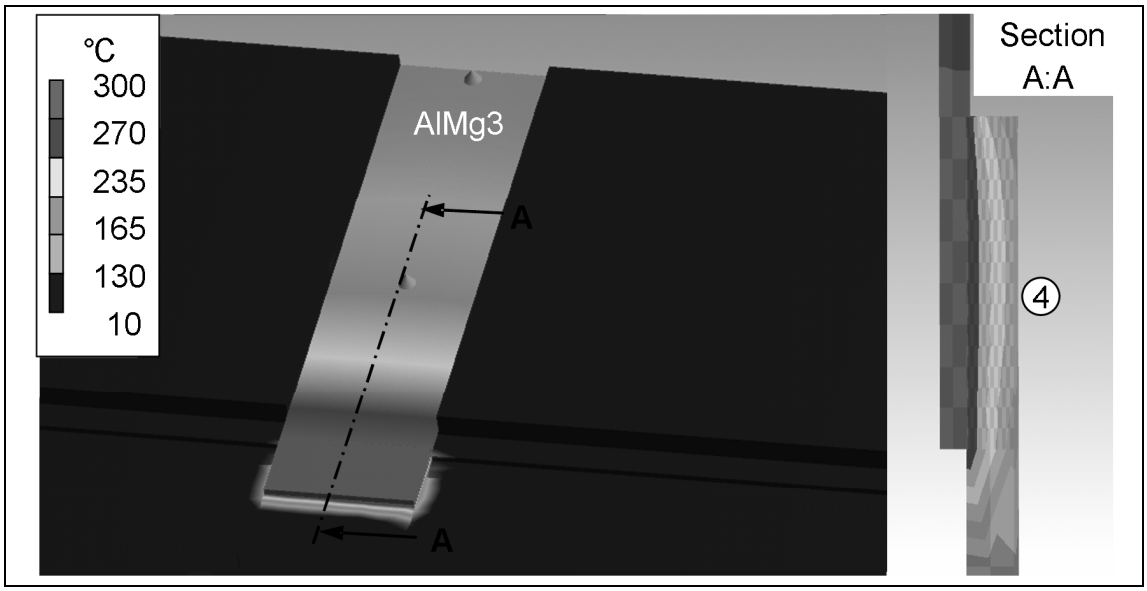

Figure 6.8: Temperature distribution after 50 seconds of heating with an internal heat source of 8.0 x 10^7 W/m³ and the temperature at position 4

Here it can be clearly observed that the thermal conductivity of the AlMg3 is much higher than in the CF/PA66. For position 4 experimentally a temperature of 150 °C was determined (Figure 6.2), the simulation leads to a value of approx. 165 °C. The good correspondence between the experiment and the FE-calculations are also proven by comparing the results of heating after 50 seconds from the infra red camera observation and the FE-model (Figure 6.9).

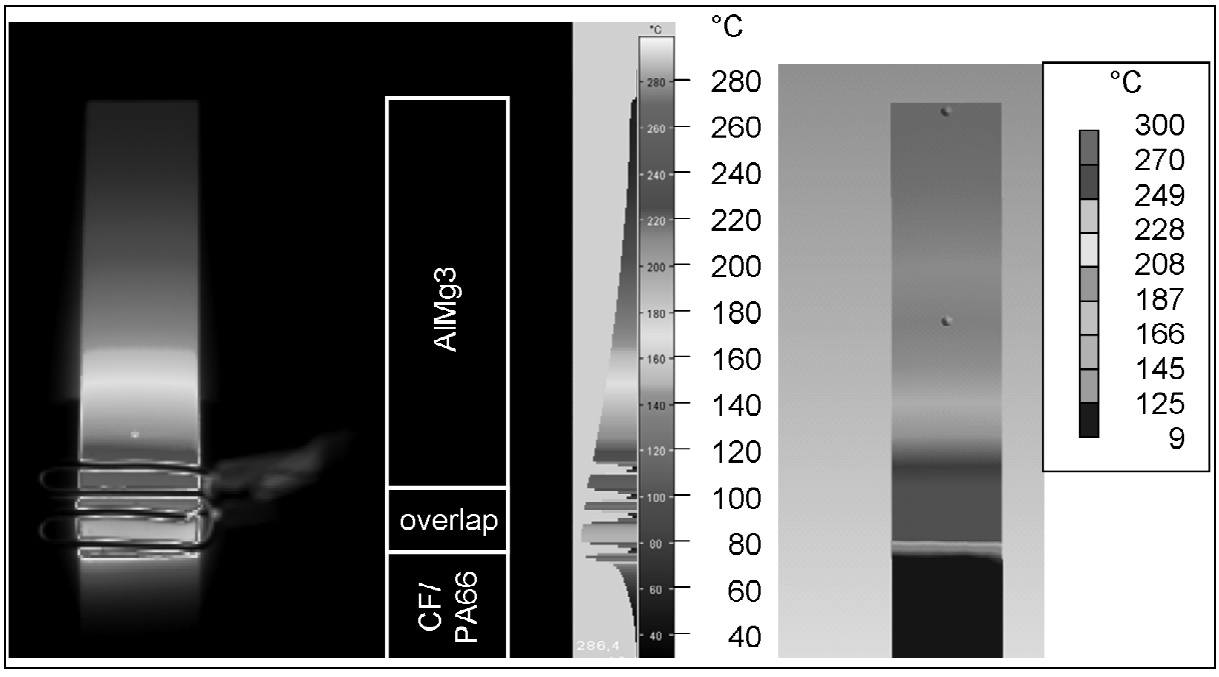

Figure 6.9: Temperature distribution after 50 seconds of heating with an internal heat source of 8.0 x 10^7 W/m³ and infra red camera observation

Summarizing the results from the experiments, the analytical calculations, and the FE-simulations, it was shown that a very good conformity between these three different methods was achieved and the FE-software can be used to predict the heat transfer into the joining partners. Finally, a prediction of the manufacturing parameters for the heating can be accomplished with this tool.

7 Summary

Induction welding can be used to weld FRPCs as well as for joining of metal/TP-FRPC. After evaluation of the achievement potential of this type of bonding, it was concluded that the surface treatment of the metallic and the polymeric joining partner, as well as process conditions, influence bonding quality.

Various new equipment (e.g. sample holder, tempered pressing tool, heating and compaction roller) was designed and introduced in the induction welding device to manufacture the metal/polymer joints. The topographical investigations by SEM and laser profilometry show a large influence of the roughness parameter as a result of the surface treatment. Moreover, the surface treatment also results in a change of physical (surface energy) and chemical (atom concentration) properties. The characteristics of the welded samples were studied, first by shear tensile testing and afterwards by surface fracture analysis. The main results of the investigations are:

- Pre-treatment methods, corundum blasting and acidic pickling, give the metallic joining partners higher bonding strength. The atmospheric plasma treatment of the polymeric joining partner produces an increase of shear tensile strength of about 10 % and also a decrease of the confidence intervals.
- The shear tensile strength depends on the applied pressure and, therefore, on the flow behavior of the polymer in the joining zone.
- The orientation of the testing force had no influence on the fabric types used.
- The plain weave, with more polymer rich areas, produces a higher bonding strength compared to the 5H Satin-weave. The NCF resulted in a similar shear tensile strength. This indicates that bonding is determined by polymer.
- An intermediate polymer layer made of additional polymer sheets leads to an increase of the shear tensile strength. Micrographs show a polymer layer with an average thickness of 5 – 20 µm.
- By combining several treatment parameters (corundum blasted with additional polymer layer) the bonding strength is almost doubled to 14 MPa for AlMg3-CF/PA66-joints and 19 MPa for DC01-CF/PEEK-joints.

Further investigations of the process conditions show that the best CF/PEEK-joints are achieved when the following settings are chosen:

- A pressing temperature of 370 °C for CF/PEEK.
- A holding time of 7 minutes.
- A cooling rate of 6 °C/min.

Shear tensile strength of 14.5 MPa for AlMg3-CF/PA66 by using a pressing temperature of 10 °C and 19.1 MPa for DC01-CF/PEEK are achieved. This shear tensile strength is only about 15 and 16 % less than that of adhesively bonded joints.

Initial investigations on galvanic corrosion were performed. Here a rapid decrease of the shear tensile strength is observed for water-submerged samples. After 21 days in water the shear tensile strength is reduced to 25 % of its original value for corundum blasted AlMg3-CF/PA66. No strength was left for acetone treated AlMg3-CF/PA66 with additional polymer. The glass fiber joints out of corundum blasted AlMg3-GF/CF/PA66 only lost 30 % strength. The corrosion is accelerated by using an artificial sea water solution. In case of direct contact of the carbon fiber to aluminum corrosion products are formed. After 7 days the shear tensile strength is reduced to 25 % of its original value for acetone treated samples; the corundum blasted AlMg3-CF/PA66 sample were corroded, but still had 90 % of its original value. The AlMg3-GF/CF/PA66-joints showes no corrosion products and no strength loss was observed. The experiments show that the induction welded joints are mainly bonded by physical bonding forces and after corundum blasting also by mechanical interlocking.

Dynamic thermogravimetric analyses in various environmental gases were performed to increase the degradation temperature of the polymer. In the case of PA66 this did not lead to an increase of the process window as the polymer degradation is almost solely thermally controlled instead of oxidative controlled. The observed degradation temperature for PEEK in air was about 550 °C. However, this kind of welding shows a large potential for welding of fiber reinforced olefins, like GF/PP. An increase of the degradation temperature from 230 °C in air to 390 °C in nitrogen was measured.

A demonstrator was made out of an aluminum profile welded on a CF/PA66-plate and shows the possible transfer of the information obtained in these investigations to industrial applications. By means of analytical and FE-calculations the heating during induction welding were successfully reproduced.

8 Appendix

8.1 Appendix 1: Mechanical properties of CF/PA66, and CF/PEEK, the metals used

The mechanical properties of the composite joining partner for the mechanical simulations by Schmeer [146, 147] are summarized in Table 8.1.

Table 8.1: Mechanical properties of CF/PA66 and CF/PEEK

Material	**CF/PA66 (woven fabric)**			**CF/PEEK (woven fabric)**			**CF/PA66 (NCF)**	
Testing temperature [°C]	**-30**	**RT**	**80**	**-30**	**RT**	**80**	**RT**	**80**
Tensile strength [MPa]	590	580	520	430	500	470	760	660
Young modulus [GPa]	56	55	50	49	46	41	48	46

The mechanical properties of the metallic joining partner for the mechanical simulations [148] are summarized in Table 8.2.

Table 8.2: Mechanical properties of AlMg3, AlMg0.4Si1.2, and DC01

Material	**AlMg3**			**AlMg0.4Si1.2**			**DC01**		
Testing temperature [°C]	**-30**	**RT**	**80**	**-30**	**RT**	**80**	**-30**	**RT**	**80**
Tensile strength [MPa]	247	250	246	259	244	219	346	313	284
Young modulus [GPa]	72	70	75	66	67	69	174	167	127
$R_{p,\,0.2}$ [N/mm²]	170	178	176	136	134	132	198	171	163
Strength [MPa] for an overlap area of 312.5 mm² with 0.2 % deformation and joining partner breakage (sample width: 25 mm, thickness: 1 mm)	13.6 19.8	14.2 20.0	14.1 19.7	10.8 20.7	10.7 19.5	10.6 17.5	15.9 27.7	13.6 25.0	13.0 22.7

8.2 Appendix 2: Thermal properties of the metals and fiber reinforced polymers used

The enthalpy (H) is the sum of the inner energy (U) and the work (p·V)

$$H = U + pV \tag{8.1}$$

When considering these parameters for a given mass (m) one obtains the specific values:

$$h = \frac{H}{m};\quad u = \frac{U}{m};\quad v = \frac{V}{m} \tag{8.2}$$

Furthermore, the specific enthalpy is given by:

$$h = u + p \cdot v \tag{8.3}$$

The specific heat capacity at constant pressure is obtained by:

$$c_p = \left(\frac{\partial h}{\partial T}\right)_p \tag{8.4}$$

and for constant volume by:

$$c_v = \left(\frac{\partial h}{\partial T}\right)_v \tag{8.5}$$

Solid and liquid materials can in a first approximation, especially at low pressures, be considered incompressible, so:

$$c_p = c_v = c \tag{8.6}$$

The specific heat capacity at constant pressure (c_p) of CF/PA66, CF/PEEK, AlMg3, and DC01 depend on the temperature can be seen in Figure 8.1.

Moreover, it can be seen that the semi-crystalline thermoplastics undergo a phase-transition near the melting point (T_m) by opening the crystalline structure, which requires energy. The measured specific heat capacities are in correspondence with those given in [125, 126].

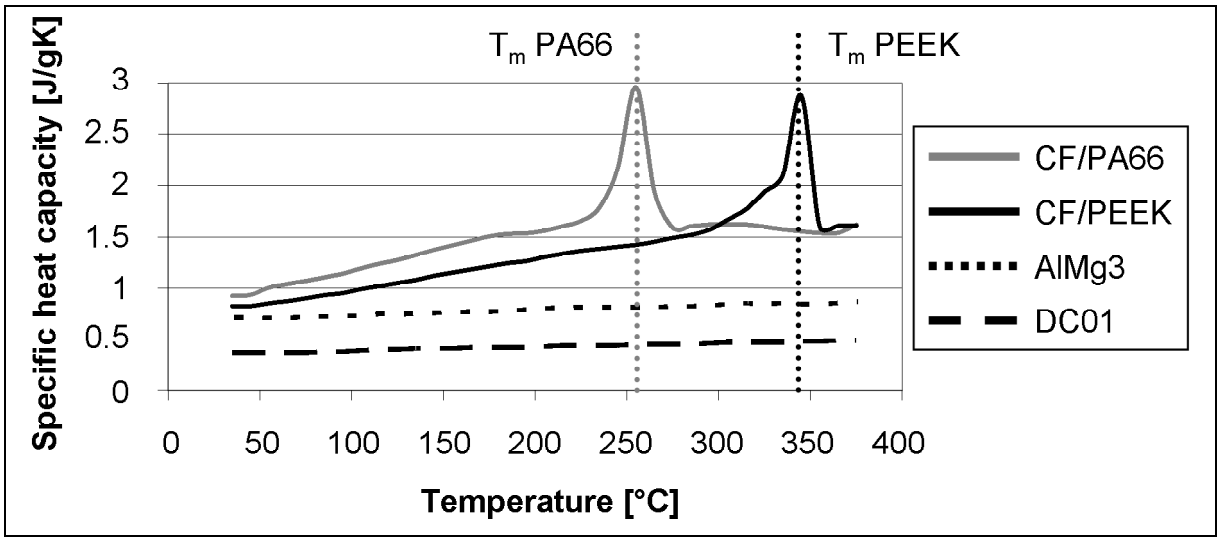

Figure 8.1: Specific heat capacity of the materials used as function of temperature

The change of the specific inner energy is then given by:

$$\Delta u = u_2 - u_1 = \int_{T_1}^{T_2} c(T)dT \tag{8.7}$$

By using formula (8.7) the area underneath the heat capacity profile is determined. This area equals the specific inner energy in the case that no work (p·V) is performed. This is called enthalpy and indicates how much energy is needed to heat up a certain mass of material up to the requested temperature.

Another important material property for the heat transfer is the thermal conductivity coefficient λ. Figure 8.2 shows that the thermal conductivity of PA66 and AlMg3 also depends on the temperature.

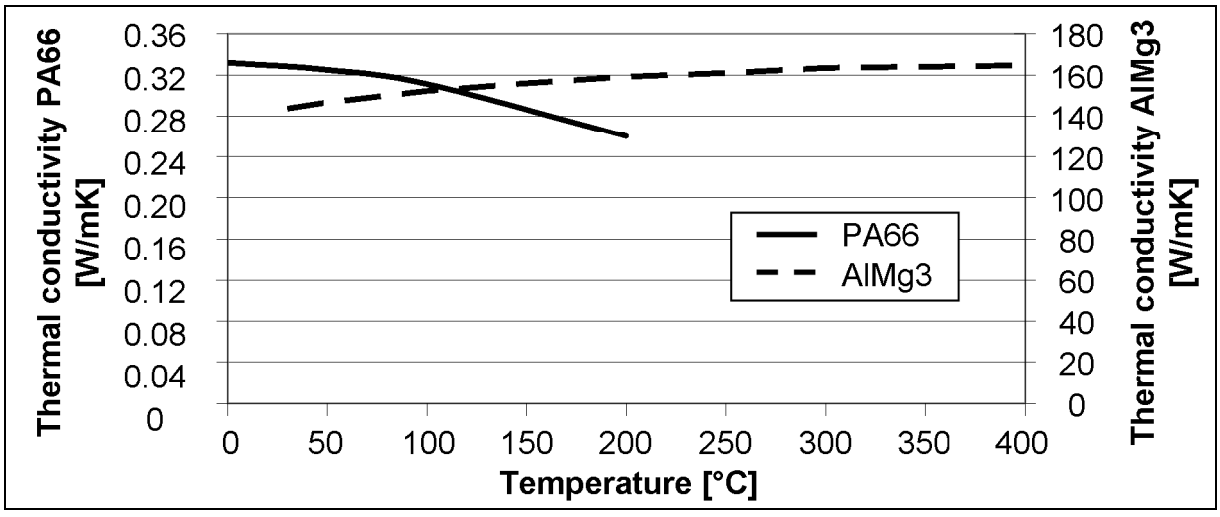

Figure 8.2: Thermal conductivity in dependence of the temperature

8.3 Appendix 3: Properties of the polymer, fibers, fabrics, and composites used

Table 8.3: Data about the polymers used

Characteristic	Unit	Polymer		
Polymer type		PA66	PEEK	PEEK-compound
Polymer manufacturer		DuPont Packaging Polymers	Victrex	Lehmann&Voss &Co. (Germany)
Polymer designation		Dartek® SF502	150pf	LUVOCOM 1105 – 7373 VP
Density	[kg/dm³]	1.13	1.3	1.62
Tensile strength, yield	[MPa]	45	100	-
Tensile strength at break	[MPa]	76	-	165
Modulus of elasticity	[GPa]	-	-	14
Coefficient of thermal expansion	[10^{-6}/°C]	-	47 (23 °C) 47 (100 °C) 94 (250 °C)	-
Specific heat capacity	[J/g·K]	1.6 (50 °C) 2.4 (235 °C) 5.0 (260 °C)	0.95 (50 °C) 1.9 (300 °C) 4.2 (345 °C)	-
Thermal conductivity	[W/m·K]	0.32 (23 °C) 0.26 (300 °C)	0.25	-
Melting point	[°C]	260	344	340
Glass transition temperature	[°C]	70	143	Approx. 143
Degradation temperature (5 % weight loss of the base line)	[°C]	350 (oxygen) 370 (air) 395 (nitrogen)	550 (air)	-
Reference		[149]	[150]	[151]

Table 8.4: Data about the carbon fibers and fabrics used

Characteristic	Unit	Carbon fiber		
Fiber manufacturer		Toray	Toray	Fortafil
Fiber designation		T300	T300J	510
Fiber type		Standard modulus carbon fiber	Standard modulus carbon fiber	Standard modulus carbon fiber
Density	[kg/dm³]	1.76	1.78	1.8
Filament diameter	[µm]	7	7	6
Tensile strength	[MPa]	3,530	4,210	3,800
Tensile modulus	[GPa]	230	230	231
Strain	[%]	1.5	1.8	1.64
Coefficient of thermal expansion	[10^{-6}/°C]	-0.41	-0.43	-0.1
Specific heat	[J/g·K]	0.80	0.75	0.92
Thermal conductivity	[W/m·K]	10.46	9.33	20.2
Electric resistivity	[Ω·10^{-8} m]	$1.7 \cdot 10^{3}$	$1.5 \cdot 10^{3}$	-
Chemical composition	[%]	Carbon (93%)	Carbon (94%)	-
Reference		[123]	[152]	[153]

Fabric manufacturer		**Ten Cate Advanced Composites**	**ECC GmbH & Co. KG**	**Sigmatex (UK) Ltd.**
Fabric type		5H Satin (Woven)	Plain (Woven)	+/- 45° (Non-crimped fabric)
Fabric designation		CD 0282. 040.000.0000	Style 475	MCX0481270
Sizing type and amount		40B / 1 %	- / 1 %	- / 0.4 %
Number of filaments	[-]	3,000	3,000	80,000
Area weight	[g/m²]	285	285	300
Ratio warp / weft		50/50	50/50	
Ratio longitudinal / transversal				50/50
Reference		[154]	[155]	[156]

Table 8.5: Data about the carbon fiber reinforced polymer composite used

Characteristic	**Unit**	**Carbon fiber reinforced polymer composite**							
		CF/PA66			CF/PEEK			CF/PA66	
Fabric type		5H Satin			5H Satin			+/- 45° NCF	
Fiber volume fraction	[-]	0.48			0.48			0.48	
Testing temperature	[°C]	-30	RT	80	-30	RT	80	RT	80
Tensile strength (0°/90°-direction)	[MPa]	590	580	520	430	500	470	760	660
Young modulus (0°/90°-direction)	[GPa]	56	55	50	49	46	41	48	46
Stain at break (0°/90°-direction)	[%]	1.04	1.06	1.14	0.94	0.97	1.09	1.9	1.4
Shear tensile strength (-45°/+45°-direction)	[MPa]	108	114	80	121	118	108	61	45
Shear tensile modulus (-45°/+45°-direction)	[GPa]	4.2	2.7	1.1	4.7	3.9	3.1	3.0	1.6
Specific heat capacity	[J/g·K]	1.0 (50 °C) 1.8 (235 °C) 3.0 (260 °C)			0.85 (50 °C) 1.6 (300 °C) 2.9 (345 °C)				
Degradation temperature (5 % weight loss of the base line)	[°C]	410 (oxygen) 415 (air) 415 (nitrogen)			560 (air)				
Reference mechanical data		[146]			[146]			[147]	
Reference thermal date		(Figure 5.25 and Figure 8.1)			(Figure 5.25 and Figure 8.1)				

9 References

[1] Kuhn, D.: Ein Riese hebt ab. Maschinenmarkt, 12 (2005), 18-19

[2] Burton, R.: Nosing ahead. Aerospace Manufacturing, September (2006), 22-24

[3] Schlarb, A.K.: Glasmattenverstärkte Thermoplaste, Eine Werkstoffklasse mit Zukunft. Plastverarbeiter, 48, 10 (1997), 87-90

[4] Bigg, D.M.; Preston, J.R.: Stamping of thermoplastic matrix composites. Polymer Composites, 10, 4 (1989), 261-268

[5] O´Brien, K.T.; Kasturi, S.; Mekkaoui, A.M.: A computational analysis of the heating of glass mat thermoplastic (GMT) sheets by dual beam microwave sources. Polymer Composites, 15, 3 (1994), 231-239

[6] Bigg, D.M.: Processing-property relationships for pet sheet composites. Makromol. Chem., Makromol. Symp. 70/71, Basel: Hüthig & Wepf Verlag, (1993), 245-254

[7] Seeber-Röchling Automotive: Kunststoffanwendungen im Motorraum. Die Bibliothek der Technik Band 259, Landsberg am Lech: Verlag Moderne Industrie, 2004

[8] Neitzel, M.; Mitschang, P.: Handbuch Verbundwerkstoffe, Munich: Hanser-Verlag, 2004

[9] Bültjer, U.: Die Produktion von GFK und duroplastischen Formmassen in Europa 2002/2003, 6th AVK-TV Conference, Baden-Baden, 2003, P1–1-P1–9

[10] Jansz, J.: Polypropylene in automotive applications. In: Karger-Kocsis, J.: Polypropylene: An A-Z Reference, Dordrecht: Kluwer Academic, 1999. 643-651

[11] Wacker, M.: Leicht und Sicher – Serienanwendungen aus thermoplastischen Faserverbundbauweisen im Automobil. Proceedings of the 2nd Landshuter Leichtbau-Colloquium. 24th-25th February 2005, 187-196

[12] Mitschang, P.; Blinzler, M.; Wöginger A.: Processing Technologies for continuous Fibre Reinforced Thermoplastics with novel Polymer Blends, Composite science and technology, 63, 14 (2003), 2099-2110

[13] Wöginger, A.: Prozesstechnologien zur Herstellung kontinuierlich faserverstärkter thermoplastischer Halbzeuge. Kaiserslautern: Dissertation, IVW-Schriftenreihe Band 41, 2004

[14] Spelz, U.: Thermoplastics Composites: Continuous Compression Moulding. JEC-Composites, 14 (2005), 57-58

[15] Giehl, S.; Mitschang, P.: Fibre-Reinforced Sandwich and Profile Structures in One Step. Kunststoffe Plast Europe, 11 (2005), 76-78

[16] Lahr, R.; Velthuis, R.; Giehl, S.; Mitschang, P.: Fügen und Thermoformen von thermoplastischen FKV. In: Neitzel, M. (Ed.): Proceedings of the IVW colloquium, Kaiserslautern, 2002, 231-235

[17] Lahr, R.; Mitschang, P.: Thermoforming of continuous carbon fiber reinforced thermoplastics and integration of a bearing element in an one step process, SAMPE Europe Symposium, 2006

[18] Mitschang, P.; Velthuis, R.; Rudolf, R.: Fügeverfahren für FKV. In: Neitzel, M.; Mitschang, P. (Ed.): Handbuch Verbundwerkstoffe, München: Carl Hanser-Verlag, 2004

[19] Ageorges, C.; Ye, L.: Fusion Bonding of Polymer Composites, London: Springer, 2002

[20] Offringa, A.: Thermoplastics in Aerospace, New Products through innovative Technology. SAMPE Journal, 41, 7 (2005), 19-27

[21] Rudolf, R.; Mitschang, P.; Neitzel, M.; Rückert, C.: Welding of High-Performance Thermoplastic Composites. Polymers and Polymer Composites 7 (1999), 5, 309-315

[22] Velthuis, R.; Mitschang, P.: Induction welding technology – Joining fiber reinforced thermoplastic polymer (composites) for aerospace applications.

International Aeronautical Federation, IAC-03-I.3.06, 54th IAF-Congress, Bremen, September 2003

[23] Velthuis, R.; Mitschang, P.: Induction welding of fibre reinforced thermoplastic composites in case of a rear seat back support, 6th AVK-TV Conference, Baden-Baden, 2003, A13–1-A13–9

[24] Wacker, M.: Thermoplastische Hochleistungsverbunde auf dem Weg zu Serienanwendungen. In: Schlarb, A.K. (Ed.): IVW-Kolloquium 2004, Kaiserslautern: IVW Schriftenreihe Band 48, 5th-6th October 2004, 140-149

[25] Hailer, R.; Sedlmaier, H.; Lohse, H.; Schumacher, R.: CFK-Dach M3 CSL – erfolgreiche Leichtbaustrategie dank Klebtechnik. Adhäsion – Kleben und Dichten, 48, 12 (2004), 11-16

[26] Lohse, H.: Joining plastics by adhesive bonding in automotive engineering. JEC Composite Magazine, 27 (2006), 46-49

[27] Deinzer, G.; Wetter, H.; Schmid, G.; Bangel, M.: Fügetechnologien zur Integration von FVK-Bauteilen in metallische Karosseriestrukturen. Proceedings: Plastics in Automotive Engineering, VDI Kunststofftechnik, Germany, Mannheim, 29th March 2006, 275-292

[28] Rotheiser, J.: Joining of plastics - Handbook for designers and engineers, Munich: Hanser-Verlag, 1999

[29] Benatar, A.; Grewell, D.A.; Park, J.B.: Plastics and Composites Welding Handbook, Munich: Hanser-Verlag, 2003

[30] Ehrenstein, G.W.: Handbuch Kunststoff-Verbindungstechnik, Munich: Hanser-Verlag, 2004

[31] Potente, H.: Zur Theorie des Heizelement-Stumpfschweißens. Kunststoffe, 67, 2 (1977), 98-102

[32] Schlarb, A.K.: Zum Vibrationsschweißen von Polymerwerkstoffen – Prozess - Struktur - Eigenschaften. Kassel: Dissertation, 1989

[33] Schlarb, A.K.; Ehrenstein, G.W.: Vibrationsschweißen – Prozess bestimmt Verbindungsqualität. Kunststoffe, 83, 8 (1993), 597-602

[34] Egen, U.: Gefügestruktur in Heizelementschweißnähten an Polypropylen-Rohren. Kassel, Dissertation, 1984

[35] Ehrenstein, G.W.; Schlarb, A.K.: Vibrationsschweißen – Ein Schweiß-verfahren für Kunststoffe aus werkstofftechnischer Sicht. Kunststoffe, 78, 6 (1988), 541-546

[36] Potente, H.; Natrop, J.: Quality assurance of computer controlled hot-tool welding for mass production. Polymer Engineering and Science, 31, 7 (1991), 519-525

[37] Potente, H.; Heil, M.: Hochtemperaturbeständige Kunststoffe mit Infrarotstrahlern schweißen. Kunststoffe, 82, 8 (1992), 655-658

[38] Potente, H.; Übbing, M.: Von der Messdatenerfassung zur Produktbeurteilung – eine Methode der Qualitätssicherung beim Vibrationsschweißen. Schweißen und Schneiden, 46, 11 (1994), 559-564

[39] Ehrenstein, G.W.; Künkel, R.; Gehde, M.: Bemessungskennwerte für die Verbindungsauslegung und werkstoff-/ prozessabhängige Nahteigenschaften beim Vibrationsschweißen verstärkter Thermoplaste. Abschlussbericht: AiF 13.512 N / DVS 11.003, 2005

[40] Bonten, C.; Schmachtenberg, E.: A new hypothesis to describe the mechanisms acting in a welded joint of semicrystalline thermoplastics. Polymer Engineering and Science, 41, 3 (2001), 475-483

[41] Potente, H.; Natrop, J.; Klit Pedersen, T.; Uebbing, M.: Vergleichende Untersuchung beim Schweißen von glasfaserverstärkten PES. Plastverarbeiter, 44, 6 (1993), 26-33

[42] Potente, H.; Brüssel, A.: Heizelementschweißen von gefüllten und verstärkten Thermoplasten. Schweißen & Schneiden, 50, 3 (1998), 172-179

[43] Giese, M.; Ehrenstein, G.W.: Vibration welding of random glass mat reinforced thermoplastic composites. ANTEC 1992, 884-887

[44] Gehde, M.; Giese M.; Ehrenstein G.: Welding of thermoplastics reinforced with random glass mat. Polymer Engineering and Science, 37, 4 (1997), 702-714

[45] Messler, R.W.: Joining composite materials and structures: Some thought-provoking-possibilities. Journal of Thermoplastic Composite Materials, 17, 1 (2004), 51-75

[46] Rudolf, R.: Entwicklung einer neuartigen Prozess- und Anlagentechnik zum Fügen von thermoplastischen Faser-Kunststoff-Verbunden. Kaiserslautern: Dissertation, IVW-Schriftenreihe Band 10, 2001

[47] Kwok, D.Y.; Neumann, A.W.: Contact angle measurement and contact angle interpretation. Advances in Colloid and Interface Science, 81, (1999), 167-249

[48] Kinloch, A.J.: Adhesion and Adhesives. London: Chapman and Hall, 1987

[49] Brockmann, W.; Geiß, P.L.; Klingen, J.; Schröder, B.: Klebtechnik – Klebstoffe, Anwendungen und Verfahren, Weinheim: Wiley-VCH Verlag GmbH, 2005

[50] Kinloch, A.J.; Kodokian, G.K.A.; Watts, J.F.: Relationship between the surface free energies and surface chemical compositions of thermoplastics fibre composites and adhesive joint strengths. Journal of Materials Science Letters, 10 (1991), 815-818

[51] Saechtling, H.: International Plastic Handbook: for the Technologist, Engineer, and User, 3. Edition, Munich: Hanser-Verlag, 1995

[52] Bischof, C.: ND-Plasmatechnik im Umfeld der Haftungsproblematik bei Metall-Polymer-Verbunden. Mat.-wiss. u. Werkstofftech, 24 (1993), 33-41

[53] Möller, S.: Phosphorsäure-Haftvermittler – ein Beitrag zur Adhäsion an Aluminiumoberflächen. Bielefeld: Dissertation, 1998

[54] Brockmann, W.: Durability of Adhesion between Metals and Polymers. Journal of Adhesion, 29 (1989), 53-61

[55] Brockmann, W.; Hennemann, O.: Eine andere Modellvorstellung über die Adhäsion in Polymer/Metall-Verbunden. Adhäsion, 11 (1989), 33-35

[56] Brockmann, W.; Emrich, S.: Wie lange halten vorbehandelte Aluminiumklebungen? Teil 1. Adhäsion, 5 (2002), 34-39

[57] Brockmann, W.; Emrich, S.: Wie lange halten vorbehandelte Aluminiumklebungen? Teil 2. Adhäsion, 7-8 (2002), 36-41

[58] Neeb, T.: Adhäsionsmechanismen an mechanisch vorbehandelten Metalloberflächen. Kaiserslautern: Dissertation, 1999

[59] Buske, C.; Knopse, A.: Plasma processes In-Line. Kunststoffe Plast Europe, 11, (2005), 82-86

[60] Chan, C.-M.; Ko, T.-M.; Hiraoka, H.: Polymer surface modification by plasmas and photons. Surface Science Reports, 24, (1996), 1-54

[61] Comyn, J.; Mascia, L.; Xiao, G.; Parker, B.M.: Plasma-treatment of polyetheretherketone (PEEK) for adhesive bonding. International journal of adhesion and adhesives, 16, (1996), 97-104

[62] Lommatzsch, U.: Vorbehandeln mit Plasma bei Atmosphärendruck. MO Metalloberfläche, 57, (2003)

[63] McKnight, S.H.; McBride, M.G.; Gillespie, J.W.: Joining of Polypropylene and Aluminum: Evaluation of environmental Durability. 25th International SAMPE Technical Conference, 26-28 October, 1993

[64] Marinelli, J.M.; Lambing, C.L.T.: Advancement in Welding Technology for Composite-to-Metallic Joints. Journal of Advanced Materials, April 1994, 20-27

[65] Ramani, K.: Process-Induced Effects in Thin-Film Bonding of PEKEKK in Metal-Polymer Joints. Polymer Composites, 17, 6 (1996), 879-886

[66] Skiles, J.A.; Wightman, J.P.: Heat-resistant thermoplastic/chromic acid anodized Ti-6Al-4V single lap bond evaluation. Int. J. Adhesion and Adhesives, 8, 4 (1988), 201-206

[67] Progar, D.J.; St.Clair T.L.: Evaluation of a novel thermoplastic polyimide for bonding titanium. Int. J. Adhesion and Adhesives, 6, 1 (1986), 25-30

[68] Mayhew, R.T.; Kohli, D.K.: Development of high Temperature Service Polyimide based Adhesives for Titanium and Composite Bonding Applications, 41st International SAMPE Symposium, 1996, 1026-1034

[69] Chan-Park, M.B.; Ngew, H.S.; Yip, D.C.F.; Er, C.J.; Zee, S.W.: Heating methods for bonding thermoplastics to aluminum alloy, Journal of Advanced Materials, 33, 4 (2001), 52-61

[70] Riedler, M.: Untersuchung des Einflusses der Prozessparameter auf das Wärmeimpulsschweißen von PEEK und Stahl. Institut für Verbundwerkstoffe GmbH, Technical Report 06-013, 2006

[71] Anagreh, N.; Dorn, L.: Klebflächenvorbehandlung von Aluminiumoberflächen mit SIP-Haftvermittler. Mat-wiss. U. Werkstofftech., 33 (2002), 657-666

[72] Jansen, I.; Simon, F.; Häßler, R.; Kleinert, H.: Aluminum treatment and the properties of adhesively bonded joints. Macromol. Symp., 164 (2001), 465-478

[73] Ramani, K.; Tagle, J.; Devanathan, D.; Nazre, A.; Swarts, D.; Lin, S.: Thermoplastic bonding for structural applications: “The Role of Processing”. Proceedings ICCM-10, Whistler, Canada, August 1995

[74] Day, M.; Suprunchuk, T; Cooney, J.D.; Wiles, D.M.: Thermal degradation of Poly(aryl-Ether-Ether-Ketone)(PEEK): A Differential Scanning Calorimetry Study. Journal of Applied Polymer Science, 36, (1988), 1097-1106

[75] Kadi, H.; Denault, J.: Effects of processing conditions on the mechanical behavior of carbon-fiber-reinforced PEEK. Journal of Thermoplastic Composite Materials, 14, 1 (2001), 34-53

[76] Suwanwatana, W.; Yarlagadda, S.; Gillespie Jr., J.W.: Hysteresis heating based induction bonding of thermoplastic composites. Composite Science and Technology, 66, 11-12 (2006), 1713-1723

[77] Oster, F.: Hochtemperaturbeständige Polymer-Beschichtungen für tribologische Anwendungen. Dissertation, Kaiserslautern: IVW-Schriftenreihe Band 53, 2005

[78] Neuwald, A.: Kristallisationsverhalten von unverstärktem und gewebeverstärktem PA66. Institut für Verbundwerkstoffe GmbH, Technical Report 98-64, 1998

[79] Elsner, H.: Grundlegende Untersuchungen an Kunststoff-Metall-Klebungen als Basis einer Entwicklungsmethodik. Berlin: Dissertation, Polymertechnik - Kunststofftechnikum, 1991

[80] DIN EN 1465 - Klebstoffe - Bestimmung der Zugscherfestigkeit hochfester Überlappungsklebungen. 1995-01

[81] Velthuis, R; Bos, M.; Emrich, S.; Schmeer, S.; Huber, U.; Kopnarski, M.; Maier, M; Mitschang, P.; Renz, R.: Diskontinuierliches Induktionsschweißen von Metall/Faser-Kunststoff-Verbunden. In: Schlarb, A.K. (Ed.): Proceedings of the IVW colloquium, Kaiserslautern, 2006, 178-179

[82] DIN EN 14869-2 - Strukturklebstoffe - Bestimmung des Scherverhaltens struktureller Klebungen - Teil 2: Scherprüfung für dicke Fügeteile (ISO 11003-2:2001, modifiziert), 2004-10

[83] Pocius, A.V.: Adhesion and Adhesives Technology: An Introduction. München: Carl Hanser-Verlag, 1997

[84] Boyd, J.; Speak, S.; Sheahen, P.: Galvanic Corrosion Effects on Carbon Fiber Composites: Results from accelerated tests. 37th International SAMPE Symposium, Coriva, California, 9-12 March 1992, 1184-1198

[85] Lide, D.R.: CRC Handbook of Chemistry and Physics. 76th Edition. New York: CRC Press, 1997

[86] Feldmann, M.; Völling, B.; Geßler, A.; Wellershoff, F.; Geiß, P.L.; Wagner, A.: Kleben im Stahlbau. Stahlbau, 75, 10 (2006), 834-846

[87] Lüderitz, K.: Korrosionsschutz von Aluminium durch Beschichtungen. Mat.-wiss.u. Werkstofftech., 28, (1997), 301-302

[88] Stevens, M.P.: Polymer Chemistry - An Introduction. New York: Oxford University press, 1990

[89] Potente, H.: Fügen von Kunststoffen. Grundlagen, Verfahren, Anwendung. Munich: Hanser-Verlag, 2004

[90] Schaffer, M.A.; Marchildon, E.K.; McAuley, K.B.; Cunningham, M.F.: Thermal nonoxidative degradation of nylon 6,6, J.M.S. – Rev. Macromol. Chem. Phys., C40, 4 (2000), 233-272

[91] Pielichowski, K.; Njuguna, J.: Thermal Degradation of Polymeric Materials, Shawbury: Rapra Technology, 2005

[92] Ehrenstein, G.W.; Riedel, G.; Trawiel, P.: Thermal Analysis of Plastics. Munich: Hanser-Verlag, 2004

[93] Jain, A.; Vijayan, K.: Effect of thermal ageing on Nylon 6,6 fibres. Journal of Material Science, 37, 13 (2002), 2623-2633

[94] Augh, L; Gillespie, J.W.; Fink, B.K.: Degradation of continuous fiber reinforced polyetherimide composites during induction heating. Journal of Thermoplastic Composite Materials, 14, 3 (2001), 96-115

[95] Ye, L.; Lu, M.; Mai, Y.-M.: Thermal de-consolidation of thermoplastic matrix composites - I. Growth of voids. Composites Science and Technology, 62 2002, 2121-2130

[96] Emrich, S.: Untersuchungen zum Einfluss von Oberflächenchemie und -morphologie auf die Langzeitbeständigkeit geklebter Aluminiumverbunde. Kaiserslautern: Dissertation, 2003

[97] Geiß, P.L.; Brockmann, W.: Creep Resistance of Pressure Sensitive Mounting Tapes. Journal of Adhesion, 63 (1997), 253-263

[98] Final report BMBF-project „Angepasste Faser-Kunststoff-Verbunde durch verfahrensintegrierte Eigenschaftsbeeinflussung“ (Förderzeichen: 03N3113C), 2005

[99] Wiedmer, S.; Gellner, D.; Friedrich, K.: Effect of electron-beam radiation on thermoplastic composites. Plastics, Rubbers and Composites, 34, 2 (2005), 76-84

[100] Zinn, S.; Semiatin, S.L.: Elements of induction heating, Metals Park, Ohio: ASM International, 1988

[101] Benkowsky, G.: Induktionserwärmung. 5. Edition, Berlin: Verlag Technik GmbH, 1990

[102] Ahmed, T.J.; Stavrov, D.; Bersee, H.E.N; Beukers, A.: Induction welding of thermoplastic composites – an overview. Composites: Part A, 37 (2006), 1638-1651

[103] Mitschang, P.; Rudolf, R; Neitzel, M.: Continuous induction welding process, modelling and realisation. Journal of thermoplastic composites materials, 15 (2002), 127-153

[104] Fink, B.K. Gillespie, J.W.; McCullough, R.L.: Experimental verification of models for induction heating of continuous-carbon-fiber composites. Polymer Composites, 17, 2 (1996), 198-209

[105] Yarlagadda, S.; Kim, H.J.; Gillespie, J.W.; Shevchenko N.B.; Fink, B.K.: A study on the induction heating of conductive fiber reinforced composites. Journal of Composite Materials, 36, 4 (2002), 401-412

[106] Fink, B.; McCullough, R.; Gillespie, J.: A Local Theory of Heating in Cross-Ply Carbon Fiber Thermoplastic Composites by Magnetic Induction. Polymer Engineering and Science, 32, 5 (1992), 357-369

[107] Stokes, V.K.: Experiments on the Induction Welding of Thermoplastics. Polymer Engineering and Science, 43, 9 (2003), 1523-1541

[108] Yousefpour, A.; Hojjati, M.; Immarigeon, J.-P.: Fusion Bonding/Welding of Thermoplastic Composites. Journal of Thermoplastic Materials, 17, 7 (2004), 303-341

[109] Ageorges, C.; Yea, L.; Hou, M.: Advances in fusion bonding techniques for joining thermoplastic matrix composites: a review. Composites: Part A, 32 (2001), 839-857

[110] Yarlagadda, S.; Fink, B.K.; Gillespie, Jr. J.W.: Resistive Susceptor Design for Uniform Heating During Induction Bonding of Composites. Journal of Thermoplastic Composites, 11 (1998), 321-337

[111] Mathur, R.; Advani S.G.; Yarlagadda, S.; Fink, B.: Genetic Algorithm based Resistive Susceptor Design for Uniform Heating During the Induction Bonding Process. Journal of Thermoplastic Composite Materials, 16, 11 (2003), 529-550

[112] Ahmed, T.J.; Stavrov, D.; Bersee H.: An experimental investigation into resistance and induction welding for aerospace structures: A comparison. 47th AIAA/ASME/ASCE/AHS/ASC Structures, Structural Dynamics, and Materials Conference, Newport, Rhode Island, 1 - 4 May 2006, AIAA 2006-2245

[113] Wijngaarden, M. van,: Welding technologies for a generic carbon fiber reinforced thermoplastic assembly. Proceedings: International Symposium for Composite Manufacturing (ISCM), Braunschweig, Germany, May 2004.

[114] Rudnev, V.; Loveless, D.; Cook, R.; Black, M.: Handbook of induction heating, New York - Basel: Dekker, 2003

[115] Nichols, R.J.: Advances in the Emabond Induction Welding Process for High-Performance Assembly of Demanding Thermoplastics. Assembly Technology Expo, 2003

[116] Wesley Cable, J.: Betriebspraxis der induktiven Erwärmung. Stuttgart: Berliner Union, 1961

[117] Orfeuil, M.: Electric Process Heating – Technologies / Equipment / Applications. Columbus (USA): Battelle Press, 1987

[118] Dolocan, V.; Dolocan E.: Temperature and magnetic field dependence of permeability in amorphous magnetic materials. Journal Physics France, 4 (1994), 1901-1911

[119] Bordin, G.; Buttino, G.; Ceccheti, A.; Poppi, M.: Temperature dependence of magnetic properties and phase transitions in a soft magnetic Co-based nanostructured alloy. J. Phys. D: Appl. Phys., 32 (1999), 1795-1800

[120] Kittel, C.: Introduction to Solid State Physics. New York: Wiley, 1996

[121] Keller-Flaig, R.M.; Arzt, E.: Mechanical and thermal expansion properties of thin Fe-36 wt.-% Ni Invar films. Advanced Engineering Materials, 4, 5 (2002), 305-307

[122] Patent: WO/0185827 A2, (15 November 2001). Stark, P. et al.: Pr.: 09/562,188 2000-5-2

[123] Data sheet, CFA-001, T300, Toray Carbon Fibers America, Inc., 2007

[124] Data sheet SGL Carbon 1501 G, 2006

[125] Scharff, A.; Allmeier, S.: Temperaturabhängige Werkstoffuntersuchungen an Aluminiumlegierungen in der Umgebung von Schweißnähten. Proceedings of „Große Schweißtechnische Tagung“, DVS Band 237, Essen, 12th-14th September 2005, 467-475

[126] Becker, G.W.; Braun, D.; Bottenbruch, L.; Binsack, R.: Kunststoff-Handbuch Band 3/4: Technische Thermoplaste Polyamide, Munich: Hanser-Verlag, 2004

[127] Zach, T.; Jew, J.; North, T.H.; Woodhams, R.T.: Joining of High Strength Oriented Polypropylene using Electromagnetic Induction Bonding and Ultrasonic Welding. Materials Science and Technology, 5 (1989), 281-287

[128] Border, J.; Salas, R.: Induction Heated Joining of Thermoplastic Composites Without Metal Susceptors. 34th International SAMPE Symposium, 1989, 2569-2578

[129] Yousefpour, A.; Hoijati, M.; Talbot, E.; Hubert, P.: Manufacturing process modelling of resistance welding. In: Proceedings CanCom 2005, Vancouver, Canada, August 2005

[130] Stavrov, D.; Nino G.; Bersee, H.: Process Optimization for Resistance Welding of Thermoplastic Composites. 47th AIAA/ASME/ASCE/AHS/ASC Structures, Structural Dynamics, and Materials Conference, Newport, Rhode Island, 1 - 4 May 2006, AIAA 2006-2246

[131] Velthuis, R.; Mitschang, P.; Schlarb, A.K.: Prozessführung zur Herstellung und Eigenschaften von Metall/Faser-Kunststoff-Verbunden. In: Schlimmer, M. (Ed.) 15. Symposium: Verbundwerkstoffe und Werkstoffverbunde. Kassel, 4-6 April 2005

[132] Mitschang, P.; Velthuis, R.; Schlarb, A.K.: Induction welding of hybrid composite-metal-parts. 12th ICCE Conference, Tenerife, Spain, August 2005

[133] DIN 50905-4 Korrosion der Metalle; Korrosionsuntersuchungen; Korrosionsgrößen bei ungleichmäßiger und örtlicher Korrosion ohne mechanische Belastung, 1987-01

[134] DIN EN ISO 10365: Adhesives - Designation of main failure pattern, 1995-08

[135] ASTM D 3528–96 (Reapproved 2002) Standard Test Method for Strength Properties of Double Lap shear Adhesive Joints by Tension Loading, 2002

[136] Mitschang, P.; Velthuis, R.; Emrich, S.; Kopnarski, M.: Induction welding of aluminum and carbon fiber reinforced nylon 66. Journal of Thermoplastic Composites, prepared for submission in November 2007

[137] Velthuis, R.; Mitschang, P.; Schlarb, A.K.: Manufacturing and Properties of Metal/Thermoplastic Fiber Reinforced Polymer Composites. In: Proceedings CanCom 2005, Vancouver, Canada, August 2005

[138] Bos, M.; Renz, R.: Characterisation of welded metal-plastic single-lap-joints with the Q300 ESPI system. 13th international user meeting and conference; Ulm, Germany, 11-12 October 2006

[139] Bauer, A.: Eigenschaften im Grenzbereich. Kleben & Dichten - Adhäsion, 38, 6 (1994), 29-32

[140] Velthuis, R.; Mitschang, P.; Kötter, P.; Geiß, P.; Schlarb, A.K.: Leichtbau aus Metall und Faser-Kunststoff-Verbunden / Lightweight Structures made of Metal and Fiber-Reinforced Polymers. Kunststoffe / Kunststoffe international, 11, 2007, 55-57

[141] Patent: DE102005018478A1, (26 October 2006). Velthuis, R; Collet, C.: B29C 65/32, 2005-4-21

[142] Moser, L.; Velthuis, R.; Mitschang, P.; Schlarb, A.K.: Three-dimensional induction welding of fiber reinforced thermoplastic polymers. In: Proceedings SAMPE Europe 2007, Paris, France, 3-5 April 2007

[143] Collet, C.: Temperaturführung beim Induktionsschweißen von Metall/Faser-Kunststoff-Verbunden, IVW Technical Report 07-006, 2007

[144] Velthuis, R.; Schlarb, A.K.: Induktionsschweißen von faserverstärkten Kunststoffen - Eine grundlegende Untersuchung zur Machbarkeit. IVW Technical Report 05-014, 2005

[145] VDI-Wärmeatlas, VDI-Gesellschaft Verfahrenstechnik und Chemieingenieurwesen, Berlin – Heidelberg: Springer. 9th edition, 2002

[146] Schmeer, S.; Huber, U.; Maier, M.: Werkstoffkennwertkatalog CF-PA66 & CF-PEEK - DFG-Forschergruppe 524, 2005

[147] Schmeer, S.; Maier, M.: Werkstoffkennwertkatalog CF-PA66-Gelege - DFG-Forschergruppe 524, 2007

[148] Lehrstuhl für Werkstoffkunde, University of Kaiserslautern: Werkstoff-kennwertkatalog AlMg3 & DC01 - DFG-Forschergruppe 524, 2005

[149] http://www.matweb.com (DuPont Dartek® SF-502 Nylon 6,6 Super Formable Film, 76 µm Thickness) (May 2007)

[150] http://www.matweb.com (Victrex PEEK™ 150PF, Easy Flow) (May 2007)

[151] Preliminary data sheet “LUVOCOM 1105 – 7373 VP” (May 2007)

[152] Data sheet, CFA-002, T300J, Toray Carbon Fibers America, Inc., 2007

[153] www.supershine.co.kr/pls003.htm (May 2007)

[154] Data sheet “Product Selector Guide Standard” Ten Cate Advanced Composites b.v. (October 2006)

[155] Data sheet “Technisches Datenblatt Style 475” - GL-011/3-09/02, ECC GmbH & Co. KG (May 2007)

[156] Data sheet “MCX0481270”, Sigmatex (UK) Ltd., (October 2006)

List of the supervised students research and graduation projects:

Moser, L.: Umbau einer Laboranlage zum diskontinuierlichen Induktionsschweißen von Metall/Faser-Kunststoff-Verbunden, 2004

Sánchez, B.: Surface preparation influences of bonding metal to fiber reinforced thermoplastics by means of induction welding, 2004

Collet, C.: Ermittlung und Optimierung des Energieeintrags in die Fügezone beim Schweißen von glasfaserverstärkten Thermoplasten, 2005

Collet, C.: Temperaturführung beim Induktionsschweißen von Metall/Faser-Kunststoff-Verbunden, 2007